STUDY OF THE p + ^{3}H AND n + ^{3}He FINAL-STATE INTERACTIONS IN THE REACTIONS ^{7}Li(p, α) AND D(^{3}He, p)

Thesis by

Wen Kuan Lin

In Partial Fulfillment of the Requirements

For the Degree of

Doctor of Philosophy

California Institute of Technology

Pasadena, California

1969

(Submitted May 1, 1969)

ACKNOWLEDGMENTS

I would like to thank the faculty and the staff of Kellogg Radiation Laboratory for the efforts that have made this work possible. In particular, special thanks must go to Professor R. W. Kavanagh who has led the interest of studying these reactions and has given me his continued guidance and encouragement, and also to Professor T. A. Tombrello for his constant interest and his close supervision during the period when Professor Kavanagh was away in France.

The author is particularly grateful to Dr. F. Scheibling for his active participation in these experiments and for his introduction to some of the useful computing techniques. The part on the theoretical interpretations has profited from the discussions with Dr. K. Nagatani and Dr. K. Kolltveit.

Extra special thanks must go to my wife, Bella, for her patience and confidence and to my mother who is always a source of inspiration.

Finally I would like to express my gratitude for the financial support from the California Institute of Technology in the form of tuition scholarships and assistantships. The research project has been supported by the Office of Naval Research and the National Science Foundation.

ABSTRACT

The α-particle energy spectra from the bombardment of ^{7}Li with 9.1-MeV protons have been obtained at $2.5° \leq \Theta_{\alpha} \leq 120°$. The high-energy ends of the spectra are interpreted as due to the ^{1}S p + ^{3}H final-state interaction through the first excited state of ^{4}He at 20.06 MeV. The factored-wave-function method is used to deduce the resonance parameters of this state. Consistency in the use of this method is obtained by a PWBA calculation based on the triton-transfer mechanism to account for the forward-peaking in the angular distribution. Coincidence measurements between α-particles and the other charged particles give additional evidence for the 0^{+} assignment to the state, and indicate that the α + ^{3}H and α + H final-state interactions are important as the ^{4}He excitation energy gets higher. To reduce the effects of these final-state interactions, the reaction D(^{3}He, p), at a ^{3}He bombarding energy of 16.5 MeV, has been investigated. The protons emitted from the reaction have been measured at $\Theta_{p} = 30°$ in coincidence with the other charged particles. Angular correlations have been obtained for 6.6 MeV $\leq E_{p} \leq$ 8.6 MeV, and compared with a modified Born approximation calculation based on the stripping of ^{3}He. The angle-energy correlation and the p - ^{3}H to p - ^{3}He branching ratio can be reproduced, if Meyerhof's p + ^{3}H phase shifts and Bransden's n + ^{3}He phase shifts are used to describe their respective interactions in the final states. In agreement with the reported 0^{-} state at 21.2 MeV, the p-wave final-state interactions are found to be important in this energy range.

TABLE OF CONTENTS

I. INTRODUCTION

The question of the existence of excited states of the α-particle was first raised by Crane, Delsasso, Fowler and Lauritsen (1935) A series of very energetic γ-rays with energies as high as 16 MeV were detected in a cloud chamber, when a ^{7}Li target was bombarded with 1-MeV protons. Those γ-rays were attributed to the decay of α-particles produced in excited states. Using a sum-rule argument, Feenberg (1936), Bethe and Bacher (1936) pointed out that the α-particle may possess excited states. An upper energy limit of 20 MeV was proposed. As was shown later by Austern (1960), these calculations suffer from the fact that the α-particle radius and the nature of nuclear forces were inadequately known in early 1935. When the appropriate corrections are made, the upper limit rises to 50 MeV, indicating that the existence of an excited bound state is not probable.

One of the first indications of an excited state of ^{4}He at about 20 MeV was suggested by Frank and Gammel (1955), who considered a ^{1}S resonance at 20.44 MeV to be necessary to explain the energy dependence of the p+^{3}H elastic-scattering cross section. In agreement with this, Bergman et al. (1958) also found a ^{1}S resonance at 20.1 MeV essential to account for the observed departure of the ^{3}He(n, p)^{3}H reaction cross section from a 1/v law. Stronger evidence for such a resonance was later given by Werntz (1962) in his analysis of the neutron energy spectra from the reaction ^{3}H(d, n) [Lefevre et al., 1962; Poppe et al., 1963]. A strong ^{1}S p+^{3}H interaction in the final state gives a maximum as required by the data at the high-energy end of the neutron energy spectra. Interpreting the interaction as a resonance, the resonance energy was found at 20.2 MeV. The reduced widths for p+^{3}H and n+^{3}He channel were

equal to each other, if the channel radius was taken as 3.0 F. From this Werntz and Brennan (1963) were able to argue that the resonance concerned is a state of definite isobaric spin.

The assignment of an isobaric spin to this resonance stimulates various interesting experimental and theoretical efforts and yields useful knowledge about the mass-four system. If the resonance was a T = 1 state, the analog ^{4}Li should be seen also as an s-wave resonance at about 0.36 MeV (c.m.) in the p+^{3}He system and ^{4}H would be stable against neutron emission by about 0.18 MeV. The experiments of $^4H(\beta^- \bar{\nu})^4He$ [Spicer, 1963, Nefkens et al., 1964], $^4H(\beta^- \bar{\nu})^4He^*$ [Janecke, 1965] and $^3H(d,p)^4H$ [Rogers et al., 1964] failed to establish any particle stable ^{4}H state. The phase-shift analysis of the n+^{3}H elastic scattering cross section and polarization data by Tombrello (1966) also indicated that ^{4}H neither possesses particle-stable states nor low-lying resonances except for two broad p-wave resonances at higher energies (3.4 MeV and 5.1 MeV). Similar results from the p+^{3}He elastic scattering were obtained for the ^{4}Li system. They include Frank and Gammel's original work, and the phase-shift analyses of Tombrello (1962, 1965) and Kavanagh and Parker (1966). The two corresponding p-wave resonances were also found by Tombrello at 4.7 MeV and 6.2 MeV in the p+^{3}He system. Taking the coulomb interaction into account, Tombrello's results suggested that the first T = 1 state in ^{4}He should appear as a p-wave resonance with an excitation energy higher than 24 MeV.

The recent phase-shift analyses by Meyerhof and McElearney (1965) and by Balashko, Kurepin and Barit (1966) also confirmed the ^{1}S resonance and showed an increase in p-wave phase shift with energy. One therefore believes that this ^{1}S resonance at 20 MeV has isobaric spin T = 0 [assuming isobaric-spin conservation, a direct evidence of the T = 0 assignment for this resonance has been

reported by Hungerford et al. (1968) from the reaction $^4He(\alpha,\alpha)^4He^*$], and that the T = 1 states may exist at higher excitation energies in p-wave states. This speculation was also supported by the theoretical shell-model calculations of deShalit and Walecka (1966) and Kramer and Moshinsky (1966). The calculation, however, predicts a series of T = 0 negative-parity states around 22 MeV. Whether the observed increase in p-wave phase shift corresponds to a T = 0 or T = 1 state is still a question requiring further investigations.

Besides the reaction $^3H(d,n)$, the excited states of ^4He were studied by many other three-body reactions. Young and Ohlsen (1964), using 6 to 10 MeV deuteron beams and ^3He gas targets, obtained the proton energy spectra from the mirror reaction $^3He(d,p)$ over laboratory angles from 14° to 30°. The peak close to the highest-energy end of the spectra was also identified as due to the 0^+ resonance of the $p+^3H$ final-state interaction. Using a deuterated polyethylene foil target and a ^3He beam from a 60-in cyclotron, Donovan (1965) and Parker et al., (1965) measured the protons in coincidence with the ^3H or the ^3He. Another excited state in ^4He at 21.2 MeV of 1.1 width was found, in addition to the 0^+ resonance discussed previously. Taking these results, Cerny et al. (1965) were able to resolve a third small peak at 22.5 MeV in the ^3He energy spectra from the reaction $^6Li(p,^3He)$. The state that gives rise to this peak, however, is not certain, since no such peak was seen also in Cerny's α-particle energy spectra from the $^7Li(p,\alpha)$ reaction.

The present work started with the purpose of re-examining the reaction $^7Li(p,\alpha)$ by using the tandem electrostatic accelerator and the 61-cm magnetic spectrometer. With better energy resolution and particle identification, it was believed possible to deduce the resonance parameters for the 0^+ state and to resolve peaks around

22 MeV, if any. The α-particle energy spectra taken at 9.1-MeV bombarding energy at various angles ranging from 2.5° to 120° show consistent evidence of the existence of the 0^+ state in the ^{4}He system. The obtained resonance parameters and therefore the ^{1}S p+^{3}H scattering phase shifts are in good agreement with the published values derived from other reactions.

The angular distribution of the α-particle group leading to this 0^+ state, in contrast to Cerny's results obtained at 43.7-MeV proton bombarding energy, turns out to be very different from that for the ground state α-particle group. The forward peaking in the angular distribution indicates the importance of the triton-pick-up process.

Other peaks which may contribute evidence for the existence of higher excited ^{4}He states were also seen in the spectra taken at smaller angles. But as the coincidence measurements to be described have shown, the strong α+^{3}H, α+H and possibly α+N final-state interactions become important as the energy of the detected α-particles gets smaller. These make the deduction of any useful information about the p+^{3}H or n+^{3}He interaction very difficult.

The coincidence measurements give the angular correlations of the α-particle and other charged particles from the reaction, e.g., between α-particle and ^{3}He in ^{7}Li+p → α+^{3}He+n. When the α-particle momentum was chosen such that there was 20.014-MeV excitation energy in the recoil ^{4}He system, the correlations obtained can be interpreted as if the recoil ^{4}He system were decaying isotropically in its center-of-mass system. This strongly confirms the 0^+ assignment of the first excited state of ^{4}He. But when the α-particle momentum was chosen such that the excitation energy of the recoil ^{4}He system was 21.272 MeV, the protons were found to be very strongly correlated with the α-particles along a certain direction.

This corresponds to the situation that the third particle, i.e., the triton, is interacting strongly with the α-particle through the 4.63-MeV excited state of ^{7}Li. Similarly the α+H final-state interaction via the ground state of ^{5}Li and possibly the α+N final-state interaction through the ground state of ^{5}He were also seen in the α-^{3}H and α-^{3}He correlations, respectively.

To reduce the effects of such competing final-state interactions, the reaction D(^{3}He, p) was then investigated. Because the phase shifts of the singlet two-nucleon system stay relatively small at low energies, it was believed that the final-state interactions in the diproton and singlet deuteron system are not as strong as those of interest. Using 16.5-MeV ^{3}He bombarding energy, the protons were detected at 30° with respect to the beam. The angular correlations of the other charged particles were obtained at proton energies ranging from 6.6 MeV to 8.6 MeV in steps of 0.4 MeV. They all had an axis of symmetry along the momentum of the recoil ^{4}He system and suggested the importance of the ^{3}He stripping reaction mechanism. A modified Born approximation calculation [Yu and Meyerhof, 1966] based on this mechanism was made to estimate the relative amplitudes of producing the final-state interacting pair of particles in s-wave and p-wave states. It was found that both the angular and energy correlations and the ratio of the contributions from p+^{3}H to n+^{3}He interaction can be reasonably well reproduced, if the p+^{3}H phase shifts of Meyerhof and McElearney (1965) and the n+^{3}He phase shifts of Bransden et al. (1956) were used to describe the respective final-state interactions.

Very recently, assuming the isobaric spin invariance, Werntz and Meyerhof (1968) have made a R-matrix analysis of the ^{4}He system [cf., Meyerhof and Tombrello, 1968]. An energy level diagram

shown in Figure 1 was proved to be consistent with the differential cross section and the neutron polarization data from the reaction $^{3}H(p,n)^{3}He$. The 0^{-} and 2^{-} assignments to the second and third T = 0 excited states are also consistent with p-wave interactions observed in this work.

In Part II the experimental details and the data obtained are discussed. The data reduction along with the kinematics involved is described in Part III. The assumptions of the Watson-Midgal approximation in treating the interaction in final state of a three-body reaction and the applications of such an approximation for data-analyses are discussed in Part IV. A summary and discussion of the results is presented in Part V. The appendices are included to supplement the calculations made in Part IV.

II. EXPERIMENTAL DISCUSSIONS

The 61-cm double-focusing magnetic spectrometer employed in the present experiments is used in conjunction with the ONR-CIT tandem accelerator. It has been described in detail by Groce (1963). With the installation of a nuclear magnetic resonance (NMR) magnetometer, the spectrometer was carefully calibrated by McNally (1966) in his Q-value measurements. When a particle of mass M and of charge Z passes through the magnet, its kinetic energy E, as a function of the magnetometer frequency f is given by

$$E = k f^2 Z^2 \frac{M_p}{M} \left(1 - \frac{E}{2Mc^2}\right),$$

where M_p is the proton mass and k is a parameter to be determined experimentally. Because of the location of the magnetometer and the dependence of the magnetic field profile on the field strength, k was found to increase by 0.88% as the frequency changes from 20 MHZ to 44 MHZ. A conversion table from frequency to energy, constructed by using two measured k values for two separate frequency ranges, was used in all the energy measurements of these experiments. A correction to this table, which is less than 30 keV for both protons and α-particles, was made at the frequencies around 33.8 MHZ. This is the frequency where the division into two separate frequency ranges occurs.

Disregarding the relativistic correction, particles of the same kinetic energy and of the same Z^2/M will correspond to one magnetometer frequency. Another measurement, usually the energy loss of the particle in certain stopping material, is needed to remove this ambiguity for proper particle identification. This is done by placing either a ΔE-counter or an appropriate stopping foil plus an

E-counter on the focal plane of the magnetic spectrometer. As the energy loss is roughly inversely proportional to the particle kinetic energy, the conditions, such as the bias on the ΔE-counter or the stopping-foil thickness, must be suitably adjusted as the energy changes from one range to another. To make these adjustments more manageable, a single surface-barrier counter (200 mm^2, 140μ thick at 50-volts maximum bias) was used. Using thin nickel foil as the stopping material, α-particles of energy as low as 900 keV could be separated out from the protons. As seen from Figure 2, the measurement of low energy α-particles by the spectrometer was limited by the presence of continuously distributed pulses below 600 keV. From the width of proton group, the over all electronic noise was estimated to be less than 250 keV. Those continuously distributed pulses probably come from the randomly scattered particles by the wall of the spectrometer. The energy resolution $\delta E/E$ of the spectrometer, controlled by a slit of adjustable size in front of the counter, was set either at 1.11% or 0.56%. The entrance slits, target chamber, and target holder used have been discussed in detail in Groce's work, and no further description will be given here.

Each of the surface-barrier counters used in the experiments was connected through a cable of minimum length to a TENNELEC Model 100A low noise preamplifier. The pulses from the preamplifier were amplified by an ORTEC model 410 linear amplifier and were then analyzed by a RIDL 400-channel analyzer. After each run the memory of the analyzer was read onto paper tape for subsequent determination of yields from the peak areas.

A. The Reaction $^{7}Li(p, \alpha)$.

In order to investigate the effects of $p+^{3}H$ and $n+^{3}He$ final-state interactions on the α-particle energy spectra, a high bombarding energy is desirable. The α-particles can then escape from the recoil pair of particles with large relative velocity without interacting with either particle of the pair. Without knowing anything about the reaction mechanism beforehand, one wishes, however, to choose a beam energy such that the compound system of the target ^{7}Li nucleus plus the incident proton may have a resonance (for increased yield). Thus the proton bombarding energy was chosen to be 9.1 MeV, corresponding to the 2^{+} 25.2-MeV excited state of ^{8}Be [Lauritsen and Ajzenberg-Selove, 1966].

The 9.1-MeV proton beam was obtained from ONR-CIT tandem accelerator. A negative proton beam ~ 20 μA was extracted from the negative ion source and was stripped to a positively charged beam at the center terminal of the tandem. It was then analyzed by a 86.3-cm uniform 90°-magnet. When the object and image slits were set at 3.81 mm, and the beam-defining slits in front of the target chamber were set at 1.53 mm along the horizontal and vertical direction, a beam of ~ 1 μA was normally obtainable on target.

In the target chamber, there was an additional surface-barrier counter. Except in the coincidence measurements, it was fixed at 145° with respect to the beam direction and measured the flux x target density of the reaction. An accurate integration was thus not required except for the runs during which the target thickness was being measured.

1. Target preparation.

The ^{7}Li targets were prepared from 99.99% ^{7}Li enriched

metal in the target-chamber furnace illustrated by Groce (1963). The lithium metal in a tantalum boat was preheated to eliminate the kerosene in which the lithium had been stored. As the current through the boat increases, the pressure of the target chamber will rise suddenly when one of the compounds in the target material starts to evaporate. A compound, presumedly the lithium hydroxide which has a boiling point considerably lower than that of the lithium metal, was found to evaporate first. The preheating process is finished, if the pressure stays at normal value $\sim 1.5 \times 10^{-6}$ mm Hg as long as the current is kept below the value at which the lithium metal would start to evaporate.

The gold backing foils $\sim 80 \mu g/cm^2$, mounted on the target holder are now lowered down to the level of the tantalum boat. To evaporate the lithium onto the foil, the temperature should be built up gradually to avoid breaking the foils.

From the time duration of the evaporation, or from the color that the foils appeared, the amount of the lithium deposited on the foils is roughly known. It can be checked by measuring the yields from the reaction $^7Li(p, \alpha_0)$ with the monitor-counter in the target chamber. Additional evaporations can be done easily without opening the vacuum system.

2. Particle spectra.

The monitor-counter (50 mm^2, 300μ thick at 85-volts maximum bias) located in the target chamber provided quick surveys of the particles emitted from the reaction. Figure 3 shows the spectra obtained at 60° and 90°. In spite of the elaborate precautions taken in the target preparation, the oxygen and carbon contaminations were not avoided.

In the energy region where the contribution due to the reaction $^{7}Li(p,\alpha)^{4}He^{*}$ is expected, one finds the presence of strong competing processes, such as $^{16}O(p,p')$, $^{12}C(p,p')$, $^{7}Li(p,d_0)$ and possibly some other three-body reactions. The usefulness of applying the magnetic spectrometer to identify the particle species is manifest.

3. Target thickness.

In the first attempt to measure the target thickness, a gold foil ~ 80μg/cm^2 uniformly coated with a CaF_2 layer ~ 20 μg/cm^2 was prepared by vacuum-evaporation. The thickness of the ^{7}Li, evaporated later on top of the CaF_2 layer in the target chamber, was determined by measuring the energy loss in ^{7}Li of the 3.85-MeV α-particles produced from the reaction $^{19}F(p,\alpha')$ with 5-MeV protons as the bombarding particles. The energy loss was then converted into the number of ^{7}Li atoms per cm^2 by using the atomic stopping cross sections given by Demirlioglu and Whaling (1962). The results are shown in Figure 4 and the differential cross section of $^{7}Li(p,\alpha_0)$ at 30° was found to be 1.39 ± 0.35 mb/sr. This is considerably lower than the 2.33 ± 0.43 mb/sr calculated from the coefficients of the Legendre polynomials published by Mani et al. (1964). The uncertainty in the oxygen and carbon contamination leads to an underestimation in the actual average stopping cross section.

A target of some lithium compound with known chemical composition should be preferable. Also by vacuum-evaporation a LiF target ~ 80μg/cm^2 on gold backing was then prepared. Its thickness was determined by measuring the energy loss of a 9.1-MeV α-particle beam from the tandem accelerator. Without including the errors of scaling the proton stopping cross section to that of the

α-particle and the assumption on the LiF chemical composition, the differential cross section of $^{7}Li(p,\alpha_0)$ at 30° was found to be 1.88 ± 0.08 mb/sr. This value will be taken to convert the measured relative differential cross sections into the absolute ones.

4. $^{7}Li(p, \alpha_0)$ angular distribution.

Besides for checking the normalizations, the $^{7}Li(p, \alpha_0)$ angular distribution is interesting for a comparison with that from the reaction $^{7}Li(p, \alpha_1)$. Since the first excited state of the α-particle was found to have the same spin and parity as the ground state of the α-particle, it was expected that the two angular distributions should bear some resemblance [Cerny et al., 1965]. As would be anticipated for a reaction involving two identical bosons in the final state, the angular distribution shown in Figure 6 has a 90° symmetry in the center-of-mass system. The data obtained at higher bombarding energies by Maxson (1962) are also included for comparison. The shapes and the absolute values of the angular distributions for these bombarding energies appear approximately the same. This confirms the direct triton-pick-up reaction mechanism that Maxson has discussed in his analyses.

5. Single α-particle energy spectra.

In the three-body reaction $^{7}Li + p \rightarrow \alpha + p + {}^{3}H$, the excitation energy of the $p+{}^{3}H$ system is fixed, if an α-particle of known energy is detected at a given angle. As a typical procedure in obtaining an α-particle energy spectrum, the spectrometer frequency was first set to a value such that an associated ^{4}He of 20.0-MeV excitation energy is expected to be formed. The protons having the same energy and the same Z^2/M as the α-particles were separated out by varying the bias voltage of the counter or the thickness of the stop-

ping foil. For further assurance of detecting the correct group of particles, the spectrometer frequency was then increased step by step. If the group of particles was due to the α-particles emitted from the reaction, the counting rate of the group should reduce to zero when the magnetic field strength of the spectrometer reaches a value such that the corresponding excitation energy of the recoil ^{4}He system crosses its p+^{3}H threshold from above.

Once the α-particles group had been established, the change in pulse height of the group could be followed as the spectrometer frequency decreased when the lower-energy part of the spectra were taken. Some adjustments on either the bias voltage or the stopping foil thickness were necessary to keep the proton group away from the α-particle group. The yield from ^{7}Li(p, α_0) was measured at 145° with the monitor-counter during each run for normalizing the flux x density.

At the beginning it was considered to be interesting to investigate the α-particle energy spectra over a wider energy range. Two of these spectra are shown in Figure 7. When the phase space factor has been taken out [cf., equation (5) in Part III], the transition probability is plotted out in Figure 8 as a function of the ^{4}He excitation energies.

The contribution due to the second excited state of ^{4}He appears as a peak in the spectra near 21.2 MeV in agreement with the value that Parker et al., (1965) and Cerny et al., (1965) have found. This becomes less obvious and is masked by the contributions from other final-state interacting pairs at larger angles. To unfold any useful information about the second excited state would require a rather complicated analysis [Morinigo, 1963; Bacher, 1966].

Limiting the interest to study of the first excited state of ^{4}He, only the high-energy ends of the spectra were taken in the later stage of the experiment. It includes the ^{4}He excitation energies from the p+^{3}H threshold, 19.814 MeV, up to 21 MeV. Figure 9 shows the spectra obtained at the laboratory angles from 10° to 120°.

6. Coincidence measurements.

For a three-body reaction 1 + 2 → 3 + 4 + 5, nine variables are required to describe the momentum vectors of all particles in the final state. The conservation of total energy and momentum reduces this number to five. The range that these five independent variables are allowed is ordinarily referred to as the phase space. Only three out of the five variables were measured with known resolutions in the measurements of energy spectra described in the previous section. Except for the pair (4 + 5), the pair excitation energies were not fixed. The coincidence measurements go one step further to measure these energies and consequently are limited to a smaller region of phase space. As will be explained in Part III, this is done by measuring the direction along which the particle 4 is emitted.

If the pair interactions of (3 + 4) and (3 + 5) in the final state of the reaction are not strong as compared with that of the pair (4 + 5) over the kinematically allowed phase space region, the angular correlation of particles 3 and 4 should include the same information about the spin, parity and some other characters of the state that the pair interaction (4 + 5) leads to.

From the single α-particle energy spectra of the reaction ^{7}Li(p, α)^{4}He*, the p+^{3}H final-state interaction is seen definitely to imply a ^{4}He first excited state. It would be interesting to check if the state prepared in this way agrees with the 0^+ spin-parity assignment from other sources of experimental data.

Keeping the incident proton energy still at 9.1 MeV, the α-particles were detected also by the magnetic spectrometer at 30° in coincidence with other charged particles of the reaction products. With $\delta\Theta = 1°$, $\delta\Phi = 4°$ and $\delta E/E = 1.11\%$, the spectrometer was set to detect 5-MeV α-particles. Its exact field strength, depending on the thickness of backing foil and that of target, was found and fixed at the value that maximized the α-particles counting rate. Other charged particles were detected by the monitor-counter in the target chamber. Its angular apertures were set at 3.8° and 15.5° respectively along the polar and azimuthal directions.

Since the protons and tritons were detected around -110°, the counting rate was not high, and a slow coincidence circuitry was sufficient. Figure 10 shows the electronic arrangements. Due to the transit time of the α-particles through the vacuum box of the spectrometer, the pulses from the counter in the target chamber were delayed by 0.2 μs before entering the coincidence circuit. The ORTEC Model 420 timing single-channel analyzer, having a 10-turn control to delay its outputs up to 1 μs, provides this amount of delay. The coincidence resolving time of the ORTEC Model 409 linear gate and slow coincidence is equal to 1 μs (the sum of the two input-pulse widths). The coincidence output gives enable pulses to open the linear gate through which the pulses from the counter in the target chamber were directly put into the ADC of a multi-channel analyzer. A 1.7-μs delay to these pulses was necessary to assure the gate to be opened at the right time. The coincidence outputs were also used to gate another multi-channel analyzer in setting the window of the single-channel analyzer for the pulses from the magnetic spectrometer.

The obtained coincidence spectra are shown in Figure 11. They were taken with ^{7}Li target facing the counter in the target chamber. The α-particles have to pass through the gold backing and suffer the spreadings in both the energy and the direction of motion. The resolution in the coincidence spectra was found to improve a little, if the target was rotated around by 180°. But the kinematic $dE/d\Theta$ spreading, the most important one, cannot be improved without cutting down the coincidence counting rate. No attempt, therefore, was tried to separate out the tritons and protons in the coincidence spectra.

A single spectrum was taken right after each of the coincidence runs. From the counts in the coincidence spectrum under the proton peak from the elastic scattering by the gold backing, the randoms per channel can be estimated. After these randoms were subtracted, the sum of coincidences due to protons and tritons is shown in Figure 12. The curve is the total coincidence efficiency predicted by assuming an isotropic decay of the ^{4}He system. The agreement gives additional evidence to support the 0^{+} assignment for the first excited state of ^{4}He.

When the spectrometer is set to detect a 4.1-MeV α-particle, more energies are then available for the decay of the recoil ^{4}He system. It is now excited above the n+^{3}He threshold, so that among the reaction products there are also neutrons and ^{3}He's. Carbon foils $\sim 20\,\mu g/cm^{2}$ were tried to reduce the spreadings of both the energy and angle due to the target backing. In this case larger angular apertures for the counter in the target chamber are allowable, because $dE/d\Theta$ is smaller. Keeping the same width in azimuthal direction, the width along the polar direction was increased by a factor of two. Figure 13 shows some of the coincidence spectra. The co-

incidence data after subtracting the randoms are plotted in Figure 14.

By detecting an α-particle at a certain momentum, the excitation energy of the pair (p+^{3}H) or (n+^{3}He) is fixed regardless of where the proton or ^{3}H (neutron or ^{3}He) is detected. The relative energy of the other two pairs of particles depends symmetrically on where particles other than the α-particle are detected [cf., Part III]. It has the same value on a cone determined by an axis of revolution around the ^{4}He recoil axis in the center-of-mass of the entire system.

Because of the experimental arrangement, the particle 4 is always detected almost opposite to the direction of motion of the particle 3, i.e., the α-particle, particle 4 escapes from the α-particle with higher relative velocity than the undetected particle 5 does. Since the final-state interaction is stronger for the pair of particles having lower relative velocity, the α-H coincidences are enhanced by the α+^{3}H final-state interaction through the 4.63-MeV excited state in ^{7}Li at the two angles determined by the intersections of the cone and the scattering plane. Similarly the effect of the α+H final-state interaction through the ground state of ^{5}Li is also seen in the α-^{3}H coincidences. The enhancement of this kind, however, is not so obvious in the case of the α-^{3}He coincidences shown in Figure 14.

B. The Reaction D(^{3}He, p).

From the coincidence measurements described in Section A6, it was found that the strong final-state interaction of pair (3 + 5) may come in to mask that of the pair (4 + 5) which is the primary

interest of this work. To overcome this difficulty, one may try to change the beam energy or the angle where the particle 3 is detected. Hopefully a phase-space region may be found, such that particle 3 won't interact as strongly as particle 4 with the particle 5 in the final state of the reaction.

Instead of trying to search for such a phase space region, the reaction D(^{3}He, p) was investigated. The interactions that may come in to mask the effects of the p+^{3}H and n+^{3}He final-state interactions are respectively those for the diproton and the singlet deuteron systems.

As mentioned in Part I, this reaction was studied before by Donovan and Parker (1965) [cf., Zürmuhle, 1965]. Only the positions of the first two excited states were reported. It would be interesting to look into the angular correlations of the decaying particles to study some other properties of the states. From the standpoint of studying the reaction mechanism, Yu and Meyerhof (1966) have analyzed the single-nucleon energy spectra from the reactions ^{3}He(d, p) and ^{3}H(d, n). From their modified Born approximation calculations, they concluded that the singles only cannot distinguish between the different break-up modes and suggested that the coincidence measurements would help to resolve this difficulty.

To separate different groups of particles from one another in the coincidence spectra, and also for the same reason described at the beginning of Section A, it is better to use the ^{3}He beam energy as high as possible. However it was found that the tandem accelerator can give a more stable beam by using 5.5 million volts as the terminal voltage rather than 6 million volts (its nominal maximum).

A singly charged negative ^{3}He beam was extracted from the negative ion source and was stripped to a double positive charge at the center terminal of the tandem. Using the same sizes of object, image and beam defining slits as described in Section A of this Part, a 16.5-MeV ^{3}He beam of 5 to 20 nA was obtained on target.

1. Target preparation.

In Donovan and Parker's experiment, a thin deuterated polyethylene foil target ~ 1 mg/cm^2 was used. A solid target is more convenient than a gas target, since for a coincidence measurement a well defined beam spot is essential. At the time when the present experiment was planned, the deuterated polyethylene was not commercially available. A compound called the deuterated dotriacontane, suggested and supplied by its manufacturer (Merck, Sharp and Dohme of Canada), was used for the target preparations.

To prevent loss of dotriacontane which would be incurred during vacuum evaporation, it was instead put in carbon tetrachloride, stirred until it dissolved completely, and then the solution was carefully transferred onto a mounted backing foil with a medicine dropper. When the carbon tetrachloride had dried, the target was ready to be used.

Using the heavier particle as projectile, reaction products such as ^{3}H's and ^{3}He's are emitted in forward directions. It is important to choose a low-Z material as target backing in order to reduce the contribution to the counting rate from the Rutherford scattering. On the other hand, the melting point of the material

is only 68° C, and for better target stability against the heat deposited as the beam particles go through, a metal with high thermal conductivity is preferred. Taking those factors into consideration, copper ~ 50 $\mu g/cm^2$ was chosen.

The deuterated dotriacontane, $CD_3(CD_2)_{30}CD_3$, was indicated by the manufacturer to be 99.7 atom % in D by mass analysis. Use of the proton yields detected by spectrometer to normalize the coincidence spectrum has the shortcoming that the target may deteriorate and pick up carbon during the run. Likely the protons could come from the reaction $^{12}C(^3He, p)^{14}N^*$. In the energy range of interest, many excited states of ^{14}N [Ajzenberg-Selove and Lauritsen, 1959] may contribute to the proton counts. The total number of proton counts is therefore proportional to some linear combination of deuterium and carbon atoms in unit area of the target, while the coincidence counting rate is proportional only to the number of deuterium atoms per unit area. It is all right to use the proton counts as normalizer, if the chemical composition of the target material does not change [cf., Section B, Part III].

To check if the chemical composition of the target material changes, another surface-barrier counter was set up at 60° in the target chamber in the last day of this experiment. It detected the deuterons from the elastic scattering $D(^3He, d)^3He$ and its yields should be proportional to the number of deuterium atoms per unit area. The number of protons counted by the spectrometer divided by the number of deuterons counted by the additional counter was plotted in Figure 15 against the total integrated charge on target. The ratio, within a 10% deviation from its average, is reasonably constant for the integrated charge less than 70 μC. Most of the

targets broke before they had accumulated this much of a charge. Figure 15 also shows the ratio plotted out as a function of proton energies. These numbers were used to normalize the coincidence runs taken at different proton energies including an additional 10% deviation.

2. Particle spectra.

Due to the presence of carbon nuclei in the target material, the spectra shown in Figure 16 reflect a rather complicated structure. The processes such as $^{12}C(^{3}He, ^{3}He)^{12}C^{*}$, $^{12}C(^{3}He, \alpha)^{11}C^{*}$, $^{12}C(^{3}He, p)^{14}N^{*}$ and $^{12}C(^{3}He, d)^{13}N^{*}$ are possible. All of these recoil nuclei possess many excited states, and no attempt was made to identify each of these possible contributions. The limiting angle of detecting a ^{3}He from the $D+^{3}He$ elastic scattering is 42°, therefore no such group was seen in the particle spectrum at 46°. The recoiled deuteron from the elastic scattering was not obvious at 26° and smaller angles.

3. Angle calibration.

In the coincidence measurement, one of the counters was set up to detect a particle at certain fixed momentum, while the other counter was moved around. The angular correlation obtained in this way is essentially an angular distribution of the breakup of the recoil system. The conversion to the recoil center-of-mass system will be explained in Section A, Part III. As will be noticed, both the cross-section conversion factor and the recoil center-of-mass angle are very rapidly varying functions of the laboratory angle especially when it approaches one of the limiting angles.

The precision of knowledge of the angles was therefore an important consideration.

The polar angle of the counter in the target chamber could be set to an accuracy of ±0.1° [Groce, 1963]. It was controlled by a dial (36° per turn) attached to the lucite cover of the target chamber. Since the target chamber rotates with the spectrometer, the angle that a particular dial reading indicates also changes with the position of the spectrometer. Originally the dial was so adjusted that it read 90°, when the counter was actually 90° with respect to the beam and the spectrometer was set at 0°. The precision in measuring the polar angle of the counter in the target chamber, therefore depends on how well the lucite cover can be reproducibly set to the correct position. The following method provides a check to this question.

For an elastic-scattering process such as $D + {}^3He \rightarrow d + {}^3He$, there exists a unique pair of angles on the scattering plane given by

$$\Theta_c = \pm \tan^{-1} \frac{M_{{}^3He} - M_d}{2M_d} ,$$

where both the deuteron and ^3He can be detected in coincidence with each other. Unless the spectrometer has been set at Θ_c, the angles that the counter in the target chamber should be set to detect deuteron in coincidence with ^3He in spectrometer and vice versa are different. By measuring this difference, the absolute angle of either of the counters can be calculated. Since Θ_c and the difference as a function of the spectrometer angles shown in Figure 17 are independent of the energies, this calibration requires only a measurement of the difference in angles.

To begin with, the spectrometer with $\delta\Theta = 0.2°$, $\delta\Phi = 4°$ and $\delta E/E = 1.11\%$ was fixed at 37.75° according its reading. The NMR magnetometer frequency was respectively set to detect ^{3}He's and deuterons from the elastic-scattering process. Figure 17 also shows the number of coincidences versus the dial readings, corresponding to different angles of the counter in the target chamber. Because the spectrometer was so closely set to Θ_c, the ^{3}He- and deuteron-coincidences almost peaked at the same position. The small difference in the positions of centroids was calculated to be 2.4 ± 0.5 units of the dial reading (0.24 ± 0.05°). The actual angle of the spectrometer was then found to be 37.62 ± 0.04°, and a dial reading of 300 would imply that the counter in the target chamber was set at 38.11 ± 0.08°.

When the spectrometer was changed to 30° for the coincidence measurements of the reaction D(^{3}He, p), the same reading of 300 became an angle of 45.73 ± 0.09°, which would be otherwise taken as 45° if the lucite cover of the target chamber was assumed to be set at the correct position.

4. Coincidence measurements.

The protons produced in the reaction D(^{3}He, p) were detected by the magnetic spectrometer at 30°. To separate the α-particles that may be present from the protons, a 0.25-mm thick aluminum sheet was put in front of the counter. The other charged particles from the reaction, namely protons, tritons and ^{3}He's, were detected in the target chamber by a surface-barrier counter. This counter could be set on the plane determined by the beam direction and the center of the spectrometer entrance

slits within ± 0.5 mm [Groce, 1963]. The angular apertures were 2° and 8° respectively along the polar and azimuthal direction. As discussed in a previous section, the counter in the target chamber had to be set at quite forward angles to permit coincidence counts. The Rutherford scattering from both the target and the backing then contribute most of the counting rate, and a fast-slow coincidence system [cf., Figure 18] was used to reduce the randoms. As in the coincidence measurements for the $^{7}Li(p,\alpha)$ reaction, the pulses from the counter in the target chamber were delayed by 80 ns before going into the fast-coincidence circuit to take account of the proton transit time in the vacuum box of the spectrometer. The fast-coincidence output gives the enable pulses to open the linear gate for those pulses directly from the linear amplifier for the counter in the target chamber (1.5 μs delayed). The outputs from the linear gate were then put into a multi-channel analyzer which again was promptly gated by the stretched fast-coincidence outputs. The delays and the fast-coincidence resolving time (110 ns) were checked by a coincidence measurement of the elastic scattering $D(^{3}He,d)^{3}He$ at the beginning of each running day.

In all the coincidence runs, the resolutions of the magnetic spectrometer were set at $\delta\Theta = 1°$, $\delta\Phi = 4°$ and $\delta E/E = 1.11\%$. By changing the detected proton energy with the counter in the target chamber fixed at - 20°, one has the coincidence spectra for the energy-correlation shown in Figure 19. Fixing the proton energy at 7.8 MeV instead, those obtained for the angular correlation are shown in Figure 20.

The p-H correlation for the reaction $D + {}^{3}He \rightarrow p + H + {}^{3}H$ can be converted to a $p - {}^{3}H$ correlation, since the proton and

triton are emitted oppositely in the center-of-mass of the recoil ^{4}He system. By using the formula to be described in the next part, the p - ^{3}H and p - ^{3}He correlations shown in Figure 21 were normalized and converted to the recoil center-of-mass system. The randoms were subtracted in the same manner as described in Section A6.

If the final-state interaction of pair (3 + 5), i.e., the pair (p + H) or (p + N), was strong, its effect should show, depending on the energy of proton detected by the spectrometer, in the p-^{3}H or p-^{3}He angular correlation around $\Theta_{LAB} = 30°$ ($\Theta_{RCM} = -70°$) where the excitation energy of the two-nucleon system was smaller. No enhancement, however, was seen at these positions.

When the angular correlations in the recoil center-of-mass system at $E_p = 7.8$ MeV were analyzed by a least-square fit to an even order of Legendre polynomials, the p-^{3}H to p-^{3}He branching ratio was found to be 7.86 ± 0.69. The other interesting feature about the correlations is that they all appear to have an axis of symmetry along the ^{4}He recoil direction. As will be discussed in Section D, Part IV, it is possible to use this symmetric property to show that the mechanism representing the stripping of incident ^{3}He is the dominant process of the reaction.

III. KINEMATICS AND DATA REDUCTION

A. Three-body Kinematics.

If T_{fi} is the transition matrix element for a process from a certain initial state i to a certain final state f, then by the famous golden rule the transition rate is given by

$$\text{Prob./Sec.} = \frac{2\pi}{\hbar} |T_{fi}|^2 \frac{dN}{dE},$$

where dN/dE is the density of final states per unit energy interval. It is expressed as

$$\frac{dN}{dE} = \frac{d\vec{P}_1}{(2\pi\hbar)^3} \cdot \frac{d\vec{P}_2}{(2\pi\hbar)^3} \cdots \frac{d\vec{P}_{n-1}}{(2\pi\hbar)^3} \quad \frac{1}{dE}$$

for an n-particle final state. A more symmetrical form can be obtained [Feynman, 1962], if one adds a factor of

$$\frac{d\vec{P}_n}{(2\pi\hbar)^3} (2\pi\hbar)^3 \delta(\vec{\pi} - \sum_{j=1}^{n} \vec{P}_j)$$

and replaces $1/dE$ by $\delta(\epsilon - \sum_{j=1}^{n} E_j)$, where $\vec{\pi}$ and ϵ are the total momentum and energy available for the transition. Defined by the experimental resolutions, the transition leads only to a finite part of the phase space region $\Delta\tau$. Let the corresponding transition rate be denoted by Δw_{if}, then

$$\Delta w_{if} = \frac{2\pi}{\hbar} \int_{\Delta\tau} |T_{fi}|^2 (2\pi\hbar)^3 \delta(\vec{\pi} - \sum_{j=1}^{n} \vec{P}_j) \delta(\epsilon - \sum_{j=1}^{n} E_j) \prod_{m=1}^{n} \frac{d\vec{P}_m}{(2\pi\hbar)^3}$$

If the initial continuum-state wave function is normalized to one particle per unit volume, the flux is numerically equal to the relative velocity of the two particles in the initial state, and the differential cross section is just $\Delta\sigma = \Delta w_{if}/\text{flux}$.

For a reaction leading to a three-particle final state, the integration can be carried out easily. Let the particles involved be labelled as $1 + 2 \rightarrow 3 + 4 + 5$, where "1" is the bombarding particle, "2" represents the target and "3" is taken to be the particle detected in the magnetic spectrometer. The differential cross section for the three-body reaction is now given as

$$\Delta\sigma = \frac{2\pi}{\hbar v_{12}} \frac{1}{(2\pi\hbar)^6} \int_{\Delta\tau} |T_{fi}|^2 \delta(\vec{P}_1 + \vec{P}_2 - \vec{P}_3 - \vec{P}_4 - \vec{P}_5) \delta\left(\frac{P_1^2}{2m_1} + \frac{P_2^2}{2m_2} + Q - \frac{P_3^2}{2m_3} - \frac{P_4^2}{2m_4} - \frac{P_5^2}{2m_5}\right) d\vec{P}_3 d\vec{P}_4 d\vec{P}_5 . \tag{1}$$

In this expression, non-relativistic energy, i.e., $E_i = P_i^2/2m_i + m_i c^2$, is used. v_{12} is the relative velocity of the particles 1 and 2, and $Q = (m_1 + m_2 - m_3 - m_4 - m_5)c^2$ is the Q-value for the reaction. After having integrated over $\vec{P}_5$ and P_4, the expression (1) becomes

$$\Delta\sigma = \frac{2\pi m_{12}}{\hbar q_{12}} \frac{1}{(2\pi\hbar)^6} \Delta E_3 \, \Delta\Omega_3 \, \Delta\Omega_4 \, m_3 \, P_3 \left|T_{fi}\right|^2 \frac{P_4^2}{\left|\frac{P_4}{m_{45}} - \frac{\hat{P}_4}{m_5} \cdot (\vec{\pi}_{12} - \vec{P}_3)\right|} , \tag{2a}$$

with $$\frac{\pi_{12}^2}{2(m_1+m_2)} + \frac{q_{12}^2}{2m_{12}} + Q - \frac{P_3^2}{2m_3} - \frac{P_4^2}{2m_4} - \frac{(\vec{\pi}_{12} - \vec{P}_3 - \vec{P}_4)^2}{2m_5} = 0 \qquad (2b)$$

to represent the conservation of energy. Here ΔE_j and $\Delta\Omega_j$ are respectively the energy and angle resolutions of the detector that particle j enters, and $\hat{P}_4$ is the unit vector in the direction of $\vec{P}_4$. The total and relative momenta of the particles i and j, $\vec{\pi}_{ij}$ and $\vec{q}_{ij}$, are

$$\vec{\pi}_{ij} = \vec{P}_i + \vec{P}_j, \quad \vec{q}_{ij} = \frac{m_i \cdot m_j}{m_i+m_j}\left(\frac{\vec{P}_i}{m_i} - \frac{\vec{P}_j}{m_j}\right) \equiv m_{ij}\vec{v}_{ij}.$$

In the study of final-state interactions, the relative momenta $\vec{q}_3$ and $\vec{q}_{45}$ are found more convenient to be used. The vector $\vec{q}_i$, defined as

$$\vec{q}_i = \frac{m_i(m_j+m_k)}{m_i+m_j+m_k}\left(\frac{\vec{P}_i}{m_i} - \frac{\vec{P}_j+\vec{P}_k}{m_j+m_k}\right),$$

where i, j and k are in cyclic order of (3, 4, 5), is the relative momentum of particle i with respect to the recoil pair of particles (j + k). In terms of these momenta, the expressions corresponding to (2a) and (2b) are written as

$$\Delta\sigma = \frac{2\pi m_{12}}{\hbar q_{12}} \frac{1}{(2\pi\hbar)^6} \Delta E_3 \, \Delta\Omega_3 \, \Delta\Omega_{45} \, m_3 \, P_3 \, |T_{fi}|^2 \, m_{45} \, q_{45}, \qquad (3a)$$

and $$\frac{q_{12}^2}{2m_{12}} + Q - \frac{q_{45}^2}{2m_{45}} - \frac{m_3+m_4+m_5}{2m_3(m_4+m_5)} q_3^2 = 0, \qquad (3b)$$

where $\Delta\Omega_{45}$ is the angular resolution $\Delta\Omega_4$ seen in the recoil center-of-mass system of particles 4 and 5. The ratio $\Delta\Omega_4/\Delta\Omega_{45}$ is obtained by equating the expressions (2a) and (3a), and is given by

$$\frac{\Delta\Omega_4}{\Delta\Omega_{45}} = \frac{q_{45}}{P_4^2} \left| P_4 - \frac{m_{45}}{m_5} \hat{P}_4 \cdot (\vec{\pi}_{12} - \vec{P}_3) \right|. \tag{4}$$

This is just the result that one would obtain in transforming an elementary solid angle from one system to another, the vector $(\vec{\pi}_{12} - \vec{P}_3)/(m_4 + m_5)$ is the relative velocity of the two systems. In the laboratory system, the target is at rest, thus $\vec{P}_2 = 0$, $\vec{\pi}_{12} = \vec{P}_1$ and $\vec{q}_{12}/m_{12} = \vec{P}_1/m_1$.

If only the single spectrum of particle 3 is measured, such as in the measurements of α-particle energy spectra discussed in Section A5, Part II, the differential cross section has to be integrated over all the directions that particle 4 may be emitted. That is

$$\Delta\sigma = \frac{2\pi}{\hbar} \frac{m_{12}}{q_{12}} \frac{1}{(2\pi\hbar)^6} m_3 P_3 m_{45} q_{45} \Delta E_3 \Delta\Omega_3 \int |T_{fi}|^2 \, d\Omega_{45}. \tag{5}$$

In the coincidence measurements, $\hat{P}_4$ is also fixed. The relative energies for all pairs of particles in the final state, depending on the squares of the relative momenta,

$$\vec{q}_{45} = - \frac{m_4 \vec{\pi}_{12}}{m_3 + m_4 + m_5} + \frac{m_4 \vec{q}_3}{m_4 + m_5} + P_4 \hat{P}_4, \tag{6a}$$

$$\vec{q}_{34} = m_{34} \left[\frac{m_3 + m_4 + m_5}{m_3 (m_4 + m_5)} \vec{q}_3 - \frac{\vec{q}_{45}}{m_4} \right], \tag{6b}$$

and $$\vec{q}_{35} = m_{35}\left[\frac{m_3+m_4+m_5}{m_3(m_4+m_5)}\,\vec{q}_3 - \frac{\vec{q}_{45}}{m_5}\right] \qquad (6c)$$

are known. As is seen from the expression (3b), q_{45} is fixed by q_3 and is independent of where the particle 4 is detected. But both $\vec{q}_{34}$ and $\vec{q}_{35}$ depend linearly on $\vec{q}_{45}$, and each of them obtains the same value on a cone determined by an axis of revolution $\hat{q}_3$ and the angle between $\hat{q}_3$ and $\hat{q}_{45}$.

For a specific example, the velocity vector diagram of the reaction $p + {}^7Li \rightarrow \alpha + {}^3H + p$ at $E_p = 9.1$ MeV is shown in Figure 22. A 4.1-MeV α-particle was detected at 30° with respect to the beam axis, while the recoil system of $(p + {}^3H)$ was moving with the same speed in the opposite direction in the center-of-mass system. This recoil direction was indicated by $\hat{q}_3$. The proton and triton, i.e., the particles 4 and 5, were emitted oppositely in their center-of-mass system along the direction $\hat{q}_{45}$. As long as the protons were detected on the cone determined by $\hat{q}_3$ and $\hat{q}_{45}$, the relative velocities v_{34} and v_{35}, thus the relative energies of the corresponding pairs (3 + 4) and (3 + 5), remained the same. In the discussions of Section A7, Part II, the protons and the α-particles were found to be very strongly correlated when the protons were detected at 26° with respect to the recoil axis $\hat{q}_3$. Because the relative energy of the pair $(\alpha + {}^3H)$ was equal to 1.96 MeV, the enhancement in the angular correlation was attributed to the final-state interaction of the pair through the 4.63-MeV excited state of ^7Li.

B. Normalization.

In this work, there are two major types of experimental

data. Those presented in Figures 7, 9 and 15b are the energy spectra. The data which were expressed in terms of the particle-particle correlations belong to the second type, and are shown in Figures 12, 14 and 21. The normalizations made in reducing the data are explained in this section.

The yield of the magnetic spectrometer is expressed in terms of the spectrometer resolutions and the differential cross sections $d^2\sigma/dE_3 d\Omega_3$ by

$$Y_{spe} = \left(\frac{d^2\sigma}{dE_3 d\Omega_3} + \frac{d^2\sigma_c}{dE_3 d\Omega_3} \frac{\Delta N_c}{\Delta N_t} \right) \Delta N_t \Delta N_B \Delta E_3 \Delta\Omega_3 , \qquad (7)$$

where ΔN_t and ΔN_c are the numbers of the target nuclei and the contaminating nuclei per unit area. ΔN_B is the total number of beam particles that have struck the target.

For the reaction $^7Li(p,\alpha)$, either $d^2\sigma_c/dE_3 d\Omega_3$ or $\Delta N_c/\Delta N_t$ was small, so that the second term in the expression (7) was neglected as compared with the first term. With the $^7Li(p,\alpha_0)$ yield Y_{mon} monitored at 145° during the same run, Y_{spe} was then converted to differential cross section in a unit of mb/sr-MeV as

$$\frac{d^2\sigma}{dE_3 d\Omega_3} = 2.643 \times \frac{90}{E_3} \times \frac{Y_{spe}}{Y_{mon}} \times 0.86 \text{ mb/sr-MeV},$$

where the first constant is the ratio of solid angle of the monitor counter to that of the spectrometer, and $\Delta E_3 = E_3/90$ is the energy resolution of the spectrometer. The last constant is the $^7Li(p,\alpha_0)$ differential cross section at 145°. From the measurements of the

target thickness and the $^{7}Li(p,\alpha_0)$ angular distribution described in Sections A3 and A4, Part II, it was found to be 0.86 ± 0.09 mb/sr.

The coincidence yield, with the randoms subtracted, is related to the third order differential cross section derived from the expression (2a) by

$$Y_{coin} = \frac{d^3\sigma}{dE_3\, d\Omega_3\, d\Omega_4}\ \Delta N_B\, \Delta N_t\, \Delta E_3\, \Delta\Omega_3\, \Delta\Omega_4 . \qquad (8)$$

The number of gates from the spectrometer, given also by Y_{spe} in the expression (7), was a measure of the flux x density, i.e., $\Delta N_B \times \Delta N_t$. For the coincidence measurements on the reaction $^{7}Li(p,\alpha)$, the coincidence counts were normalized to 1000 gates of the α-particles, and are plotted out versus the laboratory angles in Figures 12 and 14.

The complications in the reaction $D(^{3}He,p)$, due to the possibilities of the carbon and oxygen deposition and the deterioration in chemical compositions of the deuterated dotriacontane during the run, have been discussed in Section B1, Part II. A direct measurement of $\Delta N_B \times \Delta N_t$ was made by using a third counter to monitor the $D(^{3}He,d)^{3}He$ elastic scattering yield at 60° in the last day of this experiment. Since most of the coincidence spectra were obtained without this counter, the number of gates was used to normalize the corresponding coincidence spectrum. The number of protons counted by the spectrometer normalized to 10^4 of those deuterons from the third counter, plotted in Figure 15b, was used to account for the energy-dependent factor of the expression (7). Denoting this factor by $N(E_3)$, the relative yield versus the recoil

center-of-mass angles given in Figure 21 is expressed in terms of the various yields as

$$\text{Relative yield} = 0.0796 \times \frac{90}{E_3} \times N(E_3) \times \frac{Y_{coin}}{Y_{spe}} \times \frac{\Delta\Omega_4}{\Delta\Omega_{45}}$$

$$= \text{const.} \times \frac{d^3\sigma}{dE_3\, d\Omega_3\, d\Omega_{45}} \ ,$$

where the first constant was chosen such that the product of the first three factors is unity for the coincidence spectra taken at $E_3 = 7.8$ MeV. The ratio $\Delta\Omega_4/\Delta\Omega_{45}$, given by the expression (4), transforms the differential cross section from the laboratory system to the recoil center-of-mass system. The recoil ^{4}He direction, i.e., $\hat{\pi}_{45}$, was used as an axis of reference.

IV. THEORETICAL INTERPRETATION

The discussions carried on in Part II and Part III relate the experimental data to some appropriate differential cross sections. Besides the kinematic factors, these differential cross sections contain the squared modulus of some transition matrix elements. In this part some assumptions will be made to construct an approximate form for the transition matrix element T_{fi}. The object is to see if the data could be understood in terms of these assumptions. Some parameters concerning the properties of the final-state interactions will be discussed.

A. Interaction in the Final State of a Reaction.

The interaction between particles produced as a result of a certain reaction may have a sizable effect on their distributions in energy and in angle. This effect becomes particularly noticeable when the reaction proceeds into a phase space region where the relative velocity of the interacting pair of particles is small. In case of a three-body reaction, this part of the phase space region is usually reached by detecting the particle 3 near its maximum possible energy.

Approximate treatments of final-state interactions are found in the works by Migdal (1955), Watson (1952), Goldberger (1964) and Gillespie (1964). Here only the basic idea of the so-called factored-wave-function method or the Watson-Migdal approximation will be discussed.

By virtue of the short range nuclear interaction, the particles in the final state of a reaction are created in the vicinity

of one another, and would escape from there in forms of plane waves, if there were no final-state interactions acting among themselves. Because of these interactions, the wave function of the relative motion of a certain pair of particles may be distorted. This distortion, in some sense, is a measure of the final-state interaction between that particular pair of particles. It becomes conspicuous especially when the relative velocity of the pair is small, and the other particle, from energy conservation [cf., expression (3b), Part III], can escape with a larger relative velocity without distorting the wave function of the relative motion of the pair.

Under these assumptions, the transition rate of the reaction is proportional to the probability that the pair of particles are formed at their range of nuclear interaction, i.e., at $r \approx a$ apart [Fermi, 1951; Landau, 1965]. As was stated by Landau, this is just the squared modulus of the wave function of the particles formed when they are in the "reaction zone" multiplied by the size of the phase space region into which the reaction proceeds. The statement can be also visualized by considering the inverse reaction [Watson, 1952]. The probability, that the two final-state-interacting particles be found in the vicinity of each other such that the subsequent transition may occur, is proportional to the squared modulus of the wave function of the pair at $r \approx a$.

The actual form of the wave function at $r \approx a$ is not known, but just for the purpose of estimating the dependence of the wave function on the energy of the relative motion, it is sufficient to

continue inward the wave function from the region $r > a$ to $r \approx a$. As is always implied in the application of the zero-effective-range approximation to the low-energy scattering problems, this is permissible when the energy of the relative motion is small. At low energies, the Schroedinger equation in the region $r \lesssim a$ is essentially energy independent, so the dependence of the wave function on energy in this region is entirely determined by matching its value and derivative to the solution in the external region.

Since the pair of particles is created in a state of continuous spectrum moving in a definite direction, the boundary conditions for the wave function should be chosen in such a way that it contains incoming waves and a plane wave in the asymptotic region. The plane wave is replaced by a coulomb wave with only incoming waves in the asymptotic region, if there is also coulomb interaction acting between the pair of particles. This type of solution has been used by Lane and Thomas (1958) in their treatment of a three-body disintegration in terms of two successive two-body disintegrations. Since only the final-state interactions at low energies are of interest, one may disregard the contributions due to the spin-orbit interaction and the possibility of rearrangement scattering. The wave function in the external region was taken as

$$\Psi_c = \frac{1}{k_c r} \sum_{\ell m} (O_{c\ell} - U_{ccs\ell}{}^{*} I_{c\ell}) x_{c\ell} Y_\ell{}^{m*}(\hat{k}_c) Y_\ell{}^{m}(\hat{r}) \qquad (1)$$

for a particular channel c. Here $O_{c\ell}$ and $I_{c\ell}$ are respectively the outgoing and incoming wave solutions. The complex conjugate of the scattering matrix element $U_{ccs\ell}$ was taken, since the state described by the expression (1) is just the time-reversal state of

the ordinary scattering state. Because of the boundary conditions just described, all of the outgoing waves should be coulomb waves of the form [Messiah, 1962]

$$\Psi_c' = \Gamma(1-i\eta_c)e^{-\frac{\pi}{2}\eta_c} e^{i\vec{k}_c\cdot\vec{r}} F(i\eta_c, 1, -i(k_c r + \vec{k}_c\cdot\vec{r})), \qquad (2)$$

where F is the confluent hypergeometric function, and $\eta_c = z_1 z_2 e^2/\hbar v$ is the coulomb parameter. Comparing the expression (1) with the spherical harmonics expansion of the expression (2), the coefficients $x_{c\ell}$'s are found to be

$$x_{c\ell} = 2\pi i^{\ell-1} e^{-i\sigma_{c0}}$$

where $\sigma_{c\ell} = \arg\Gamma(\ell + 1 + i\eta_c)$ is the ℓ-th wave coulomb phase shift. If there is no nuclear interaction, i.e., $U_{ccs\ell} = \exp[2i(\sigma_{c\ell} - \sigma_{c0})]$, Ψ_c is reduced identically to Ψ_c'. The factor

$$|\Psi_c'(0)|^2 = \frac{2\pi\eta_c}{e^{2\pi\eta_c} - 1}$$

is known as the coulomb correction (non-relativistically) in many atomic and nuclear problems such as the photoelectric effect and β-decay where the electron produced in the final state is interacting with the residual nucleus by the coulomb force between them.

If one writes Ψ_c as

$$\Psi_c = \Psi_c' + \frac{1}{k_c r} \sum_{\ell m} [e^{-2i(\sigma_{c\ell} - \sigma_{c0})} - U_{ccs\ell}^{*}] I_{c\ell}{}^{x}{}_{c\ell} Y_{\ell}^{m^{*}}(\hat{k}_c) Y_{\ell}^{m}(\hat{r}) \tag{3}$$

and evaluates it at $r \approx a$, one finds that the main contributions come from those terms containing $1/r$. Since the square bracket in expression (3) is just the partial-wave elastic-scattering amplitude, the transition rate can be also approximated as something proportional to the scattering cross section of the interacting pair of particles [Watson, 1952; Migdal, 1955].

The approximations discussed so far amount to a factorization of the wave function of the relative motion from a complicated three-body transition matrix element. The possibility of this factorization can also be rediscovered in making some model calculation based on some reaction mechanisms. To the first order of the plane-wave Born approximation, it is found that the transition matrix element, for each channel in the final state, can usually be put in a form as

$$T_{fi} = \int \psi^{*}(\vec{r}, \vec{k})\, v(\vec{r})\, \phi(r, \vec{p})\, e^{i\vec{q} \cdot \vec{r}}\, d\vec{r}, \tag{4}$$

where $\psi(\vec{r}, \vec{k})$ is the wave function of the relative motion of the pair of particles interacting in the final state and $\hbar\vec{k}$ is their relative momentum. $v(\vec{r})$ is the interaction acting between them and the vector $\hbar\vec{q}$ is the momentum transfer to the relative motion of the pair. $\phi(r, \vec{p})$, depending parametrically on other momentum transfers denoted by $\vec{p}$, is some bound function left over after the integrations over all degrees of freedom other than $\vec{r}$ have been

carried out. The expression (4) can be evaluated by assuming a certain form for $v(\vec{r})$, by solving for $\psi(\vec{r}, \vec{k})$ from the Schroedinger equation and carrying out the integration numerically. Alternatively the integral was simplified by following the idea first used by Werntz (1962). Analyzing $\psi(\vec{r}, \vec{k})$ into partial waves, the expression (4) becomes

$$T_{fi} = \frac{1}{k} \sum_{\ell m} x_\ell^* Y_\ell^m(\hat{k}) \int \frac{f_\ell^*(kr)}{r} v(\vec{r}) \phi(r, \vec{p}) Y_\ell^{m*}(\hat{r}) e^{i\vec{q}\cdot\vec{r}} d\vec{r},$$

where the radial wave function $f_\ell(kr)$ is equal to $(O_\ell - U_{s\ell}^* I_\ell)$ for $r > a$. If only central force is assumed, the angular part of the integration can be made readily. That is

$$T_{fi} = \frac{1}{k} \sum_{\ell} i^\ell (2\ell+1) x_\ell^* P_\ell(q \cdot k) \int_0^\infty f_\ell^*(kr) v(r) \phi(r, \vec{p}) j_\ell(qr) r\, dr,$$

where $P_\ell(x)$ is the Legendre polynomial of x of order ℓ. Because $v(r)$ is significant only for $r < a$ and in this region the shape of $f_\ell(kr)$ is almost energy independent when k is sufficiently small, T_{fi} is approximated by

$$T_{fi} = \text{const.} \times \frac{1}{ka} \sum_{\ell} (2\ell+1)[I_\ell(ka) - U_{s\ell} O_\ell(ka)] J_\ell P_\ell(\hat{q} \cdot \hat{k}), \quad (5a)$$

where

$$J_\ell = \int_0^\infty \phi(r, \vec{p})\, v(r)\, j_\ell(qr) r\, dr. \quad (5b)$$

The radial wave function is factored out; each partial-wave amplitude, however, is modified by a factor J_ℓ. A cut-off radius can be introduced in the evaluation of the integral (5b); this has the effect of simulating the distorted waves [Yu and Meyerhof, 1966].

As is noticed from the expression (5a), $\vec{q}$ gives an axis of symmetry in the angular correlation. Since a particular reaction mechanism is characterized by the momentum transfers $\vec{q}$ and $\vec{p}$, an angular correlation, on the other hand, may indicate information about $\vec{q}$ and J_ℓ and tell which one of the reaction mechanisms is more favorable in describing the reaction.

B. Resonance Parameters of the First Excited State of ^{4}He.

Since none of the interacting pairs of particles was measured in the α-particle energy spectrum of the reaction ^{7}Li(p, α), one has to integrate $|T_{fi}|^2$ over all directions of $\hat{k}$. From the expressions (5a) and (5b), each partial wave is added up incoherently as

$$\int |T_{fi}|^2 \, d\hat{k} = \text{const.} \times \sum_\ell (2\ell+1) |J_\ell|^2 \, \frac{1}{ka} \, \rho_{s\ell}(ka), \qquad (6)$$

where $$\rho_{s\ell}(ka) = \frac{1}{ka} \, |I_\ell(ka) - U_{s\ell} O_\ell(ka)|^2 \qquad (7)$$

is usually referred as the generalized density-of-states function [Phillips et al., 1960]. To include the effect of the n + ^{3}He channel, a real scattering matrix amplitude $D_{s\ell}$ was introduced. In terms of this and the phase shifts, the scattering matrix element $U_{s\ell}$ and thus the expression (7) can be evaluated. As discussed in Appendix A, the scattering matrix element was parametrized

in the R-matrix theory by the resonance parameters (a, $E_R, \gamma_p^2, \gamma_n^2$).

The total phase shift $\delta_{s\ell}$ for the partial wave (s, ℓ) is the sum of the coulomb phase shift $\omega_\ell = \sigma_\ell - \sigma_0$, the hard-sphere phase shift

$$\phi_\ell = -\tan^{-1} \frac{F_\ell(ka)}{G_\ell(ka)}$$

and the nuclear phase shift $\beta_{s\ell}$. F_ℓ and G_ℓ are respectively the regular and irregular real coulomb functions. The final form for the expression (7) is given by

$$\rho_{s\ell}(ka) = [D_{s\ell}^2 + 1 - 2 D_{s\ell} \cos(2\beta_{s\ell})]/P_\ell(ka),$$

where $P_\ell(ka) = ka/(F_\ell^2 + G_\ell^2)$ is the penetration function. For a one-channel problem $D_{s\ell}$ reduces to unity and $\rho_{s\ell}(ka)$ becomes

$$\rho_{s\ell}(ka) = \frac{4 \sin^2 \beta_{s\ell}}{P_\ell(ka)} .$$

The generalized density-of-states function, expressed in this form, was used before by Barker and Treacy (1962) in analyzing the deuteron energy spectra from the reaction $^9Be(p, d)^8Be^*$. By assuming the contributions from the $\ell = 0$ and $\ell = 2$ states of ^8Be only, $|J_0|^2$ and $|J_2|^2$ appearing in the expression (6) were left as the free parameters adjusted to fit the experimental energy spectra.

Returning to the reaction $^7Li(p, \alpha)^4He^*$, the α-particle energy spectra shown in Figure 9 indicated a strong p + ^3H final-state interaction near the higher-energy ends of the spectra. Since a ^1S

resonance due to the p + ^{3}H interaction was established from many other sources of experimental data [cf., Part I], it was interesting to see how this resonance affects the α-particle energy spectra based on the expression (6). By restricting to the ^{1}S partial wave only, the resonance parameters derived from a least-square fit may be used to compare with existing knowledge about the low-energy p + ^{3}H interaction deduced from other experiments.

Let the experimental differential cross section at $\Theta_a = \Theta_i$ and $E_a = E_j$ be σ_{ij}, while the corresponding value predicted by the assumed transition matrix element be $\bar{\sigma}_{ij}$. By adding together the contributions from the p + ^{3}H and the n + ^{3}He channels, σ_{ij} can be written as

$$\bar{\sigma}_{ij} = f(\Theta_i) E_j^{\frac{1}{2}} \left[\frac{D_{s\ell}^2 + 1 - 2D_{s\ell}\cos(2\beta_{ps\ell})}{P_{p\ell}(k_p a)} + \frac{D_{s\ell}^2 + 1 - 2D_{s\ell}\cos(2\beta_{ns\ell})}{P_{n\ell}(k_n a)} \right], \tag{8}$$

where $|J_0|^2$ and the other energy independent factors are absorbed into $f(\Theta_i)$. Letters p and n are used to distinguish the p + ^{3}H from the n + ^{3}He channel. The factor $1/k$ in the expression (6) is canceled by an identical one in the phase-space factor given by expression (5), Part III.

Since the experimental differential cross section differs from the actual number of counts N_{ij} only by a normalization constant, the root-mean-square error of σ_{ij} was assigned as

$$\Delta\sigma_{ij} = \frac{\sigma_{ij}}{N_{if}^{\frac{1}{2}}} .$$

The fitting procedure involves a search for the minimum of the expression

$$\chi^2 = \sum_{i=1}^{M} \sum_{j=1}^{N_i} \left(\frac{\sigma_{ij} - \bar{\sigma}_{ij}}{\Delta\sigma_{ij}} \right)^2 , \qquad (9)$$

where M is the number of energy spectra, and N_i is the number of data points in each spectrum at $\Theta_a = \Theta_i$. Table I lists all the spectra included for the least-square fit. As was mentioned before, for higher excitation energies in the p + ^{3}H system, the contributions of the higher partial waves may become important, and at the same time the final-state interactions between other pairs of particles will begin to mask the effect of the p + ^{3}H final-state interaction. Expression (8) therefore is not expected to be valid for higher excitation energies. All the spectra shown in Figure 9 start with a rapid rise just above the p + ^{3}H threshold, reach a maximum at 20.06 MeV, and then decrease slowly to a minimum near the n + ^{3}He threshold. Since this is a general feature, a cut-off energy of 20.30 MeV was taken in the χ^2 evaluations.

With this cut-off energy, the number of data points included in the fit reduces to $\sum_{i=1}^{M} N_i = 229$ in a total of 26 spectra. It is possible to apply the principle of the maximum likelihood to determine all of the 30 parameters, i.e., 26 $f(\Theta_i)$'s plus four ^{1}S

resonance parameters, by the least-square fit. The resonance parameters (a, E_R, γ_p^2, γ_n^2) are expressed in Appendix A in a Breit-Wigner form through $D_{s\ell}$ and $\beta_{s\ell}$.

Table II lists the sets of resonance parameters given in literature with the χ_{min}^2 resulted from the least-square fit. These sets of resonance parameters differ from each other over a very wide range. Unfortunately the existing p + ^{3}H scattering phase shifts are not accurate enough to pin down those ambiguities. Judging from the χ_{min}^2, the α-particle energy spectra obtained in this work give, however, some preference over several sets of the resonance parameters.

The reported range of the p + ^{3}H interaction ranges from 3.0 F to 4.2 F. It was fixed in each search for the least square. The other three resonance parameters (E_R, γ_p^2, γ_n^2) were found by an iteration method discussed in Appendix B. The results obtained with a = 3.0 F and a = 4.0 F are summarized as the following:

a (F)	E_R (MeV)	γ_p^2 (MeV)	γ_n^2 (MeV)
3.0	20.35 ± 0.01	5.53 ± 0.24	2.88 ± 0.21
4.0	20.45 ± 0.02	3.38 ± 0.09	2.23 ± 0.10

where based on the Chi-square distribution [cf., Appendix B], the errors were assigned. The sensitivity of those resonance parameters to the χ^2 is shown in Figure 23, and the p + ^{3}H scattering phase shifts and the differential cross section for the reaction ^{7}Li(p, α) calculated from those resonance parameters are respectively shown in Figures 24 and 25. The curves in Figure 9 are the differential cross sections calculated with the first set (a = 3.0 F) of the parameters.

The fits at $E_x = 20.06$ MeV for all the spectra are quite satisfactory, the data points corresponding to this excitation energy are taken, without assuming any background contribution, as the angular distribution of the α-particle group leading to the first excited state of ^{4}He. The result is shown in Figures 5 and 26.

C. Triton-transfer Reaction Mechanisms in the Reaction ^{7}Li(p, α).

Nothing about how the reaction ends up with a three-body final state was asked in the previous discussions. It was assumed that the particles are produced in the vicinity of one another, and one of them escapes from the recoil pair of particles with high relative velocity. The distortion to the wave function of the relative motion of the recoil pair was due to their final-state interaction only. With these assumptions, a transition matrix element was constructed. From the least-square fit of the calculated differential cross sections to the experimental ones, an angular distribution was taken without assuming any backgrounds. Further justification can be obtained, if the angular distribution itself may be predicted from some model calculation. As is shown in Figure 26, the angular distribution has a forward peak and suggests the possibility of a pick-up process. In this section, various attempts to understand this prominent feature will be discussed.

For calculating the transition matrix element in the plane wave Born approximation, the wave functions in the initial and final state were written respectively as

$$\Psi_i = \phi_4(\vec{r}_1 - \vec{R}_1)\phi_{34}[\tfrac{1}{4}(\vec{r}_1 + 3\vec{R}_1) - \vec{R}_2] \times e^{i\vec{k}_p \cdot [\vec{r}_2 - \frac{1}{7}(\vec{r}_1 + 3\vec{R}_1 + 3\vec{R}_2)]}, \tag{10}$$

and

$$\Psi_f = \chi_4(\vec{r}_1 - \vec{R}_1)\chi_4'(\vec{r}_2 - \vec{R}_2)e^{i\vec{k}_a \cdot [\frac{1}{4}(\vec{r}_1 + 3\vec{R}_1) - \frac{1}{4}(\vec{r}_2 + 3\vec{R}_2)]} + \chi_4(\vec{r}_2 - \vec{R}_2)\chi_4'(\vec{r}_1 - \vec{R}_1)e^{i\vec{k}_a \cdot [\frac{1}{4}(\vec{r}_2 + 3\vec{R}_2) - \frac{1}{4}(\vec{r}_1 + 3\vec{R}_1)]}, \tag{11}$$

where the wave function ϕ_4 describes the relative motion of a p + ^{3}H two-particle subsystem in the ^{7}Li nucleus, and ϕ_{34} describes that of the other triton with respect to the center-of-mass of the two-particle subsystem. χ_4 and χ_4' are respectively the internal wave functions of the detected α-particle and the recoil ^{4}He system. The vector $\vec{r}_i$ ($\vec{R}_j$) designates the position of the i-th proton (j-th triton), and $\hbar\vec{k}_p$ ($\hbar\vec{k}_a$) is the initial-state proton (final-state α-particle) momentum in the center-of-mass system. The second term in the expression (11) was obtained from the first term by exchanging the protons and tritons simultaneously, and was included because the experiment is not able to tell which proton or triton is present in the detected α-particle.

If the unbound pair interactions in the final state are neglected [Banerjee, 1960], the interaction responsible for the triton-transfer reaction contains only $V_{pt}(\vec{r}_2 - \vec{R}_2)$. The transition matrix element is

$$T_{fi} = (\Psi_f, V_{pt}\Psi_i) \equiv T_{di} + T_{ex}.$$

Here T_{fi} is split into a direct and an exchange term, and they are given by the integrals

$$T_{di} = \int d\vec{r}\, \chi_4^*(\vec{r})\phi_4(\vec{r}) \int d\vec{r}_{pt}\, \chi_4'^*(\vec{r}_{pt})\, V_{pt}(\vec{r}_{pt}) d^{\,i\vec{q}_p \cdot \vec{r}_{pt}}$$

$$\times \int d\vec{r}_{at} \phi_{34}(\vec{r}_{at}) e^{-i\vec{q}_a \cdot \vec{r}_{at}}, \tag{12a}$$

and

$$T_{ex} = \int d\vec{r}\, \chi_4'^*(\vec{r})\phi_4(\vec{r}) \int d\vec{r}_{pt} \chi_4^*(\vec{r}_{pt})\, V_{pt}(\vec{r}_{pt}) e^{i\vec{q}_p' \cdot \vec{r}_{pt}}$$

$$\times \int d\vec{r}_{at} \phi_{34}(\vec{r}_{at}) e^{-i\vec{q}_a' \cdot \vec{r}_{at}}. \tag{12b}$$

Here the new set of integration variables are defined as $\vec{r} = \vec{r}_1 - \vec{R}_1$, $\vec{r}_{pt} = \vec{r}_2 - \vec{R}_2$ and $\vec{r}_{at} = \frac{1}{4}(\vec{r}_1 + 3\vec{R}_1) - \vec{R}_2$, and the momentum transfers $\hbar\vec{q}_p$ and $\hbar\vec{q}_a$ are given as

$$\vec{q}_p = \vec{k}_p + \frac{1}{4}\vec{k}_a \qquad \text{and} \qquad \vec{q}_a = \frac{4}{7}\vec{k}_p + \vec{k}_a. \tag{13}$$

The corresponding vectors $\vec{q}_p'$ and $\vec{q}_a'$ in the expression for T_{ex} are obtained from $\vec{q}_p$ and $\vec{q}_a$ with $\vec{k}_a$ replaced by $-\vec{k}_a$.

When the recoil ^{4}He system is in its ground state, i.e., $\chi_4' = \chi_4$, the overlap integral

$$\int \chi_4'^*(\vec{r})\phi_4(\vec{r})\, d\vec{r} \tag{14}$$

appears in both T_{di} and T_{ex}, and can be taken out as a common factor. The $\vec{r}_{pt}$-integration may be simplified, if a zero-range $p + {}^3H$ interaction is assumed. That is by setting

$$\chi_4(\vec{r}_{pt})\, V_{pt}(\vec{r}_{pt}) = W_0\, \delta(\vec{r}_{pt}) \tag{15}$$

in the integral [Tobocman, 1961]. This approximation was used by Maxson (1962) in analyzing the angular distribution of the ground-state α-particle group from the same reaction but at some what higher energies, 15.0 MeV and 18.6 MeV. The ^{7}Li nucleus $(3/2^-)$ was regarded as a two-particle system consisting of an α-particle (0^+) and a triton $(1/2^+)$ coupled with orbital angular momentum $\ell = 1$. The wave function corresponding to this model can be written as

$$\phi_{34}(\vec{x}) = \sum_{\nu m} (\tfrac{1}{2}|\nu m|\tfrac{3}{2} M_i) Y_1^m(\hat{x})\, U_{34}(x) \tag{16}$$

where M_i is the spin projection of the initial-state ^{7}Li nucleus. The transition probability, after averaging and summing over the initial- and final-state spin projections, becomes

$$\overline{|T_{fi}|^2} = \text{const. x } [\omega^2(q_a) + \omega^2(q_a') + 2\omega(q_a)\omega(q_a')\cos\Theta], \tag{17}$$

where $\cos\Theta = \hat{q}_a \cdot \hat{q}_a'$, and

$$\omega(q) = \int_0^\infty x^2\, U_{34}(x) j_1(qx) dx.$$

Introducing a cut-off radius R_c and applying the Butler theory of surface reaction, $\omega(q)$ is approximated as [Banerjee, 1960]

$$\omega(q) = \frac{R_c U_{34}(R_c)}{q^2 - \frac{2M_{34}E_{34}}{\hbar^2}} [qR_c j_0(qR_c) - (2 + \Lambda) j_1(qR_c)]. \qquad (18)$$

Here M_{34} and E_{34} are the reduced mass and the relative energy of the α-particle and triton in the ^{7}Li nucleus, and $\Lambda = R_c [d \ell n\, U_{34}(r)/dr]_{r = R_c}$ is the logarithmic derivative of U_{34} at R_c. Estimating Λ from the known binding energy and substituting $\omega(q)$ into expression (17), the calculated angular distribution for ^{7}Li(p, α_0) is shown in Figure 6. As was noticed by Maxson, the angular distribution is very sensitive to the choice of R_c and the best value of R_c for the fit is found to be energy dependent. At 9.1-MeV bombarding energy, a cut-off of 5.3 F gives a better agreement with the angular distribution, but it does not reproduce the slow decrease in differential cross section for the smaller angles.

As the recoil ^{4}He system is in its excited state, χ_4' becomes orthogonal to χ_4, since they belong to two different eigenstates of the same Hamiltonian. Thus if one takes α + ^{3}H model of the ^{7}Li nucleus seriously and assumes that ϕ_4 is identical to χ_4, i.e., the free α-particle state, the overlapping integral (14) is vanishingly small. This means that only the direct term T_{di} needs to be considered. With the same approximations, the angular distribution of ^{7}Li(p, α_1) was calculated. It starts with almost a constant value at forward directions and peaks up at backward angles. Since the direct term given by expression (12a) implies

that the incident proton knocks out an α-particle and forms an excited state of ^{4}He with the triton, this process occurs predominantly in the backward directions.

In the second attempt, the zero-range approximation implied by the expression (15) was dropped. The ground state and the first excited state of ^{4}He (0^+) was considered as in a ^{1}S state of the two-particle system consisting of a proton and a triton. The interaction V_{pt} was replaced by the operator $(\frac{\hbar^2}{2M_{pt}}\Delta + E_{pt})$ in the $\vec{r}_{pt}$-integration. The radial integral can also be simplified by using the same method with which the expression (18) was derived, as

$$\int_0^\infty U_4(r)\,V_{pt}(r)j_0(pr)r^2dr \approx (-\frac{\hbar^2}{2M_{pt}}p^2 + E_{pt})\int_{r_c}^\infty U_4(r)j_0(pr)r^2dr$$

$$= -\frac{\hbar^2}{2M_{pt}}\,r_c\,U_4(r_c)[pr_c\cos(pr_c) - (1+\lambda)j_0(pr_c)].$$

Here U_4 is the radial wave function of the ^{4}He system either in its ground state or its first excited state, and λ again is the logarithmic derivative of U_4 at a cut-off radius of r_c. The logarithmic derivative was determined by the binding energy for the ground state, while, for the first excited state, it was evaluated by the asymptotic expression (1) incorporated with the phase shift (at $E_x = 20.06$ MeV) obtained in Section B. A peak in forward angles of the angular distributions of both ^{7}Li(p, α_0) and ^{7}Li(p, α_1) can be generated, but for the latter it was too small and too broad in comparison with the data [cf., Figure 26].

It was therefore thought that the exchange term should be taken into consideration in order to reproduce the shape and magnitude of this forward peak. It is possible that the p + ^{3}H two-particle subsystem in ^{7}Li may have a definite probability of being excited to the first excited state of ^{4}He. For convenience in computing the relative amplitude of the direct and exchange processes, the wave functions involved in the overlap integral (14) were assumed as

$$\phi_4(\vec{r}) = \left(\frac{2\beta^2}{\pi}\right)^{3/4} e^{-\beta^2 r^2} \qquad \chi_4(\vec{r}) = \left(\frac{2\gamma^2}{\pi}\right)^{3/4} e^{-\gamma^2 r^2}$$

and $$\chi_4'(\vec{r}) = \frac{1}{4\pi}\,\frac{1}{kr}\, x_0\, f_0(kr).$$

Here $f_0(kr)$ is the radial wave function of the first excited state of ^{4}He, and for $r > a$, it becomes the ^{1}S component of the expression (1) in Section A. The inverse-square decay length β^2 of the p + ^{3}H subsystem in ^{7}Li is not known, and is arbitrarily taken as that of a free α-particle, i.e., $\gamma^2 = 0.21\,F^{-2}$. The wave function $U_{34}(r)$ in expression (16) was chosen as a Gaussian type given by

$$U_{34}(r) = 2\pi^{1/2} \left(\frac{2\alpha^2}{\pi}\right)^{3/4} e^{-\alpha^2 r^2}$$

where $\alpha = 0.28\,F^{-1}$ is chosen to fit the reduced width of the ground state of ^{7}Li [Tombrello and Parker, 1963]. Since $f_0(kr)$ is unknown for $r \lesssim a$, the integral involving χ_4' cannot be carried out analytically. They were approximated [cf., expressions (5a) and (5b), Section A] as

$$\int \chi_4'^*(\vec{r})\phi_4(\vec{r})d\vec{r} = \frac{1}{4\pi k}\left(\frac{2\beta^2}{\pi}\right)^{3/4} x_0^* \int \frac{1}{r} f_0^*(kr)e^{-\beta^2 r^2} dr$$

$$\approx \frac{x_0^*}{4\pi k}\left(\frac{2\beta^2}{\pi}\right)^{3/4} f_0^*(ka)\frac{2\pi}{\beta^2}$$

and

$$\int \chi_4'^*(\vec{r})\, V_{pt}(\vec{r})e^{i\vec{p}\cdot\vec{r}}d\vec{r} = -\left(\frac{\hbar^2}{2M_{pt}} p^2 + E_{pt}\right)\int \chi_4'^*(\vec{r})e^{i\vec{p}\cdot\vec{r}}d\vec{r}$$

$$\approx -\left(\frac{\hbar^2}{2M_{pt}} p^2 + E_{pt}\right)\frac{x_0^*}{2\pi k} f_0^*(ka)\frac{4\pi}{p^2}$$

The factor $f_0^*(ka) = I_0(ka) - U_{00}O_0(ka)$ appears in both T_{di} and T_{ex}, and it can be factored out in the total transition matrix element. The differential cross section therefore contains also the same generalized density-of-states function as the expression (6) does. As in the previous approximation, a cut-off radius of 5.2 F was needed for the integral

$$\int_0^\infty U_{34}(r)r^2 j_\ell(qr)dr \approx \int_{R_c}^\infty U_{34}(r)\, r^2 j_\ell(qr)dr$$

and the Simpson's rules were then used in obtaining the integral in the right hand side. Figure 26 shows the results of this calculation.

A satisfactory fit, with those simple calculations, to the experimental data seems to be not very likely. It however does indicate qualitatively that the angular distributions of both $^7Li(p, a_0)$

and $^{7}Li(p, \alpha_1)$ may be understood in terms of the triton-transfer mechanisms. The assumptions made in Section B for deducing the resonance parameters are plausible.

D. A Modified Born Approximation Calculation for the Reaction $D(^{3}He, p)$.

The angular correlations from the reaction $D(^{3}He, p)$ were obtained at the proton energies chosen such that the excitation energies of the $p + {}^{3}H$ system lay between 20.66 MeV to 22.06 MeV. As was mentioned in Part I, the P-wave interactions are important in this energy range [Meyerhof, 1965; Yu and Meyerhof, 1966]. The observed anisotropy in the angular correlations provides additional evidence about this. The modified Born approximation calculation, to be discussed in this section, was made to estimate the relative amplitude of producing the $p + {}^{3}H$ and $n + {}^{3}He$ final-state interacting pairs in S-wave and P-wave states. In terms of the usual analysis of the particle-particle angular correlation, this is equivalent to an estimation of the density matrix of the "intermediate ^{4}He" formed during the reaction.

In Yu and Meyerhof's analyses of the proton energy spectra from the reaction $D(^{3}He, p)$ and the neutron energy spectra from its mirror reaction $^{3}H(d, n)$, the following reaction mechanisms were considered:

A (D) ^{3}He picks up a neutron from the target deuteron and forms a $p + {}^{3}H$ $(n + {}^{3}He)$ interacting pair.

B (E) ^{3}He strips its deuteron to the target deuteron to form a $p + {}^{3}H$ $(n + {}^{3}He)$ interacting pair.

C (F) ^{3}He breaks up giving one of its neutron (proton) to the deuteron, the ^{3}H (^{3}He) formed then interacts with the other proton (neutron) from the breakup.

G ^{3}He interacts with the neutron from the direct breakup of the target deuteron.

In a phase space region where the nucleon + nucleon final-state interaction is of less importance than those of p + ^{3}H and n + ^{3}He, the deviation of the final-state wave function from pure plane waves can be attributed to the effects of the p + ^{3}H and n + ^{3}He final-state interactions only. By using the method described in Section A and the Wigner type of the nucleon-nucleon potential, Yu and Meyerhof have given the transition matrix element for any of those mechanisms. as

$$M_i = n_i I_i e^{-k_i^2/4A_i^2} \sum_{\ell} (2\ell + 1) N_\ell(p'') J_{\ell,i} P_\ell(\hat{p}_i \cdot \hat{p}'').$$

Here i stands for each of the mechanisms listed above, and $\hat{p}_i$ and $\hat{p}''$ are respectively the unit vectors of the momentum transfer to the relative motion and of the relative momentum of the final-state interacting pair. Other quantities appearing in this expression will be redefined in the following discussions. The angle Θ_i between $\vec{p}_i$ and the beam axis will determine an axis of symmetry in the angular correlation, if the reaction goes predominantly by the mechanism i. For the present experiment with $E_p = 7.8$ MeV and $\Theta_p = 30°$, Θ_i is calculated as

Process i	Θ_i (deg.)
A(D)	16.3
B(E)	-16.8
C(F)	- 4.0
G	-41.0

The observed angular correlations have an axis of symmetry along the ^{4}He recoil direction, which was found also to be lying at -16.8° with respect to the beam. The mechanism B(E), representing the ^{3}He stripping of its deuteron, is therefore assumed to be the dominant process in the analysis.

If one labels the nucleons in the target deuteron by 1 and 2, and those in the incident ^{3}He by 3, 4 and 5, the initial- and final-state wave functions can be written as

$$\Psi_i = \phi(\vec{r}_1, \vec{r}_2)\psi(\vec{r}_3, \vec{r}_4, \vec{r}_5)e^{i\vec{k}_\tau \cdot [\frac{1}{3}(\vec{r}_3 + \vec{r}_4 + \vec{r}_5) - \frac{1}{2}(\vec{r}_1 + \vec{r}_2)]},$$

and

$$\Psi_f = \psi(\vec{r}_1, \vec{r}_2, \vec{r}_3)\chi(4)\chi_4'[\vec{r}_4 - \tfrac{1}{3}(\vec{r}_1 + \vec{r}_2 + \vec{r}_3)]\chi(5)$$

$$\times\ e^{i\vec{k}_p \cdot [\vec{r}_5 - \frac{1}{3}(\vec{r}_1 + \vec{r}_2 + \vec{r}_3 + \vec{r}_4)]},$$

where $\hbar\vec{k}_\tau$ ($\hbar\vec{k}_p$) is the initial-state ^{3}He (final-state proton) momentum in the center-of-mass system. χ_4', as was defined in Section C, describes the relative motion of the final-state interacting pair of a nucleon and a mass three nucleus. χ, ϕ, and ψ respectively are the fully antisymmetrized internal wave functions of mass one, mass two and mass three nucleus. They are assumed to be separable in

space and spin-isospin variables, and are given by

(1) One-nucleon system

$$\chi(1) = \rho_1^{m_1} \eta_1^{\mu_1}$$

where ρ, η are the spin and isospin matrices.

(2) Two-nucleon system $^3S_1$ state

$$\phi(\vec{r}_1, \vec{r}_2) = D^{M_d, 0}(1,2) \left(\frac{2a^2}{\pi}\right)^{3/4} e^{-a^2|\vec{r}_1 - \vec{r}_2|^2}$$

with

$$D^{M_d, 0}(1,2) = \sum_{m_1 m_2} \sum_{\mu_1 \mu_2} (\tfrac{1}{2}\tfrac{1}{2} m_1 m_2 | 1 M_d)(\tfrac{1}{2}\tfrac{1}{2}\mu_1\mu_2|00)$$

$$\times \rho_1^{m_1} \rho_2^{m_2} \eta_1^{\mu_1} \eta_2^{\mu_2}.$$

(3) Three-nucleon system in $^2S_{\frac{1}{2}}$ state [Schiff, 1964]

$$\psi(\vec{r}_1, \vec{r}_2, \vec{r}_3) = R^{n\nu}(1,2,3)(\sqrt{3}/\pi)^{3/2}\gamma^3$$

$$\times e^{-\gamma^2[\frac{3}{4}|\vec{r}_1 - \vec{r}_2|^2 + |\vec{r}_3 - \frac{1}{2}(\vec{r}_1 + \vec{r}_2)|^2]},$$

and

$$R^{n\nu}(1,2,3) = \frac{1}{\sqrt{6}} \sum_{m_1 m_2} \sum_{\mu_1 \mu_2} (\tfrac{1}{2}\tfrac{1}{2} m_1 m_2 | 00)(\tfrac{1}{2}\tfrac{1}{2}\mu_1\mu_2|00)$$

$$\times \{\rho_1^{m_1} \rho_2^{m_2} \rho_3^{n} (\eta_1^{\mu_1} \eta_2^{\nu} + \eta_1^{\nu} \eta_2^{\mu_1}) \eta_3^{\mu_2} - (\rho_1^{m_1} \rho_2^{n} + \rho_1^{n} \rho_2^{m_1})$$

$$\times \rho_3^{m_2} \eta_1^{\mu_1} \eta_2^{\mu_2} \eta_3^{\mu_3}\}.$$

In accordance with Yu and Meyerhof, the inverse decay lengths of the bound wave functions were taken as $\alpha = 0.167\,F^{-1}$ and $\gamma = 0.36\,F^{-1}$ respectively for the two-nucleon and three-nucleon systems. The interactions responsible for the stripping of ^3He are $V = V_{13} + V_{14} + V_{23} + V_{24}$, where V_{ij} was generalized to include the spin and isospin dependences as a scalar type with Gaussian shape given by

$$V_{ij} = -V_0 e^{-\beta^2|\vec{r}_i - \vec{r}_j|^2} (W + BP_{ij}^{\sigma} - MP_{ij}^{\sigma}P_{ij}^{\tau} - HP_{ij}^{\tau}), \tag{19}$$

with $\beta = 0.63\,F^{-1}$. The exchange operator $P_{ij}^{\sigma}(P_{ij}^{\tau})$ acts on the spin (isospin) variables of the nucleons i and j. The two sets of constants W, B, M and H used are [Preston, 1962]

type	W	B	M	H
Rosenfeld	-0.13	0.46	0.93	-0.26
Serber	0.5	0	0.5	0

Because both Ψ_i and Ψ_f are antisymmetric under the exchange of nucleons 1 and 2, V_{1j} and V_{2j} have the identical matrix elements. The transition matrix element for the process B(E) is then reduced to

$$T_{fi} = 2(\Psi_f, (V_{13} + V_{14})\Psi_i).$$

By expressing the spin wave functions of the final-state interacting pair in its channel spin representation, i.e.,

$$R^{\bar{n}\bar{\nu}}(1,2,3)\rho_4{}^{\bar{m}_4} = \sum_{SM} (\tfrac{1}{2}\tfrac{1}{2}\bar{n}\bar{m}_4|SM)\, S_{SM}{}^{\bar{\nu}}(1,2,3;4),$$

T_{fi} was separated into a space integral and a spin-isospin overlap as

$$T_{fi} = \text{const.} \times \sum_{SM} (\tfrac{1}{2}\tfrac{1}{2}\bar{n}\bar{m}_4|SM) \sum_{j=3,4} I_j(S,\bar{\mu}_4\bar{\nu}) \langle S_{SM}{}^{\bar{\nu}}(1,2,3;4)\eta_4{}^{\bar{\mu}_4}\rho_5{}^{\bar{m}_5}\eta_5{}^{\bar{\mu}_5}, \\ O_{1j} D^{M_d,0}(1,2) R^{n\nu}(3,4,5)\rangle \,. \tag{20}$$

A bar was put on the final-state spin or isospin projection to distinguish the corresponding quantity in the initial state. The operator O_{1j} is an abbreviation for the sum of operators with i = 1 in the parentheses of the expression (19). Its matrix element $^{2S+1}\langle O_{1j}\rangle$ and the space integral I_j, for j = 3 or 4, are calculated in Appendix C. After averaging over the initial spin projections M_d and n, and summing over the final state spin projections $\bar{n}$, $\bar{m}_4$ and $\bar{m}_5$, the squared modulus of T_{fi} becomes

$$\overline{|T_{fi}|^2} = \text{const.} \times \sum_S \text{Tr} \left(\sum_{i=3,4} I_i(S,\bar{\mu}_4\bar{\nu})^{2S+1}\langle O_{1j}\rangle \right)\left(\sum_{j=3,4} I_j(S,\bar{\mu}_4\bar{\nu})^{2S+1}\langle O_{1j}\rangle \right)^{\dagger}$$

The cross sign indicates that both the transpose and complex conjugate of the matrix were taken. In terms of the abbreviations defined as

$$^{2S+1}A = (W+M-\tfrac{1}{2}B-\tfrac{1}{2}H)I_3(S,\bar{\mu}_4\bar{\nu}) + (W-\tfrac{1}{2}H)I_4(S,\bar{\mu}_4\bar{\nu}),$$

$$^{2S+1}B = +I_4(S,\bar{\mu}_4\bar{\nu})B,$$

and $^{2S+1}C = -I_4(S, \bar{\mu}_4 \bar{\nu})M.$

The final form for $\overline{|T_{fi}|^2}$ is given as the following:

(1) For $D + {}^3He \rightarrow p + {}^3He + n$, i.e., $\bar{\mu}_4 = -\frac{1}{2}$ and $\bar{\nu} = +\frac{1}{2}$

$$|T_{fi}|^2 = K\left[\tfrac{1}{12}|{}^1A|^2 + \tfrac{1}{48}|{}^1B|^2 - \tfrac{1}{12}\,\mathrm{Re}\,{}^1A\,{}^1B^* + \tfrac{1}{4}|{}^3A|^2 + \tfrac{11}{48}|{}^3B|^2 + \tfrac{1}{3}|{}^3C|^2 + \mathrm{Re}\left(\tfrac{5}{12}\,{}^3A\,{}^3B^* + \tfrac{1}{2}\,{}^3B\,{}^3C + \tfrac{1}{3}\,{}^3C\,{}^3A^*\right)\right]. \tag{21}$$

(2) For $D + {}^3He \rightarrow p + {}^3H + p$, i.e., $\bar{\mu}_4 = +\frac{1}{2}$ and $\bar{\nu} = +\frac{1}{2}$

$$|T_{fi}|^2 = K\left[\tfrac{1}{12}|{}^1A|^2 + \tfrac{1}{48}|{}^1B|^2 - \tfrac{1}{12}\,\mathrm{Re}\,{}^1A\,{}^1B^* + \tfrac{1}{4}|{}^3A|^2 + \tfrac{11}{48}|{}^3B|^2 + \tfrac{5}{12}\,\mathrm{Re}\,{}^3A\,{}^3B^*\right]. \tag{22}$$

K here is just a numerical constant independent of which one of the branches the reaction leads to.

As is indicated in Appendix C, the $p + {}^3H$ and $n + {}^3He$ final-state interactions are taken into account in terms of the scattering matrix amplitude $D_{s\ell}$ and the respective phase shifts $\delta_{ps\ell}$ and $\delta_{ns\ell}$ by the factored-wave-function method discussed in Section A. For the ^4He excitation energies $20.662 \leq E_x \leq 22.055$ MeV, $D_{s\ell}$, $\delta_{ps\ell}$ and $\delta_{ns\ell}$ given by Bransden et al. (1956) and by Meyerhof and McElearney (1965) are listed in Table III. Using an a = 3.0 F and

a cut-off radius R_c = 5.0 F [Yu and Meyerhof, 1966], the angular correlations calculated for E_p = 7.8 MeV with Rosenfeld type nucleon-nucleon potential were compared with the experimental correlations in Figure 27 by a least-square fit. The dashed curves represent the calculations from all the phase shifts and scattering matrix amplitudes given by Meyerhof and McElearney; while the solid curves are the same calculations except the triplet S-wave n + ^{3}He phase shift was changed to the value of Bransden et al. For partial waves other than the triplet S-wave, the n + ^{3}He phase shifts from Meyerhof and from Bransden agree in signs. Although Bransden's values are smaller, the data are not able to indicate any definite preference between them. It is clear that the set of the n + ^{3}He phase shifts from Meyerhof et al. cannot reproduce the observed branching ratio and the forward-to-backward peak ratio in the p - ^{3}He correlations. In the phase-shift analysis of Meyerhof and McElearney, a discrepancy was found in predicting the energy dependence of the ratio B_{nn1}/B_{nn0}, where B_{nnL}/k_n^2 is the coefficient of $P_L(\cos\Theta_n)$ in the Legendre polynomials analysis of the n + ^{3}He elastic differential cross section. Θ_n and k_n are the direction and magnitude of the neutron wave vector in the center-of-mass system. This discrepancy was considered to be caused by an incorrect n + ^{3}He phase shift. The n + ^{3}He phase shifts of Bransden et al. from the resonating group calculations, whose T = 1 phase shifts were found to be in good agreement with the p + ^{3}He and n + ^{3}H elastic-scattering data [Tombrello, 1965 and 1966], were used in computing the curves shown in Figure 21.

The normalization constant obtained from the least-square fit to the p - ^{3}H and p - ^{3}He angular correlations at 7.8 MeV was used to generate those correlations taken at other proton energies. It was found [cf., Appendix C] that the cut-off radius R_c is not very sensitive to the quality of the fit, and I_4 is very much smaller than I_3 for R_c chosen to be somewhat greater than 2.0 F. This means that only I_3 contributes to the differential cross section, and the constants that describe the nucleon-nucleon potential appear effectively in $(W + M - \frac{1}{2}B - \frac{1}{2}H)^2$ as a constant of proportionality. Consequently, the present data are not able to tell the difference in choosing among the nucleon-nucleon potentials. The agreement of the calculation with the angular correlations becomes poor for lower proton energies, i.e., for higher ^{4}He excitation energies, this may be partially due to the inappropriate phase shifts and also due to the fact that the factored-wave-function method may become less efficient.

V. DISCUSSION OF RESULTS

Nuclear reactions with three outgoing particles are very complicated in comparison with the reactions where there are only two particles in both the initial and final states. Recently substantantial progress has been made in the study of three-body problems by Faddeev (1963) and Lovelace (1964). For each of the rearrangement scatterings, the transition matrix is solved by a system of inhomogeneous integral equations. The inhomogeneities and kernels of these Faddeev's equations are directly related to the two-body transition matrices. Besides its involved mathematical technique, the method is still too difficult for an actual application at the present stage. This is because the kernels also require the two-body transition matrix element off its energy-shell. More experimental data over wider ranges therefore are needed to obtain such information by analytic continuation.

The factored-wave-function method or the Watson-Migdal approximation (referred as WMA) used in the analyses of Part IV, is crude in the sense that it is just a very primitive approximation of the solution to the Faddeev's equations [Gillespie, 1964]. From the results obtained in this work, the approximation however appears to be better than expected. An explanation may be that for the phase space region of interest, the final-state interaction of one pair of particles dominates over that of the other pairs in the reaction.

All the α-particle energy spectra of the reaction ^{7}Li(p, α) at 9.1-MeV bombarding energy, and $2.5° \leq \Theta_{\alpha} \leq 120°$, showed an enhancement of the differential cross section over the phase-space

factor near the highest possible energies. The WMA was used to predict the spectral shape for the higher energy parts of these spectra. It turns out that these parts of the spectra can be sufficiently understood by assuming a resonance in the ^1S p + ^3H system. The ^1S phase shifts derived from a least-square fit are shown in Figure 24 to compare with those given in the literature. Both the open and dark circles with the error bars represent the solutions of a point-by-point phase shift analysis of the p + ^3H elastic scattering data by Kurepin et al. (1966). The triangles and the squares indicate some of the phase shifts obtained by Werntz (1964) and Meyerhof and McElearney (1965) respectively. In addition to the p + ^3H elastic scattering data due to Jarmie et al. (1963), the total cross section of the $^3H(p,n)$, $^3He(n,p)$ and $^3He(n,n)$ reactions [Seagrave et al., 1960] were also included in the latter analyses. From the discontinuity of the energy derivative of the p + ^3H elastic scattering differential cross section, Werntz was able to argue that the ^1S p + ^3H phase shift at the n + ^3He threshold energy should be equal to 108°. With the resonance parameters obtained in this work, the phase shift at this energy was found to be 104° for a = 3.0 F or 101° for a = 4.0 F. The agreement of the phase shifts with those obtained in this work from a rather indirect approach is gratifying.

As was explained in Section B, Part IV and in Appendix A, the phase shifts here were found parametrically through a set of resonance parameters (a, E_R, γ_p^2, γ_n^2). Although in the least-square fit, the χ^2 for a given range of nuclear interaction, a, appears to be quite sensitive to the rest of the resonance parameters

near the solutions [cf., Figure 23], there still is no definite assurance that the set of parameters (E_R, γ_p^2, γ_n^2) obtained for a given a is unique. The total cross sections by thermal neutrons (0.025 eV) on ^{3}He are calculated as the following:

a	E_R	γ_p^2	γ_n^2	Wigner limit	σ_{nn}(b)		σ_{np}(b)	
					calc.	expt.	calc.	expt.
3.0	20.35	5.53	2.88	9.2	1.90	1.80	12400	5280
4.0	20.45	3.38	2.23	5.2	2.70	1.80	15000	5280

Both sets of the resonance parameters predict approximately the magnitudes of the thermal cross sections given by Seagrave et al.

Besides the phase-space factor, the WMA [cf., Section B, Part IV] predicts an angle-independent α-particle energy spectrum. An additional justification for the use of this approximation was obtained by making a model calculation to predict relative yields in the α-particle energy spectra taken at various angles. As was shown in Section C, Part IV, the angular distribution of the α-particle group leading to the first excited state of the ^{4}He system can be qualitatively understood by a PWBA calculation of the triton-transfer reaction mechanisms. In order to explain the forward-peaking in the distribution, it was found that the exchange process has to be included in the calculation.

It may be recalled that a cut-off in the proton center-of-mass energy of 0.485 MeV (E_x = 20.30 MeV in ^{4}He system) was used during the search for the least square in the fit of the spectral shapes to the α-particle energy spectra. As the energy gets higher, two sources of complications come in. The first is that the contri-

butions due to the final-state interactions of the higher partial waves have to be included. The second depends on the type of particle 3 and its relative velocity with respect to any of the other particles in the final state of the reaction. As the excitation energy of the recoil pair becomes higher, one may reach a phase-space region in which particle 3 is interacting strongly with one of the other particles. The angular-correlation measurements from the reaction ^{7}Li(p, α) [cf., Section B6, Part II], indicate that the effects of the p + ^{3}H and n + ^{3}He final-state interactions are masked by the strong final-state interactions between the α + H, α + ^{3}H and possibly α + N pairs, when the ^{4}He excitation energy is changed from 20.01 MeV to 21.27 MeV. The α - ^{3}H plus α - H angular correlations at 20.01 MeV, incidentally, showed that only the p + ^{3}H final-state interaction is important at this energy, and gave an additional confirmation about the 0^{+} spin-parity assignment of the first excited state of the ^{4}He system. To reduce the effects due the second complication just described, the reaction D(^{3}He, p) [cf., Section C, Part II] was investigated. With 16.5-MeV ^{3}He bombarding energy, the angular-correlation measurements were carried out by detecting the protons at 30° and at 6.6 MeV ≤ E_{p} ≤ 8.6 MeV. The excitation energies between these protons and the mass-three particles are higher than that of the ^{4}He system recoiled. Their corresponding final-state interactions are expected to be weaker. Although the excitation energy of the p + H or p + N system may be, in very few occasions, small, the effects of the p + H or p + N final-state interactions were not seen in the angular correlations.

The p - ^{3}H, p - H and p - ^{3}He angular correlations have an axis of symmetry along the ^{4}He recoil direction. From this and the calculations made by Yu and Meyerhof, one was able to conclude that the reaction proceeds predominantly by the ^{3}He stripping mechanism [cf., Section D, Part IV]. Based on this mechanism, a modified Born approximation with a more generalized nucleon-nucleon potential was carried out. The modification was made to account for the p + ^{3}H and n + ^{3}He final-state interactions by the factored-wave-function method.

By using the scattering matrix amplitudes and the p + ^{3}H phase shifts reported by Meyerhof and McElearney to describe the corresponding final-state interaction, the calculation reproduces both the energy and angle dependences of the p - ^{3}H correlations. (Because the protons and tritons from the decays of the recoil ^{4}He systems were emitted oppositely in their center-of-mass system, the p - H correlations were converted into the p - ^{3}H correlations.) It was thought, therefore, that the assumptions regarding the ^{3}He stripping and the factored-wave-function method are plausible. The analyses were then carried over for the p - ^{3}He correlations. In order to predict the p - ^{3}H to p - ^{3}He branching ratio and the forward-to-backward-peak ratio in the p - ^{3}He angular correlation, it was shown that at least for the triplet S-wave the n + ^{3}He phase shifts due to Bransden et al. are preferred.

As was remarked also in Section D, Part IV, the agreement of the calculations with the angular correlations becomes

poor for lower proton energies (in particular for the p - ^{3}He correlations). Since the relative energy of the n + ^{3}He system is 0.764 MeV lower than that of the p + ^{3}H system, one would be rather reluctant to assume that the factored-wave-function is not valid. It was stated in Meyerhof and McElearney's analyses that the region of validity of the scattering-matrix amplitudes and the phase shifts they obtained does not extend to the region beyond approximately 21.3 MeV. The phase shifts due to Bransden et al. from the resonating-group calculations were derived without considering the inelasticity, and are expected to be invalid for higher relative energies. It is clear that one therefore needs to obtain a better set of the scattering-matrix amplitudes and the phase shifts in order to say whether the theory of the final-state interaction employed in this work is still applicable for the higher relative energies of the pair of particles interacting in the final state.

APPENDIX A. PARAMETRIZATION OF THE PHASE SHIFTS

For ^{4}He excitation energies well below the d + d threshold energy (23.841 MeV), there are p + ^{3}H and n + ^{3}He channels to be considered. The scattering matrix satisfying the symmetric and unitary condition can be written as a 2x2 matrix [Meyerhof and McElearney, 1965] for each partial wave of channel spin s and orbital angular momentum ℓ,

$$U_{s\ell} \equiv \begin{vmatrix} U_{pps\ell} & U_{pns\ell} \\ U_{nps\ell} & U_{nns\ell} \end{vmatrix} \tag{1}$$

$$= \begin{vmatrix} D_{s\ell} e^{2i\delta_{ps\ell}} & \pm i(1-D_{s\ell}^2)^{\frac{1}{2}} e^{i(\delta_{ps\ell}+\delta_{ns\ell})} \\ \pm i(1-D_{s\ell}^2)^{\frac{1}{2}} e^{i(\delta_{ps\ell}+\delta_{ns\ell})} & D_{s\ell} e^{2i\delta_{ns\ell}} \end{vmatrix}$$

where $\delta_{ps\ell}(\delta_{ns\ell})$ is the total phase shift of the p + ^{3}H (n + ^{3}He) system. The real quantity $D_{s\ell}$ is the scattering-matrix amplitude which couples the two channels together. If there is a resonance in the partial wave (s,ℓ), the phase shifts and the scattering-matrix amplitude can be parametrized by a set of resonance parameters in the Breit-Wigner forms. The d + d channel, belonging to a negative-energy channel, is eliminated by using the method due to Teichmann and Wigner [Lane and Thomas, 1958].

Following the notations and definitions of Lane and Thomas, the scattering matrix is connected to the nuclear parameters through the reduced R-matrix for $E_n > 0$ as the following:

$$U_{pp} = \frac{I_p[(1-R_{nn}L_n^{o})(1-R_{pp}L_p^{o*}) - R_{np}R_{pn}L_n^{o}L_p^{o*}]}{O_p[(1-R_{nn}L_n^{o})(1-R_{pp}L_p^{o}) - R_{np}R_{pn}L_n^{o}L_p^{o}]}, \qquad (2a)$$

$$U_{np} = 2iP_p \frac{\rho_n^{\frac{1}{2}} I_p}{\rho_p^{\frac{1}{2}} O_n} R_{np} / [(1-R_{nn}L_n^{o})(1-R_{pp}L_p^{o}) - R_{np}R_{pn}L_n^{o}L_p^{o}], \qquad (2b)$$

and similarly for U_{nn} and U_{pn} with the subscripts p and n interchanged. Various quantities here are defined as

a_c = the range of nuclear interaction

M_c = the reduced mass of the particle-pair in channel c

E_c = the energy of the relative motion of the pair

k_c = $(2M_c E_c/\hbar^2)^{\frac{1}{2}}$ is the relative wave number of the pair

ρ_c = $k_c a_c$

I_c = the incoming wave solution in channel c

O_c = the outgoing wave solution in channel c

S_c = the shift function

P_c = the penetration function

B_c = the boundary value in channel c

L_c^{o} = $S_c + iP_c - B_c$.

In general the reduced R-matrix elements are expressed in terms of the reduced-width amplitude $\gamma_{c\lambda}$ of the resonance labelled by λ as

$$R_{cc'} = \sum_{\lambda\lambda'} \gamma_{c\lambda}\gamma_{c'\lambda'}(A)_{\lambda\lambda'}, \tag{3}$$

where $$(A^{-1})_{\lambda\lambda'} = (E_\lambda - E_p)\delta_{\lambda\lambda'} - \sum_e \gamma_{e\lambda}\gamma_{e\lambda'}(S_e - B_e),$$

and E_p is chosen as a common energy reference. The channel index e runs through all the negative-energy channels.

For $E_n \leq 0$, i.e., $E_p = E_n + E_{th} \leq E_{th}$, where E_{th} is the threshold energy of the n + ^{3}He channel, the summation in expression (3) now has to include the n + ^{3}He channel, also. The corresponding scattering matrix and the reduced R-matrix, written as $\bar{U}$ and $\bar{R}$, are related to each other by

$$\bar{U}_{pp} = \frac{I_p}{O_p} \frac{(1-\bar{R}_{pp} L_p^{o*})}{(1-\bar{R}_{pp} L_p^{o})}, \tag{4}$$

and the other matrix elements $\bar{U}_{pn}$, $\bar{U}_{nn}$ and $\bar{U}_{np}$ are no longer of physical significance.

If a single level $\lambda = (s, \ell)$ is effective in determining the main feature of the scattering process in the energy range of interest, the reduced R-matrix elements are given by expression (3) as

$$R_{pp} = \frac{\gamma_{ps\ell}\gamma_{ps\ell}}{(E_{s\ell}-E_p) + \Delta_{ds\ell}} \tag{5a}$$

and

$$R_{np} = \frac{\gamma_{ns\ell}\gamma_{ps\ell}}{(E_{s\ell}-E_p) + \Delta_{ds\ell}} \tag{5b}$$

for $E_p > E_{th}$, and as

$$\bar{R}_{pp} = \frac{\gamma_{ps\ell}\gamma_{ps\ell}}{(E_{s\ell}-E_p) + \Delta_{ds\ell} + \Delta_{ns\ell}} \quad , \tag{6}$$

for $E_p \leq E_{th}$. R_{nn} and R_{pn} can be obtained in a similar way or directly from the expressions (5a) and (5b) by exchanging the subscripts p and n. The quantity $\Delta_{cs\ell} = -\gamma_{cs\ell}^2 (S_{c\ell}-B_{c\ell})$ is the level shift. Substituting (5a) and (5b) into (2a) and (2b), and (6) into (4), the scattering matrix elements become

$$U_{pps\ell} = \frac{\epsilon_{s\ell} - \frac{i}{2}(\Gamma_{ns\ell} - \Gamma_{ps\ell})}{\epsilon_{s\ell} - \frac{i}{2}(\Gamma_{ns\ell} + \Gamma_{ps\ell})} \, e^{2i(\omega_{p\ell} + \phi_{p\ell})}, \tag{7a}$$

$$U_{nps\ell} = \frac{\Gamma_{ns\ell}^{\frac{1}{2}}\Gamma_{ps\ell}^{\frac{1}{2}}}{\epsilon_{s\ell} - \frac{i}{2}(\Gamma_{ns\ell} + \Gamma_{ps\ell})} \, e^{i(\omega_{n\ell} + \omega_{p\ell} + \phi_{n\ell} + \phi_{p\ell})} \tag{7b}$$

and similar expressions for $U_{nns\ell}$ and $U_{pns\ell}$ for $E_p > E_{th}$, and

$$\bar{U}_{pps\ell} = \frac{\epsilon_{s\ell} + \frac{i}{2}\Gamma_{ps\ell}}{\epsilon_{s\ell} - \frac{i}{2}\Gamma_{ps\ell}} e^{2i(\omega_{p\ell} + \phi_{p\ell})}, \qquad (8)$$

for $E_p \leq E_{th}$. Here $\Gamma_{cs\ell} = 2\gamma_{cs\ell}^2 P_{c\ell}$ is the level width, and $\epsilon_{s\ell}$ is an abbreviation of the quantity $E_{s\ell} - E_p + \Delta_{ds\ell} + \Delta_{ns\ell} + \Delta_{ps\ell}$.

Finally, by comparing the expressions (7a), (7b) and (8) with the expression (1), the phase shifts and the scattering-matrix amplitude are given by

(1) $E_p > E_{th}$

$$\beta_{ps\ell} = \tan^{-1}\{\Gamma_{ps\ell}\epsilon_{s\ell}/[\epsilon_{s\ell}^2 + \tfrac{1}{4}(\Gamma_{ns\ell}^2 - \Gamma_{ps\ell}^2)]\}$$

$$\beta_{ns\ell} = \tan^{-1}\{\Gamma_{ns\ell}\epsilon_{s\ell}/[\epsilon_{s\ell}^2 - \tfrac{1}{4}(\Gamma_{ns\ell}^2 - \Gamma_{ps\ell}^2)]\}$$

and
$$D_{s\ell} = \left[1 - \frac{\Gamma_{ns\ell}\Gamma_{ps\ell}}{\epsilon_{s\ell}^2 + \tfrac{1}{4}(\Gamma_{ns\ell} + \Gamma_{ps\ell})^2}\right]^{\frac{1}{2}}$$

(2) $E_p \leq E_{th}$

$$\beta_{ps\ell} = \tan^{-1}(\Gamma_{ps\ell}/2\epsilon_{s\ell})$$

and $D_{s\ell} = 1.$

The total phase shift $\delta_{cs\ell}$ is the sum of the nuclear phase shift $\beta_{cs\ell}$, the coulomb phase shift $\omega_{c\ell}$ and the hard-sphere phase shift

$$\phi_{c\ell} = -\tan^{-1}(F_{c\ell}/G_{c\ell}).$$

The level shift $\Delta_{ds\ell}$ can be set to be very small across the resonance energy $E_{s\ell}$ by choosing $B_d = S_{d\ell}(E_{s\ell})$. The other boundary values $B_{p\ell}$ and $B_{n\ell}$ are fixed respectively by the conditions that $\delta_{ps\ell}(E_{s\ell}) = \pi/2$ and $\Delta_{ns\ell}(E_{s\ell}) = 0$. In actual calculations, the shift function (a_c = 3.0 F) for d + d channel varies by 13%, and that for p + ^{3}H channel varies by 240%, per MeV in the energy range of interest. Furthermore because the deuteron reduced width was estimated [Werntz and Meyerhof, 1968] to be about one half of the nucleon reduced width, $\Delta_{ds\ell}$ was set identical to zero in the calculations of the spectral shape for the α-particle energy spectra [cf., Section B, Part IV]. The expressions for the phase shifts and the scattering-matrix amplitude are then identical to those given in the work of Meyerhof and McElearney (1965).

Including the ^{1}S resonance of ^{4}He only, i.e., $\lambda = (s, \ell) = (0, 0)$, the nuclear phase shifts and the scattering matrix amplitude, β_{p00}, β_{n00} and D_{00}, calculated from an assumed set of (a, E_R, γ_p^2, γ_n^2) $\equiv$ (a, E_{00}, γ_{p00}^2, γ_{n00}^2) were used to evaluate the expression (8) in Section B, Part IV. The procedure for the least-square fit for a = 3.0 F or 4.0 F is explained in Appendix B.

APPENDIX B. A SEARCH FOR THE LEAST SQUARE BY ITERATIONS

In estimating a number of parameters $a = \{a_1, a_2, \cdots, a_s\}$ in a theory from $N \geq s$ measured quantities $x_1, x_2, \cdots, x_N$ by a least-square fit, a search is made for the minimum of the quantity

$$\chi^2 = \sum_{i=1}^{N} \left(\frac{x_i - \xi_i}{\sigma_i} \right)^2 , \tag{1}$$

where σ_i is the standard error in measuring x_i, and ξ_i, containing the set of parameters a, is the theoretically predicted expression for x_i. If $\bar{a} = \{\bar{a}_1, \bar{a}_2, \cdots, \bar{a}_s\}$ are the values of the parameters a of the maximum likelihood, then

$$\left(\frac{\partial \chi^2}{\partial a_m} \right)_{a=\bar{a}} \equiv F_m(\bar{a}) = 0, \tag{2}$$

with m running from 1 through s. The problem therefore is essentially to solve for a from this system of equations.

If all ξ_i's in the expression (1) are linear functions of a, the system of equations (2) becomes an inhomogeneous linear one, and can be solved readily by the standard matrix algebra [Mathews and Walker, 1964]. On the other hand, if ξ_i's depend on a in a complicated fashion and a linearization of the system of equations (2) becomes too involved, the iteration method [Janossy, 1965] to be described here sometimes proves to be very useful.

It starts with an approximate set of values a'. If a' are chosen to be reasonably close to $\bar{a}$, $F_m(\bar{a})$ can be expanded in a power series in $\bar{a} - a'$ around a'. One then obtains in this way an approximate relation between $\bar{a}$ and a' given by

$$F_m(a') = \sum_n \left(\frac{\partial F_m(a)}{\partial a_n} \right)_{a=a'} (a' - \bar{a})_n . \qquad (3)$$

$\bar{a}$ solved from this system of equations are still the approximate solutions, unless a' are very well chosen to start with. By substituting $\bar{a}$ for a' in equations (3), another solution of $\bar{a}$ can be obtained, and should be closer to the real solutions step by step in each iteration. The matrix containing $(\partial F_m(a)/\partial a_n)_{a=a'}$ is a symmetric s x s matrix. The χ^2 has to be evaluated at $(2s + 1) + \frac{1}{2} s(s - 1)$ points around a' in the s-dimensional parameter space in order to construct this matrix.

The parameters involved in deducing the low-energy properties of the p + ^{3}H system from the α-particle energy spectra [cf., Section B, Part IV] are $(E_R, \gamma_p^2, \gamma_n^2)$ and the $f(\Theta_i)$'s. The latter were found for each input of $(E_R, \gamma_p^2, \gamma_n^2)$ by minimizing the χ^2 separately for each spectrum. Since the ξ_i's are linear functions of the $f(\Theta_i)$'s, these were solved by the first method. The χ^2 was then considered as a function of $(E_R, \gamma_p^2, \gamma_n^2)$, and was minimized by successive iterations. Depending on the first approximate values, usually four or five iterations were sufficient to bring the parameters in the neighborhood of their optimum values. The final values of the parameters were varied around to check if χ^2 was really a minimum there.

The expected magnitude of χ^2_{min} from the expression (1) is equal to N - s, i.e., the number of the degrees of freedom. In the actual fitting χ^2_{min}, however, was found to be considerably larger than N - s. This may be due to the fact that the standard errors were underestimated and that the theoretical expression is not equally valid for all the data points. The χ^2 obtained by re-normalizing the σ_i^2, i.e., increased by a factor of $\chi^2_{min}/N - s$, should now follow the Chi-square distribution. From the tabulated values for the Chi-square distribution, it was found that the probability that $\chi^2/(N - s)$ exceeding unity is 50% for $N - s > 30$. If two of the parameters are fixed, the probability that $\chi^2/(N - s + 2)$ not exceeding unity is also 50%. The error in determining each of the parameters (E_R, γ_p^2, γ_n^2) was taken as the range of that parameter for which the χ^2 increases by two when the other two parameters were held at some values in the neighborhood of the optimum ones.

APPENDIX C. THE SPIN-ISOSPIN OVERLAPS AND THE SPACE INTEGRALS IN THE MODIFIED BORN APPROXIMATION CALCULATION FOR THE REACTION D(^{3}He, p)

The evaluations of the spin-isospin overlaps $^{2S+1}\langle O_{1j}\rangle$, defined in Section D, Part IV for j = 3 or 4, involve systematic bookkeeping of the Clebsch-Gordan coefficients and the Kronecker deltas. The latter resulted directly from the orthogonal properties of the spin and isospin matrices. Writing the operator explicitly, the matrix $\langle O_{1j}\rangle$ is given by

$$\langle O_{1j}\rangle = W\langle 1\rangle + B\langle P_{ij}{}^{\sigma}\rangle - M\langle P_{ij}{}^{\sigma}P_{ij}{}^{\tau}\rangle - H\langle P_{ij}{}^{\tau}\rangle. \qquad (1)$$

The operator $P_{1j}{}^{\sigma}(P_{1j}{}^{\tau})$ exchanges the spin (isospin) projections of the nucleons 1 and j in the initial-state wave function. Because of the symmetry property of the wave functions used for the two- and three-nucleon systems, it was found that $\langle O_{1j}\rangle$ can be expressed as some linear combination of the three matrices $\langle 1\rangle$, $\langle P_{14}{}^{\sigma}\rangle$ and $\langle P_{14}{}^{\sigma}P_{14}{}^{\tau}\rangle$. In terms of a 2x2 matrix, defined as

$$X_{a,b} = \sum_{\sigma} (\tfrac{1}{2}\tfrac{1}{2}\sigma a|1M_d)(\tfrac{1}{2}\tfrac{1}{2}\sigma b|SM)$$

where $M_d(M)$ is the spin projection of the initial-state deuteron (the final-state ^{4}He system), the matrix elements of $\langle 1\rangle$, $\langle P_{14}{}^{\sigma}\rangle$ and $\langle P_{14}{}^{\sigma}P_{14}{}^{\tau}\rangle$ are given by

$$\langle 1 \rangle = \frac{-1}{6\sqrt{2}} \delta_{\bar{m}_5, n} \delta_{S, 1} \delta_{M, M_d} - \frac{1}{6} (\tfrac{1}{2}\tfrac{1}{2}\bar{\mu}_4\bar{\nu}|00)[\delta_{\bar{m}_5, n}(X_{-n,-n} - X_{n,n}) + 2\delta_{m_5, -n} X_{-n,n}],$$

$$\langle P_{14}^{\sigma} \rangle = \frac{-1}{4\sqrt{2}} \delta_{\bar{m}_5, n} \delta_{S, 1} \delta_{M, M_d} - \frac{(-)^{S+1}}{12} (\tfrac{1}{2}\tfrac{1}{2}\bar{\mu}_4\bar{\nu}|00) \times [\delta_{\bar{m}_5, n}(X_{-n,-n} - X_{n,n}) + 2\delta_{\bar{m}_5, -n} X_{-n,n}]$$

and

$$\langle P_{14}^{\sigma} P_{14}^{\tau} \rangle = \frac{1}{6} \delta_{\bar{m}_5, n} [\frac{-1}{\sqrt{2}} \delta_{S, 1} \delta_{M, M_d} + (-)^{S+1} (\tfrac{1}{2}\tfrac{1}{2}\bar{\mu}_4\bar{\nu}|00) \times (X_{-n,-n} + X_{n,n})].$$

The index $n(\bar{m}_5)$ is the spin projection of the initial-state ^{3}He (final-state proton).

Depending on the channel spin S of the final-state interacting pair, i.e., of the final-state ^{4}He system, these matrices are the 6 x 2 (2S+1) matrices given as the following:

(1) For producing a singlet final-state interacting pair

$$\langle 1 \rangle = \mp \frac{1}{6\sqrt{2}} \begin{vmatrix} 0 & 0 \\ -\sqrt{2} & 0 \\ -1 & 0 \\ 0 & 1 \\ 0 & \sqrt{2} \\ 0 & 0 \end{vmatrix}, \quad \langle P_{14}^{\sigma} \rangle = \pm \frac{1}{12\sqrt{2}} \begin{vmatrix} 0 & 0 \\ -\sqrt{2} & 0 \\ -1 & 0 \\ 0 & 1 \\ 0 & \sqrt{2} \\ 0 & 0 \end{vmatrix}$$

and $\langle P_{14}{}^{\sigma} P_{14}{}^{\tau} \rangle = 0.$

(2) For producing a triplet final-state interacting pair

$$\langle 1 \rangle = \frac{-1}{6\sqrt{2}} U \mp \frac{1}{6\sqrt{2}} V, \quad \langle P_{14}{}^{\sigma} \rangle = \frac{-1}{4\sqrt{2}} U \mp \frac{1}{12\sqrt{2}} V$$

and $$\langle P_{14}{}^{\sigma} P_{14}{}^{\tau} \rangle = \frac{-1}{6\sqrt{2}} (1 \mp 1)U$$

where U is a 6x6 unity matrix, and V is a 6x6 matrix given by

$$V = \begin{vmatrix} -1 & 0 & 0 & 0 & 0 & 0 \\ 0 & 1 & -\sqrt{2} & 0 & 0 & 0 \\ 0 & -\sqrt{2} & 0 & 0 & 0 & 0 \\ 0 & 0 & 0 & 0 & -\sqrt{2} & 0 \\ 0 & 0 & 0 & -\sqrt{2} & 1 & 0 \\ 0 & 0 & 0 & 0 & 0 & -1 \end{vmatrix}$$

The upper (lower) sign in those expressions describes the reaction $^3He + D \rightarrow p + p + {}^3H$ ($p + n + {}^3He$).

The other matrices are simply

$$\langle P_{13}{}^{\sigma} \rangle = -\tfrac{1}{2}\langle 1 \rangle, \langle P_{13}{}^{\tau} \rangle = \tfrac{1}{2}\langle 1 \rangle, \langle P_{13}{}^{\sigma} P_{13}{}^{\tau} \rangle = -\langle 1 \rangle$$

and $$\langle P_{14}{}^{\tau} \rangle = \tfrac{1}{2}\langle 1 \rangle.$$

By substituting those expressions into the expression (1), the trace of $\langle O_{1j} \rangle \langle O_{1i} \rangle^{\dagger}$, for i, j = 3 or 4, can be found readily, and the results were summarized in the expressions (21) and (22) of Section D, Part IV.

To carry out the space integral I_j that also appeared in Section D, Part IV, one needs to choose an appropriate set of integration variables. The purpose is to find a coordinate system in which the integrations are separable. In the center-of-mass system, there are four degrees of freedom to be integrated, since the sum of the coordinate vectors of the five nucleons vanishes.

With the bound wave functions assumed for the deuteron and the mass three systems, and with the nucleon-nucleon potential assumed, I_j is given by

$$I_j = 5\int e^{-i\vec{k}_p[\vec{r}_5-\frac{1}{4}(\vec{r}_1+\vec{r}_2+\vec{r}_3+\vec{r}_4)]}\, e^{-\gamma^2[\frac{3}{4}|\vec{r}_1-\vec{r}_2|^2+|\vec{r}_3-\frac{1}{2}(\vec{r}_1+\vec{r}_2)|^2]}$$

$$\times\ \chi_4'^*[\vec{r}_4-\tfrac{1}{3}(\vec{r}_1+\vec{r}_2+\vec{r}_3)]\, e^{-\beta^2|\vec{r}_1-\vec{r}_j|^2}\, e^{i\vec{k}_\tau[\frac{1}{3}(\vec{r}_3+\vec{r}_4+\vec{r}_5)-\frac{1}{2}(\vec{r}_1+\vec{r}_2)]} \tag{2}$$

$$\times\ e^{-\alpha^2|\vec{r}_1-\vec{r}_2|^2}\, e^{-\gamma^2[\frac{3}{4}|\vec{r}_3-\vec{r}_4|^2+|\vec{r}_5-\frac{1}{2}(\vec{r}_3+\vec{r}_4)|^2]}\, d\vec{r}_1\, d\vec{r}_2\, d\vec{r}_3 d\vec{r}_4 .$$

Transforming to the new integration variables, defined as

$$\vec{y}_1 = \vec{r}_1-\vec{r}_2, \quad \vec{y}_2 = \vec{r}_3-\tfrac{1}{2}(\vec{r}_1+\vec{r}_2), \quad \vec{\rho} = \vec{r}_4 - \tfrac{1}{3}(\vec{r}_1+\vec{r}_2+\vec{r}_3)$$

and $$\vec{r} = \vec{r}_5-\tfrac{1}{2}(\vec{r}_3+\vec{r}_4),$$

the integral (2) becomes

$$I_j = \int e^{-i\vec{k}_p(\vec{r}+\frac{1}{4}\vec{\rho}+\frac{1}{3}\vec{y}_2)}\, e^{-\frac{3}{4}\gamma^2 y_1^2}\, e^{-\gamma^2 y_2^2}\, \chi_4'^*(\vec{\rho})\, e^{-\beta^2|\vec{V}_j+\frac{1}{2}\vec{y}_1|^2} \tag{3}$$

$$\times\ e^{i\vec{k}_\tau(\frac{1}{3}\vec{r}+\frac{1}{2}\vec{\rho}+\frac{2}{3}\vec{y}_2)}\, e^{-\alpha^2 y_1^2}\, e^{-\frac{3}{4}\gamma^2|\frac{2}{3}\vec{y}_2-\vec{\rho}|^2}\, e^{-\gamma^2 r^2}\, d\vec{y}_1\, d\vec{y}_2\, d\vec{\rho} d\vec{r}.$$

Here the jacobian of the coordinate transformation is $1/5$, and the vector $\vec{V}_j$ is

$$\vec{V}_j = a_j\vec{\rho} + b_j\vec{y}_2$$

where depending on whether $j = 3$ or 4, $a_3(a_4)$ and $b_3(b_4)$ are respectively equal to $0(-1)$ and $-1(-1/3)$. The integrations over $\vec{r}$ and $\vec{y}_1$ can be done easily by using the formulas

$$\int e^{-c^2x^2} e^{i\vec{p}\cdot\vec{x}} d\vec{x} = \left(\frac{\sqrt{\pi}}{c}\right)^3 e^{-p^2/4c^2} \qquad (4)$$

and

$$\int e^{-A^2x^2} e^{-B^2|\vec{V} + C\vec{x}|^2} d\vec{x} = \left(\frac{\pi}{A^2+B^2C^2}\right)^{\frac{3}{2}} e^{-V^2A^2B^2/(A^2+B^2C^2)} \qquad (5)$$

The integral (2) is now reduced to

$$I_j = \frac{8\pi^3}{\gamma^3(4\alpha^2+3\gamma^2+\beta^2)^{3/2}} e^{-|\frac{1}{3}\vec{k}_\tau - \vec{k}_p|^2/4\gamma^2} \int e^{-i\vec{k}_p(\frac{1}{4}\vec{\rho}+\frac{1}{3}\vec{y}_2)}$$

$$\times e^{-\gamma^2 y_2^2} \chi_4'^*(\vec{\rho}) e^{i\vec{k}_\tau(\frac{1}{2}\vec{\rho}+\frac{2}{3}\vec{y}_2)}$$

$$\times e^{-\frac{3}{4}\gamma^2|\frac{2}{3}\vec{y}_2 - \vec{\rho}|^2 - |a_j\vec{\rho}+b_j\vec{y}_2|^2\beta^2(4\alpha^2+3\gamma^2)/(4\alpha^2+3\gamma^2+\beta^2)} d\vec{\rho}d\vec{y}_2 .$$

Finally to separate the last two integrations, an additional change of the coordinate system was made. If one writes

$$\vec{z}_1 = \vec{\rho} \quad \text{and} \quad \vec{z}_2 = f_j\vec{\rho} + \vec{y}_2 ,$$

and chooses f_j such that the coefficient of $\vec{z}_1\cdot\vec{z}_2$ in the exponent vanishes, the integration over $\vec{z}_2$ can be carried out by using the formula (4) again. Let $\zeta^2 = \beta^2(4\alpha^2+3\gamma^2)/(4\alpha^2+3\gamma^2+\beta^2)$, f_j is found

to be

$$f_j = \frac{2\zeta^2 a_j b_j - \gamma^2}{\frac{8}{3}\gamma^2 + 2\zeta^2 b_j^2} \quad .$$

The final result is then given by

$$I_j = 8\pi^3 [\gamma^2(4\alpha^2 + 3\gamma^2 + \beta^2)]^{-3/2} \left[\frac{\pi}{\zeta^2 b_j^2 + \frac{4}{3}\gamma^2}\right]^{3/2} e^{-|\frac{1}{3}\vec{k}_\tau - \vec{k}_p|^2/4\gamma^2}$$

$$\times e^{-|\frac{2}{3}\vec{k}_\tau + \frac{1}{3}\vec{k}_p|^2/4(\zeta^2 b_j^2 + \frac{4}{3}\gamma^2)} \int \chi_4'^*(\vec{z}_1) e^{-\xi_j^2 z_1^2} e^{i\vec{p}_j \cdot \vec{z}_1} d\vec{z}_1 , \tag{6}$$

where $$\vec{p}_j = (\tfrac{4}{3} f_j - 1)(\tfrac{1}{4}\vec{k}_p - \tfrac{1}{2}\vec{k}_\tau)$$

and $$\xi_j^2 = (\zeta^2 b_j^2 + \tfrac{4}{3}\gamma^2) f_j^2 + (\gamma^2 - 2\alpha_j b_j \zeta^2) f_j + (\zeta^2 a_j^2 + \tfrac{3}{4}\gamma^2).$$

By a method similar to that used in the general discussions of Section A, Part IV, the wave function $\chi_4'(\vec{z}_1)$ is then expanded into partial waves, and the angular part of the integration can be done readily. The last integral in expression (6) becomes

$$\int \chi_4'^*(\vec{z}_1) e^{-\xi_j^2 z_1^2} e^{i\vec{p}_j \cdot \vec{z}_1} d\vec{z}_1 = \frac{1}{k} \sum_\ell i^\ell (2\ell+1) x_\ell^* P_\ell(\hat{p}_j \cdot \hat{k})$$

$$\times \int_0^\infty f_\ell^*(kz_1) j_\ell(p_j z_1) e^{-\xi_1^2 z_1^2} z_1 dz_1 .$$

Here $f_\ell(kz_1)$ is the ℓ-th wave radial wave function of the final-state interacting pair, and the corresponding partial-wave amplitude x_ℓ

was given in Section A, Part IV. Since $f_\ell(kr)$ is not known for $r \lesssim a$, the factored-wave-function method is used to approximate the radial integral as

$$\int_0^\infty f_\ell^*(kr) j_\ell(p_j r)\, e^{-\xi_j^2 r^2}\, r^2 dr \approx \left[I_\ell(ka) - U_{s\ell} O_\ell(ka)\right] \int_{R_c}^\infty j_\ell(p_j r) e^{-\xi_j^2 r^2}\, r dr.$$

A cut-off radius R_c is introduced to simulate the distortion effects in the reaction. The integral,

$$J_{j,\ell} \equiv \int_{R_c}^\infty j_\ell(p_j r) e^{-\xi_j^2 r^2}\, r dr,$$

gives the relative amplitude of producing the final-state interacting pair in the ℓ-th wave by the interaction between nucleons 1 and j. Together with the χ^2 resulted from the least-square fit to the experimental angular correlations $J_{j,\ell}$'s are listed in the following for the cut-off radius varied from zero to 6 F.

R_c	$J_{3,0}$	$J_{3,1}$	$J_{4,0}$	$J_{4,1}$	$\chi^2_{^3H}$	$\chi^2_{^3He}$
0.0	4.70	1.41	1.06	0.06	992	548
1.0	4.22	1.41	0.66	0.06	869	501
2.0	3.07	1.22	0.16	0.02	825	485
3.0	1.79	0.89	0.02	3×10^{-3}	778	417
4.0	0.84	0.52	6×10^{-4}	1×10^{-4}	731	349
5.0	0.31	0.25	8×10^{-6}	2×10^{-6}	707	283
6.0	0.09	0.09	4×10^{-8}	2×10^{-8}	653	236

The inverse decay lengths for the bound wave functions were taken as $\alpha = 0.167\,F^{-1}$ and $\gamma = 0.36\,F^{-1}$, and the range of nuclear interaction was chosen as $a = 3.0\,F$. The χ^2 with subscript ^3H (^3He) was obtained by the fit to the p - ^3H (p - ^3He) angular correlation at $E_p = 7.8$ MeV. The total χ^2 turns out to be not very sensitive to R_c as long as it was taken to be equal or greater than 2.0 F. For these values of R_c, the contribution $J_{4,\ell}$ from V_{14} is very much smaller than that of $J_{3,\ell}$ from V_{13}, and as a result the angular correlation becomes insensitive to the type of nucleon-nucleon potential used [cf., Section D, Part IV].

REFERENCES

1. Ajzenberg-Selove, F. and Lauritsen, T., Nucl. Phys. 11, 1 (1959).

2. Austern, N., Nuclear Forces and the Few-Nucleon Problem, Volume II, Pergamon Press, London (1960), p. 549.

3. Bacher, A. D., Ph.D. Thesis, California Institute of Technology (1966).

4. Balashko, J. G. and Barit, I. J., Trudy of the Lebedev Institute (Moscow, USSR) 33, 85 (1965), (transl. by Consultants Bureau, New York, 1966).

5. Banerjee, M. K., Nuclear Spectroscopy, Part B, Academic Press, New York (1960), pp. 695-731.

6. Barker, F. C. and Treacy, P. B., Nucl. Phys. 38, 33 (1962).

7. Bergman, A. A., Isakov, A. I., Popov, J. P. and Shapiro, F. L., JETP 6, 6 (1958).

8. Bethe, H. A. and Bacher, R. F., Rev. Mod. Phys. 8, 147 (1936).

9. Bransden, B. H., Robertson, H. H. and Swan, P., Proc. Phys. Soc. (London) A69, 877 (1956).

10. Cerny, J., Détraz, C. and Pehl, R. H., Phys. Rev. Lett. 15, 300 (1965).

11. Crane, H. R., Delsasso, L. A., Fowler, W. A. and Lauritsen, C. C., Phys. Rev. 48, 125 (1935).

12. Demirlioglu, M. and Whaling, W., unpublished compilation of proton stopping cross sections (1962).

13. deShalit, A. and Walecka, J. D., Phys. Rev. 147, 763 (1966).

14. Donovan, P. F., Rev. Mod. Phys. 37, 501 (1965).

15. Evans, R. D., Methods of Experimental Physics, Volume V, Part B, Academic Press, New York (1963), pp. 803-806.

16. Faddeev, L. D., Mathematical Aspects of the Three-Body Problem in Quantum Scattering, Stekov Math. Inst. Leningrad Publ. LXIX (1963), (transl. by D. Davey and Co., New York, 1965).

17. Feenberg, E., Phys. Rev. 49, 328 (1936).

18. Fermi, E., Elementary Particles, Yale University Press, New Haven, Conn. (1951), pp. 58-64.

19. Feynman, R. P., Theory of Fundamental Processes, W. A. Benjamin, Inc., New York (1962), p. 70.

20. Frank, R. M. and Gammel, J. L., Phys. Rev. 99, 1406 (1955).

21. Gillespie, J., Final-state Interactions, Holden-Day, Inc., San Francisco, Calif., (1964).

22. Goldberger, M. L. and Watson, K. M., Collision Theory, John Wiley and Sons, Inc., New York (1964), pp. 540-553.

23. Groce, D. E., Ph.D. Thesis, California Institute of Technology (1963).

24. Hungerford, E. D., Gross, E. E., Malanify, J. J., Pugh, H. G. and Watson, J. W., ORNL-4217, May, 1968.

25. Janecke, J., Z. Phys. 183, 499 (1965).

26. Janossy, L., Theory and Practice of the Evaluation of Measurements, Clarendon Press, Oxford (1965), pp. 258-259.

27. Jarmie, N., Silbert, M. G., Smith, D. B. and Joos, J. S., Phys. Rev. 130, 1987 (1963).

28. Kavanagh, R. W. and Parker, P. D., Phys. Rev. 143, 779 (1966).

29. Kramer, P. and Moshinsky, M., Phys. Lett. 23, 574 (1966).

30. Kurepin, A. B., Trudy of the Lebedev Institute (Moscow, USSR) 33, 1 (1965), (transl. by Consultants Bureau, New York, 1966).

31. Landau, L. I. and Lifshitz, E. M., Quantum Mechanics, 2nd ed., Addison-Wesley Publ. Co., Reading, Mass. (1965), pp. 562-565.

32. Lane, A. M. and Thomas, R. G., Rev. Mod. Phys. 30, 257 (1958).

33. Lauritsen, T. and Ajzenberg-Selove, F., Nucl. Phys. 78, 1 (1966).

34. Lefevre, H. W., Borchers, R. R. and Poppe, C. H., Phys. Rev. 128, 1328 (1962).

35. Lovelace, C., Phys. Rev. 135, B1225 (1964).

36. Mani, G. S., Freeman, R., Picard, F., Sadeghi, A. and Redon, D., Nucl. Phys. 60, 588 (1964).

37. Mathews, J. and Walker, R. L., Mathematical Methods of Physics, W. A. Benjamin, Inc., New York (1964), pp. 361-369.

38. Maxson, D. R., Phys. Rev. 128, 1321 (1962).

39. McNally, J. H., Ph.D. Thesis, California Institute of Technology (1966).

40. Messiah, A., Quantum Mechanics, Volume I, John Wiley and Sons, Inc., New York (1962), pp. 426-428.

41. Meyerhof, W. E., Rev. Mod. Phys. 37, 512 (1965).

42. Meyerhof, W. E. and McElearney, J. N., Nucl. Phys. 74, 533 (1965).

43. Meyerhof, W. E. and Tombrello, T. A., Nucl. Phys. A109, 1 (1968).

44. Migdal, A. B., JETP 1, 2 (1955).

45. Morinigo, F. B., Ph.D. Thesis, California Institute of Technology (1963).

46. Nefkens, B. M. K. and Moscatti, G., Phys. Rev. 133, B17 (1964).

47. Parker, P. D., Donovan, P. F., Kane, J. V. and Mollenauer, J. F., Phys. Rev. Lett. 14, 15 (1965).

48. Phillips, G. C., Griffy, T. A. and Biedenharn, L. C., Nucl. Phys. 21, 327 (1960).

49. Poppe, C. H., Holbrow, C. H. and Borchers, R. R., Phys. Rev. 129, 733 (1963).

50. Preston, M. A., Physics of the Nucleus, Addison-Wesley, Inc., Reading, Mass. (1962), p. 179.

51. Rogers, P. C. and Stokes, R. H., Phys. Lett. 8, 320 (1964).

52. Schiff, L. I., Phys. Rev. 133, B802 (1964).

53. Seagrave, J. D., Cranberg, L. and Simmons, J. E., Phys. Rev. 119, 1981 (1960).

54. Spicer, B. M., Phys. Lett. 6, 88 (1963).

55. Tobocman, W., Theory of Direct Nuclear Reactions, Oxford University Press, London (1961), p. 35.

56. Tombrello, T. A., Jones, C. M., Phillips, G. C. and Weil, J. L., Nucl. Phys. 39, 541 (1962).

57. Tombrello, T. A. and Parker, P. D., Phys. Rev. 130, 1112 (1963).

58. Tombrello, T. A., Phys. Rev. 138, B40 (1965).

59. Tombrello, T. A., Phys. Rev. 143, 772 (1966).

60. Watson, K. M., Phys. Rev. 88, 1163 (1952).

61. Werntz, C., Phys. Rev. 128, 1336 (1962).

62. Werntz, C. and Brennan, J. G., Phys. Lett. 6, 113 (1963).

63. Werntz, C., Phys. Rev. 133, B19 (1964).

64. Werntz, C. and Meyerhof, W. E., Nucl. Phys. A121, 38 (1968).

65. Young, P. G. and Ohlsen, G. G., Phys. Lett. 8, 124 (1964).

66. Yu, D. U. L. and Meyerhof, W. E., Nucl. Phys. 80, 481 (1966).

67. Zurmühle, R. W., Nucl. Phys. 72, 225 (1965).

Table I. The magnetic spectrometer resolutions, $\delta\Theta$, $\delta\Phi$ and $\delta E/E$, used in obtaining the α-particle energy spectra from the reaction ^{7}Li (p,α) at Θ_L are listed in this table [cf., Section B5, Part II]. As was indicated in Section B, Part IV, a cut-off energy of E_x = 20.30 MeV was introduced for the least-square fit, thus only N_i data points in each spectrum were included in evaluating the χ^2. The spectrum marked with two stars is shown in Figure 25; while those marked with one star are shown in Figure 9. See pages 31 and 43 for more details.

TABLE I. The α-Particle Energy Spectra Included for the Least-Square Fit

Θ_L (deg.)	Y_{mon}	$(\delta\Theta \times \delta\Phi)$ (deg.)	$\delta E/E$ (%)	N_i
2.5	909	1.0x2	1.11	9
5	900	1.0x2	1.11	9
5	1392	1.0x4	0.56	11
10*	1443	1.0x4	0.56	11
10	770	1.0x4	1.11	9
15**	787	1.0x4	1.11	10
15	2832	1.0x4	0.56	11
20	751	1.0x4	0.56	11
20*	2227	1.0x4	0.56	7
30*	1518	1.0x4	0.56	13
30	2309	1.0x4	0.56	7
30	1563	0.6x4	0.56	13
40*	2591	1.0x4	0.56	8
45	2764	1.0x4	1.11	7
45	2839	1.0x4	1.11	8
50*	889	1.0x4	0.56	14
60	2710	1.0x4	0.56	8
60*	3430	1.0x4	1.11	9
70*	6468	1.0x4	0.56	7
80*	1859	1.0x4	0.56	7
90	1128	1.0x4	0.56	7
90*	3716	1.0x4	1.11	7
100*	1389	1.0x4	0.56	6
100	2458	0.5x4	1.11	10
110*	3955	1.0x4	1.11	5
120*	3120	1.0x4	1.11	5

Table II. Some of the resonance parameters (a, E_R, γ_p^2, γ_n^2) for the first excited state of ^{4}He given in literature were used to fit the α-particle energy spectra summarized in Table I. The nuclear phase shifts and the scattering matrix amplitudes, appearing in expression (8), Part IV, are calculated from those resonance parameters with the expressions developed in Appendix A. See pages 44 and 75 for the evaluation of χ_{min}^2.

TABLE II. Comparison of the Resonance Parameters Given in Literature

a (F)	E_R (MeV)	γ_p^2 (MeV)	γ_n^2 (MeV)	χ_{min}^2	Reference
3.0	20.59	2.1	0.0	1649	Frank et al., 1955
3.0	20.21	1.4	0.0	1214	Werntz, 1962
3.0	20.21	4.18	1.50	1579	Werntz, 1964
3.0	20.31	4.44	0.50	2215	Werntz, 1964
3.0	20.41	4.77	0.50	2089	Werntz, 1964
3.6	20.21	3.02	3.00	984	Werntz, 1964
3.6	20.31	3.84	3.00	691	Werntz, 1964
3.6	20.41	3.52	2.00	615	Werntz, 1964
4.2	20.21	2.09	2.09	1098	Werntz, 1964
4.2	20.31	2.40	1.70	789	Werntz, 1964
4.2	20.41	2.60	1.57	615	Werntz, 1964
3.0	20.36	5.20	2.10	695	Kurepin, 1965
3.0	20.36	8.40	6.70	732	Kurepin, 1965
4.0	20.31	5.30	5.30	737	Kurepin, 1965
4.0	20.31	6.60	5.40	1441	Kurepin, 1965
4.0	20.31	10.00	8.00	2151	Kurepin, 1965
3.3	20.45	3.35	1.74	1085	Meyerhof et al., 1965
3.3	20.41	3.53	1.62	650	Meyerhof et al., 1965

Table III. The scattering phase shifts $\delta_{ps\ell}(\delta_{ns\ell})$ and the scattering matrix amplitudes $D_{s\ell}$ taken to describe the p + ^{3}H (n + ^{3}He) final-state interaction in the reaction D(^{3}He, p) are listed here. E_p is the laboratory energy of the detected protons, and E_x is the corresponding excitation energy of the final-state interacting pair with respect to the ^{4}He ground state. Energies are expressed in MeV, and phases are given in radians. The columns (a) are values from Meyerhof and McElearney (1965). The region of validity of their analysis was restricted to $E_x \leq 21.3$ MeV. The corresponding $D_{s\ell}$, $\delta_{ps\ell}$ and $\delta_{ns\ell}$ for higher excitation energies were obtained by extrapolations. Those columns indicated by (b) are from the resonating-group calculations of Bransden et al. (1956). The inelasticity was not considered in Bransden's calculations, so $D_{s\ell} = 1$ for all the energies, and the phase shifts quoted here are the averages of those derived from Serber force and symmetrical force. For further discussion see pages 59, 66 and 67.

TABLE III. A Summary of the Scattering Matrix Amplitudes and the Phase Shifts used for Comparison with the Experimental Data

Partial Wave	E_p	E_x	$D_{s\ell}$	$\delta_{ps\ell}$		$\delta_{ns\ell}$	
			(a)	(a)	(b)	(a)	(b)
^1S	8.6	20.66	0.77	1.75	-0.17	-0.30	-0.04
	8.2	20.95	0.66	1.70	-0.22	-0.60	-0.12
	7.8	21.24	0.63	1.65	-0.26	-0.70	-0.20
	7.4	21.52	0.62	1.60	-0.32	-0.82	-0.26
	7.0	21.79	0.62	1.58	-0.34	-0.90	-0.30
	6.6	22.06	0.62	1.56	-0.37	-0.98	-0.33
^3S	8.6	20.66	0.94	-0.44	-0.39	0.22	-0.10
	8.2	20.95	0.85	-0.50	-0.48	0.50	-0.31
	7.8	21.24	0.77	-0.60	-0.56	0.67	-0.47
	7.4	21.52	0.72	-0.65	-0.63	0.85	-0.57
	7.0	21.79	0.67	-0.75	-0.70	1.10	-0.65
	6.6	22.06	0.62	-0.85	-0.75	1.35	-0.72
^1P	8.6	20.66	0.99	0.16	-0.02	-0.01	-0.00
	8.2	20.95	0.96	0.34	-0.03	-0.05	-0.01
	7.8	21.24	0.90	0.42	-0.04	-0.10	-0.02
	7.4	21.52	0.78	0.50	-0.05	-0.15	-0.03
	7.0	21.79	0.68	0.63	-0.06	-0.32	-0.04
	6.6	22.06	0.57	0.76	-0.07	-0.49	-0.05
^3P	8.6	20.66	1.00	0.18	0.07	0.01	0.00
	8.2	20.95	1.00	0.36	0.14	0.08	0.05
	7.8	21.24	1.00	0.40	0.21	0.13	0.10
	7.4	21.52	1.00	0.53	0.28	0.20	0.17
	7.0	21.79	1.00	0.68	0.36	0.30	0.23
	6.6	22.06	1.00	0.83	0.41	0.40	0.32

FIGURE 1. Energy Level Diagram

The energy levels of ^{4}He are shown together with all of the threshold energies and the various Q-values of the reactions that can populate the excited ^{4}He system. The energies are given in MeV relative to the ground-state energy of ^{4}He. The excitation energies involved in most of the present work were limited to the range from 19.814 MeV, the p + ^{3}H threshold, up to 22 MeV.

The 0^+ state at 20.2 MeV was seen from the α-particle energy spectra from the reaction ^{7}Li(p, α) as the ^{1}S p + ^{3}H interaction in the final state. In Section B, Part IV, the resonance parameters for this state are deduced. Near 21.5 MeV, the system was studied by the p - ^{3}H and p - ^{3}He angular correlation measurements of the reaction D(^{3}He, p). Except for the ^{3}S n + ^{3}He phase shifts, both the s- and p-wave phase shifts, as given by Meyerhof and McElearney, were found to be appropriate in describing the final-state interactions of the reaction.

The level positions, spins, parities and the isobaric spins are taken from the latest compilation of Meyerhof and Tombrello (1968). For further discussion see Table III and pages 5, 13, 14 and 62-67.

FIGURE 1

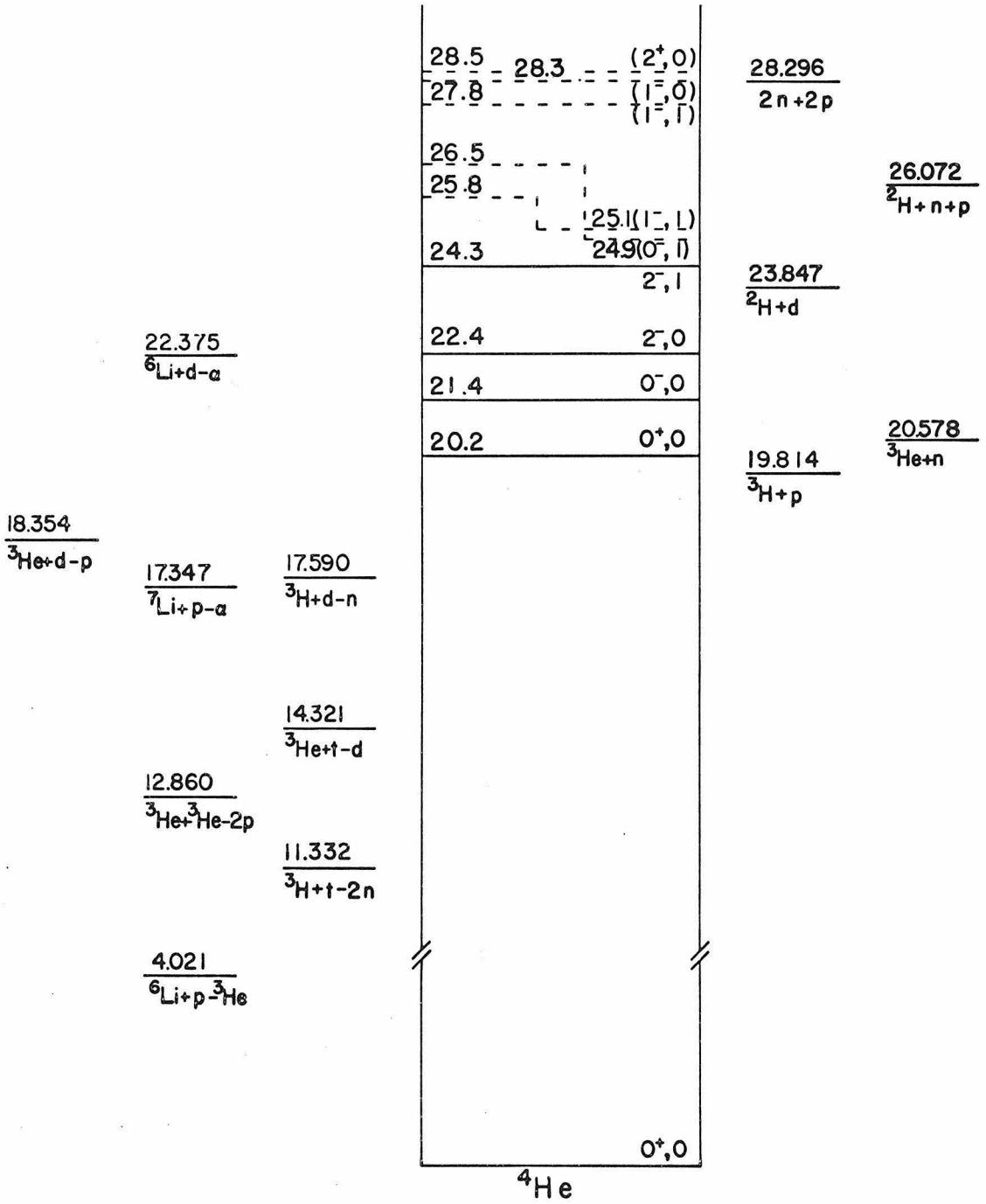
28.5
28.3
(2+,0)
27.8
(1-,0)
(1-,1)
26.5
25.8
25.1(1-,1)
24.3
24.9(0-,1)
2-,1
22.4
2-,0
21.4
0-,0
20.2
0+,0
0+,0
4He
28.296
2n+2p
26.072
2H+n+p
23.847
2H+d
20.578
3He+n
19.814
3H+p
22.375
6Li+d-α
18.354
3He+d-p
17.347
7Li+p-α
17.590
3H+d-n
14.321
3He+t-d
12.860
3He+3He-2p
11.332
3H+t-2n
4.021
6Li+p-3He

FIGURE 2. Particle Spectra from Spectrometer at 120°

The particles produced from bombardment of a ^{7}Li target with 9.1-MeV proton beam were detected at 120° at the focus of a 61-cm magnetic spectrometer in conjunction with a 200-mm^2 140-μ surface-barrier counter. The protons and α-particles, with energies ~ 1 MeV, were stopped in the counter after passing through a 5000-Å nickel foil used to separate the two kinds of particles from each other. The energy window of the spectrometer was set at $\Delta E = E/90 \sim 12$ keV. From the width of the proton peak, the over all electronic noise was found to be 120 keV (FWHM), thus the continuously distributed pulses below 600 keV are believed to be due to the scattered particles from the wall of the spectrometer. For more details see page 8.

FIGURE 2

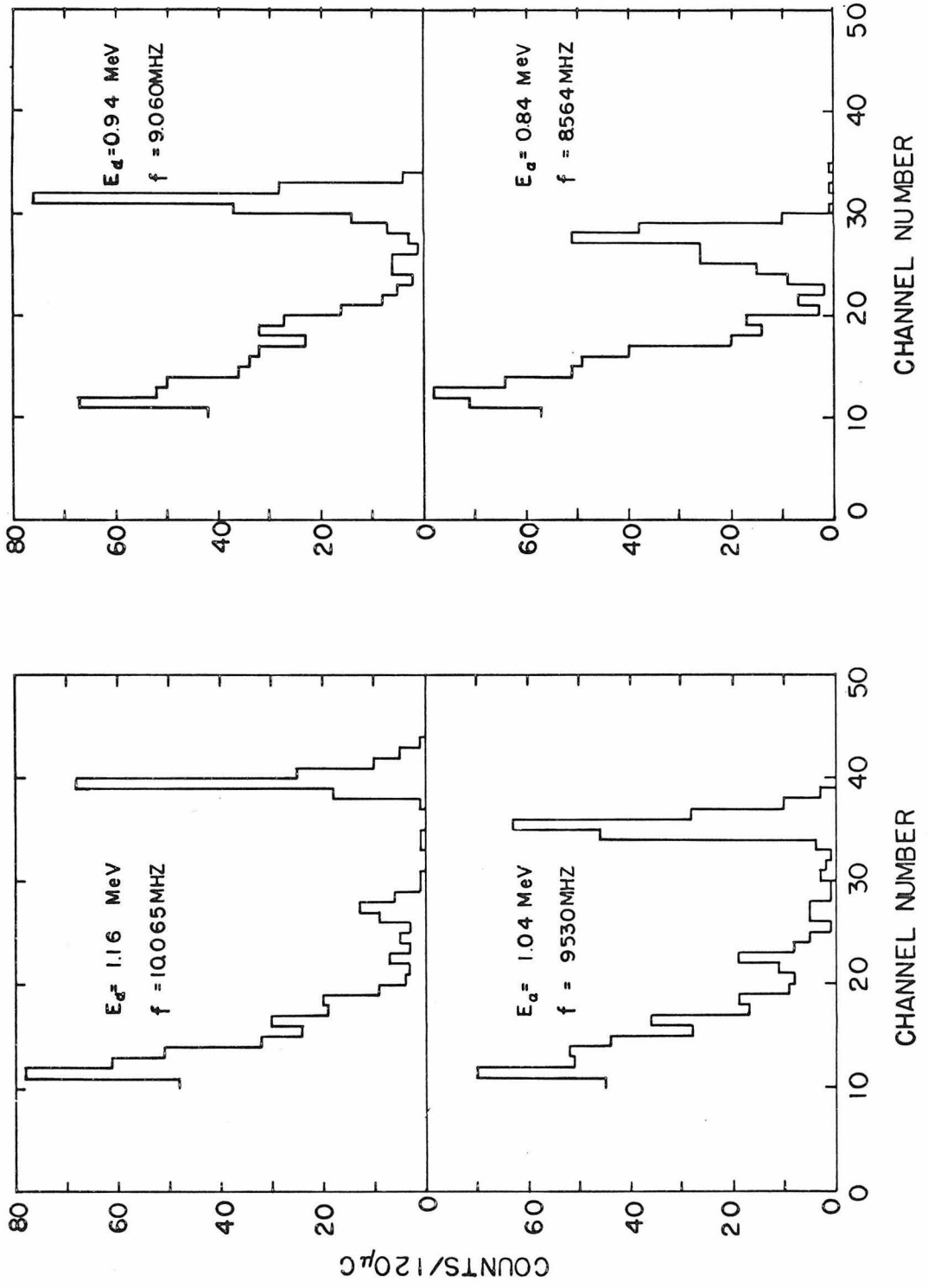
E_d= 1.16 MeV
f = 10.065MHZ
E_d= 1.04 MeV
f = 9530MHZ
E_d=0.94 MeV
f = 9.060MHZ
E_d= 0.84 MeV
f = 8564MHZ
COUNTS/120μC
CHANNEL NUMBER
CHANNEL NUMBER

FIGURE 3. Particle Spectra at 60° and 90°

The particles emitted during bombardment of a ^{7}Li target on gold foil by 9.1-MeV protons were detected in a 300-μ surface-barrier counter in the target chamber. Beam defining slits in front of the target chamber were 1.53 mm in both vertical and horizontal directions. The angular apertures of the counter were 0.9° and 11.7° along the Θ- and Φ-direction. From the spectra at 60° and 90° and some other angles, the actual thickness of the surface-barrier at 85-volts bias was found to be 500 μ, and various groups of particles were identified. The group (A) represents the elastically scattered protons from the backing or the edge of the counter collimator and stopped in the sensitive layer of the counter. (B) represents those protons that are not stopped. The group (C) is an unidentified peak. For more details see page 10.

FIGURE 3

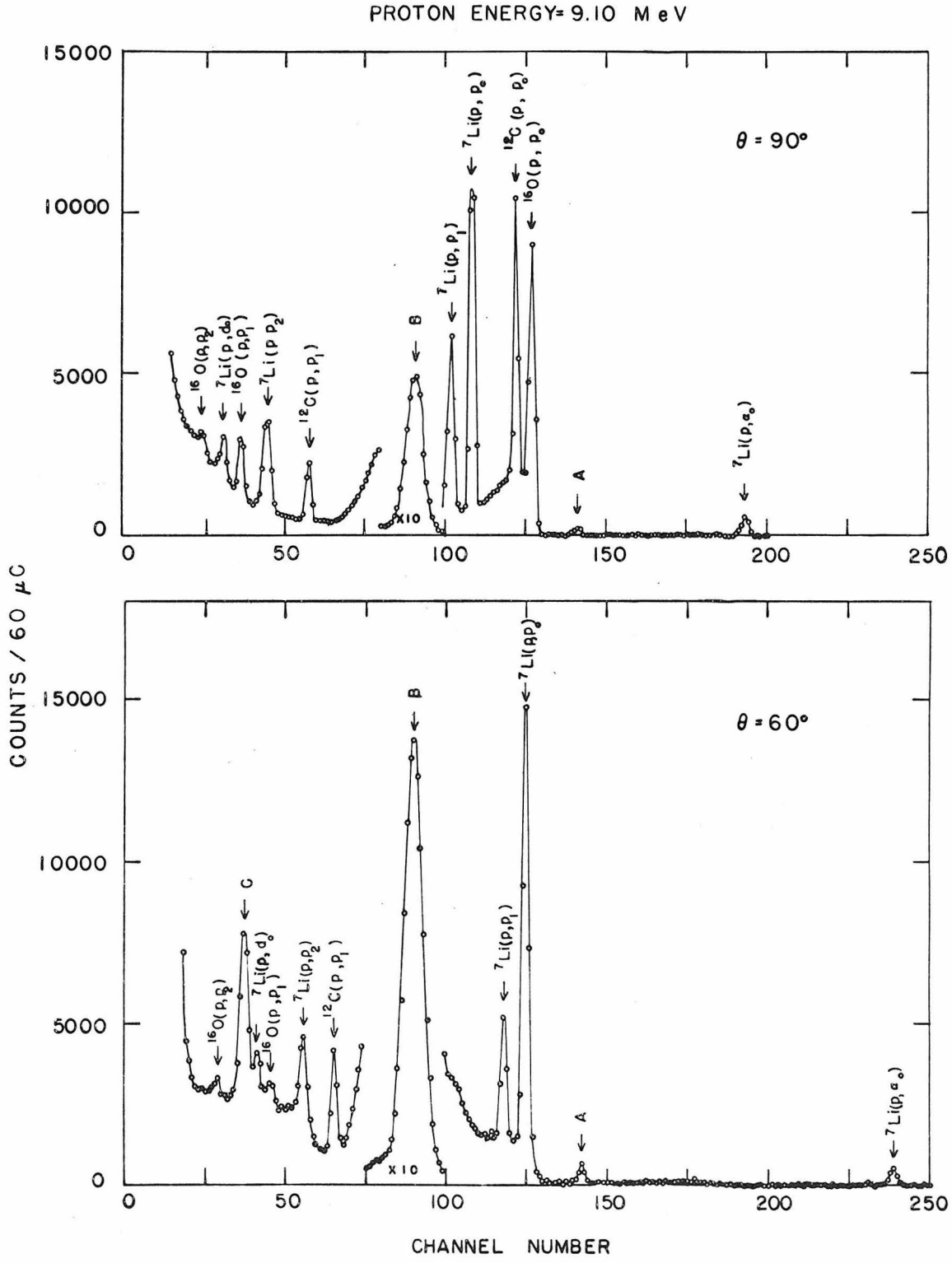
PROTON ENERGY= 9.10 MeV
θ = 90°
θ = 60°
COUNTS / 60 μC
CHANNEL NUMBER
B
A
C
x10
0
5000
10000
15000
50
100
150
200
250

FIGURE 4. The Target-Thickness Measurements

The number of ^{7}Li atoms per unit area of the target was measured by finding the energy loss to an α-particle group of well defined energy passing through it. In the geometry indicated, in the upper graph, the 3.85 MeV α-particles from the reaction $^{19}F(p,\alpha')^{16}O^{*}$ at E_p = 5.00 MeV were let through the ^{7}Li evaporated in the target chamber. The shift in the position of the energy centroid, defined by $\sum_i E_i N_i / \sum_i N_i$, was found to be 16 ± 4 keV. The differential cross section of the reaction $^{7}Li(p,\alpha_0)$ at 30° was then found to be 1.39 ± 0.35 mb/sr. The second method, shown in the lower graph, was carried out with a 9.1-MeV α-particle beam from the tandem and a LiF target. The energy loss and the corresponding $^{7}Li(p,\alpha_0)$ differential cross section at 30° were respectively found to be 136 ± 6 keV and 1.88 ± 0.08 mb/sr.

The ^{7}Li target prepared in the first method may have suffered from oxygen or carbon contamination, which would lead to an underestimate of the differential cross section. For more details see page 11.

FIGURE 4

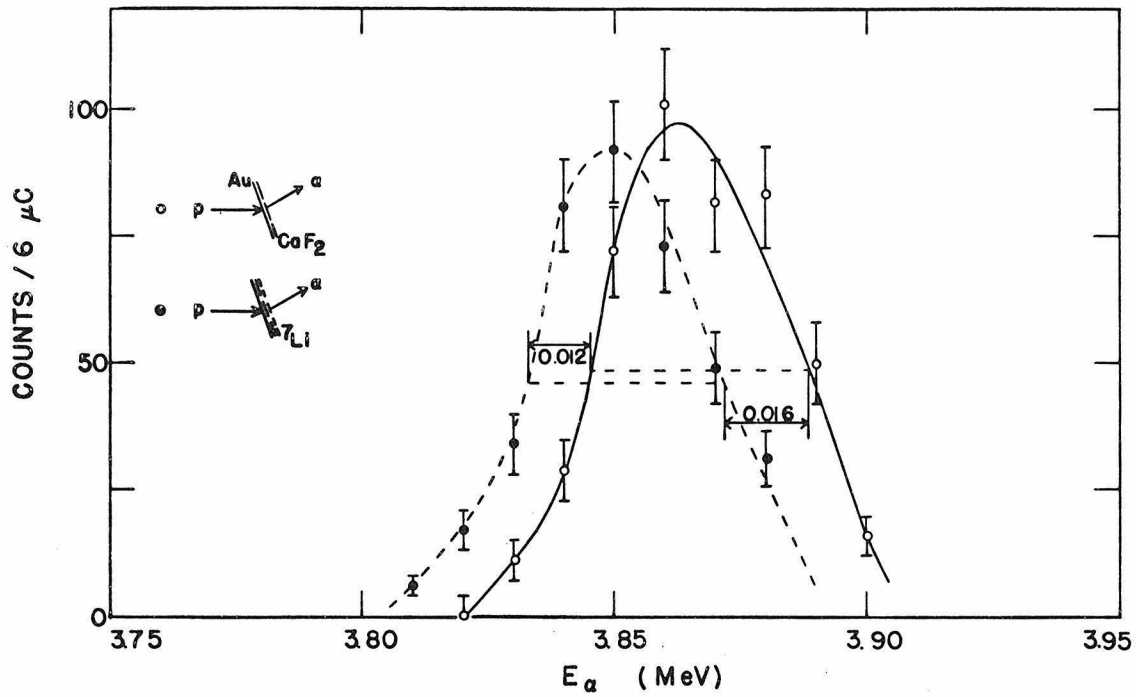
COUNTS / 6 μC
100
50
0
Au
α
p
CaF2
p
α
7Li
0.012
0.016
3.75
3.80
3.85
3.90
3.95
Eα (MeV)

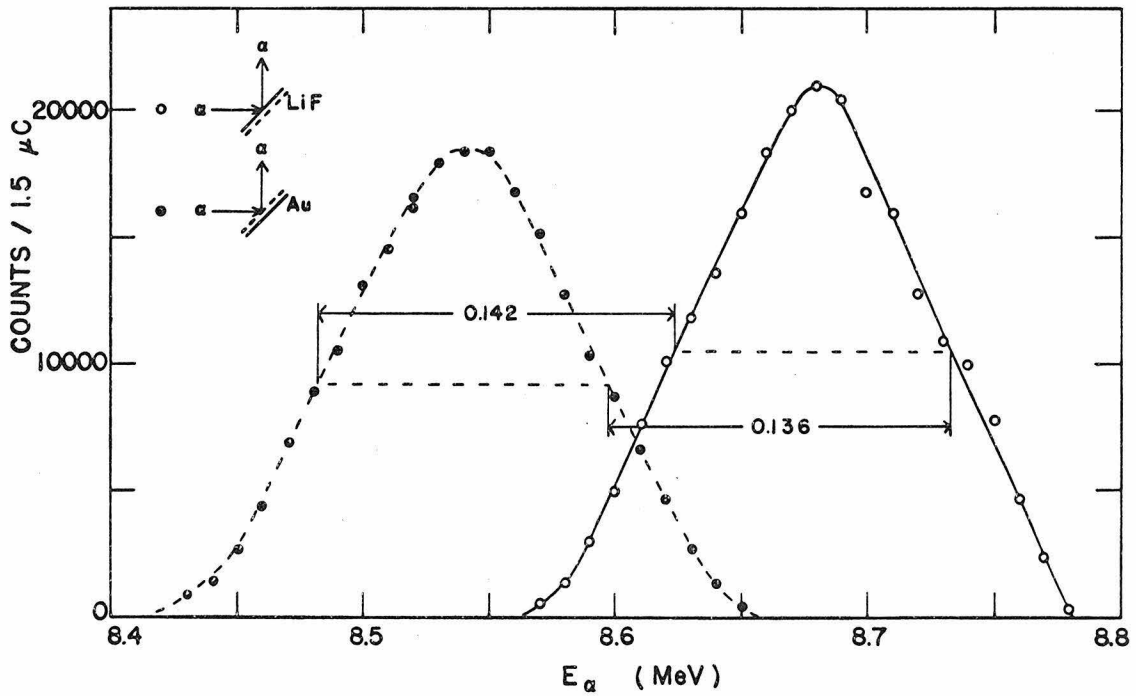
COUNTS / 1.5 μC
20000
10000
0
α
α
LiF
α
α
Au
0.142
0.136
8.4
8.5
8.6
8.7
8.8
Eα (MeV)

FIGURE 5. The Angular Distributions of $^{7}Li(p, \alpha_0)$ and $^{7}Li(p, \alpha_1)$

The angular distributions of the α-particle groups leading to the ground state and the first excited state of ^{4}He from the reaction $^{7}Li(p, \alpha_0)$ are shown in the laboratory system. The smooth curves serve only to connect the data points. The errors were estimated by "insufficient" statistics [Evans, 1963] over several repeated measurements. For the reaction $^{7}Li(p, \alpha_1)$, the differential cross sections were evaluated at the α-particle energies corresponding to an excitation energy of 20.06 MeV in the ^{4}He system. See pages 12 and 13 for additional details.

FIGURE 5

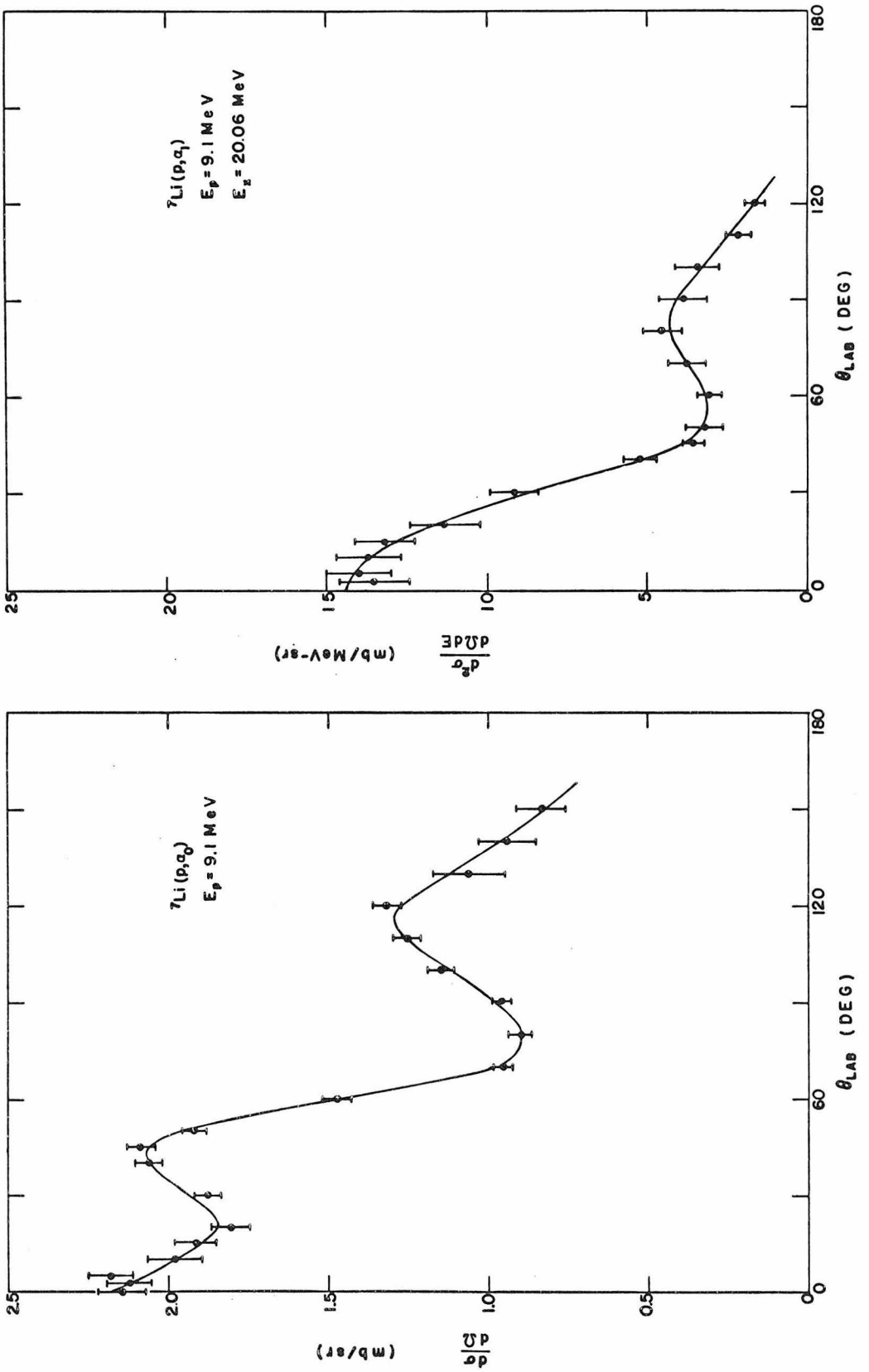
^{7}Li(p,α$_1$)
E$_p$ = 9.1 MeV
E$_x$ = 20.06 MeV
$\frac{d^2\sigma}{d\Omega dE}$ (mb/MeV-sr)
θ$_{LAB}$ (DEG)
^{7}Li(p,α$_0$)
E$_p$ = 9.1 MeV
$\frac{d\sigma}{d\Omega}$ (mb/sr)
θ$_{LAB}$ (DEG)

FIGURE 6. The $^{7}Li(p, \alpha_0)$ Angular Distribution in the C.M. System

The $^{7}Li(p, \alpha_0)$ angular distribution at 9.1 MeV, along with some higher energy data due to Maxson (1962), is plotted out in the center of mass system. Since the two final-state particles are identical bosons, there is a 90° symmetry in the angular distribution. The dark circles are those data points taken at the angles corresponding to $(\pi - \Theta_{CM})$. The curves are the model calculations based on a PWBA and a zero-range $p + {}^{3}H$ interaction in the α-particle. The parameter indicated for each curve is the cut-off radius which appeared in the Butler Theory of Stripping. For discussion see pages 12 and 49.

FIGURE 6

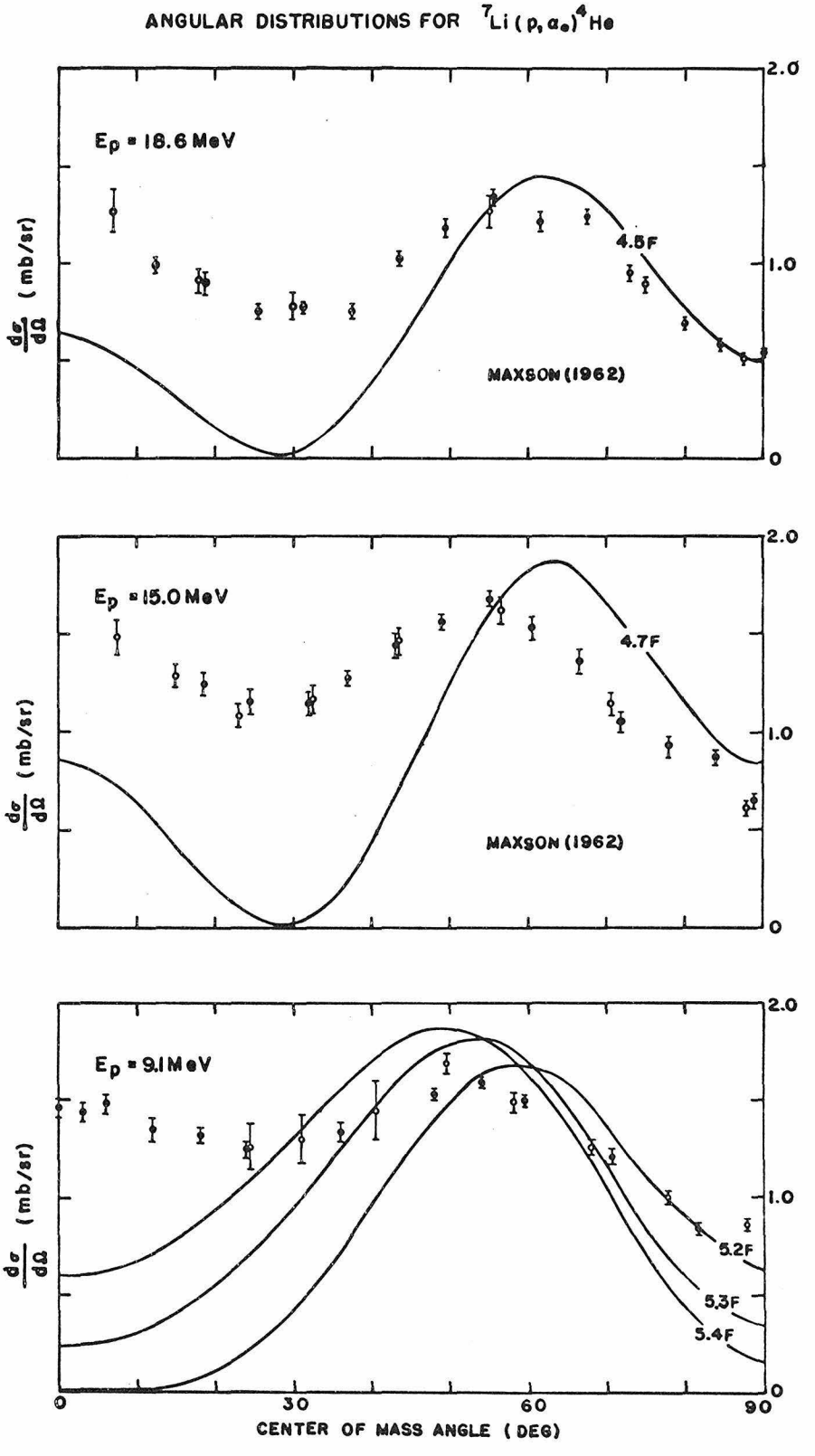
ANGULAR DISTRIBUTIONS FOR $^{7}Li(p,\alpha_0)^{4}He$
E_p = 18.6 MeV
4.5F
MAXSON (1962)
E_p = 15.0 MeV
4.7F
MAXSON (1962)
E_p = 9.1 MeV
5.2F
5.3F
5.4F
$\frac{d\sigma}{d\Omega}$ (mb/sr)
2.0
1.0
0
0
30
60
90
CENTER OF MASS ANGLE (DEG)

FIGURE 7. The α-Particle Energy Spectra at 10° and 30°

The two spectra shown here cover a wider range of the α-particle energies. Except for the contamination due to $^{16}O(p, \alpha_0)$, the spectra are quite clean. The first two peaks are due to the first and second excited states of ^{4}He. The third broad state at 22.5 MeV, reported by Cerny (1965), is not obvious. For further details see pages 3 and 12. See also Figure 8.

FIGURE 7

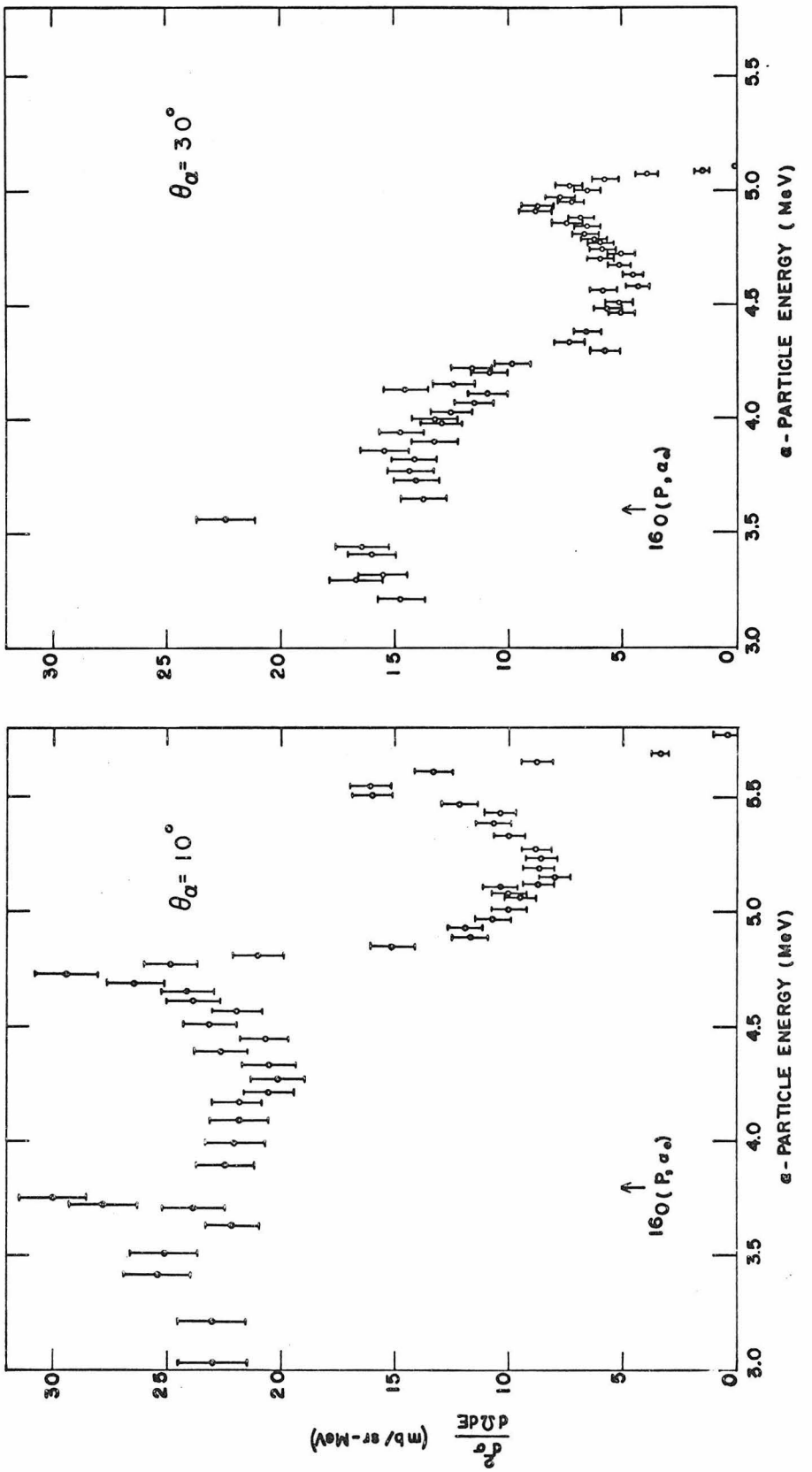
$\theta_\alpha = 10°$
$\theta_\alpha = 30°$
$^{16}O(P,\alpha_0)$
$^{16}O(P,\alpha_1)$
α-PARTICLE ENERGY (MeV)
$\frac{d^2\sigma}{d\Omega dE}$ (mb/sr-MeV)

FIGURE 8. Transition Probabilities

The α-particle energy spectra shown in Figure 7 are plotted here as functions of the excitation energies of the recoil ^{4}He system. The phase-space factor, which is proportional to $[E_\alpha(E_x - 19.814)]^{\frac{1}{2}}$, was taken out. The enhancement in the transition probability near the low-excitation end of the spectra was interpreted as due to the strong p + ^{3}H final state interaction through the first excited state of the ^{4}He system. For additional details see pages 13 and 29.

FIGURE 8

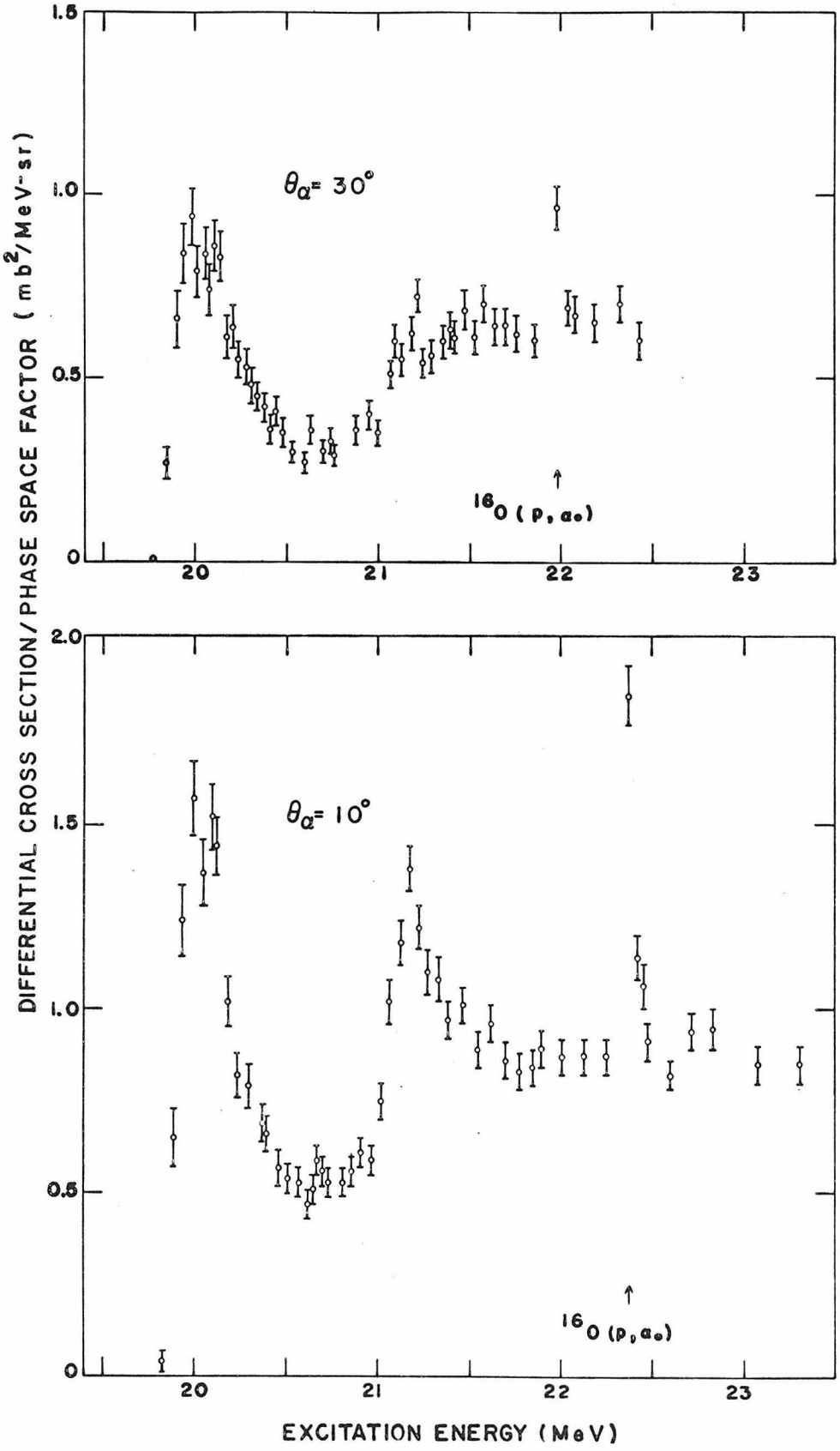
DIFFERENTIAL CROSS SECTION/PHASE SPACE FACTOR (mb²/MeV-sr)
θα= 30°
16O (p, α0)
θα= 10°
16O (p, α0)
EXCITATION ENERGY (MeV)

FIGURE 9. The α-Particle Energy Spectra from 10° to 120°

The higher-energy part of the α-particle energy spectra and the fitted spectral shapes of the reaction $^{7}Li(p, \alpha)$, are shown from 10° to 120° in steps of 10°. The arrows, corresponding to an excitation energy of 20.30 MeV, indicate that all of the data points from those energies up are included in the least-square fit. The details of the fitting procedure are discussed in Section B of Part IV, and Figures 23, 24 and 25.

FIGURE 9

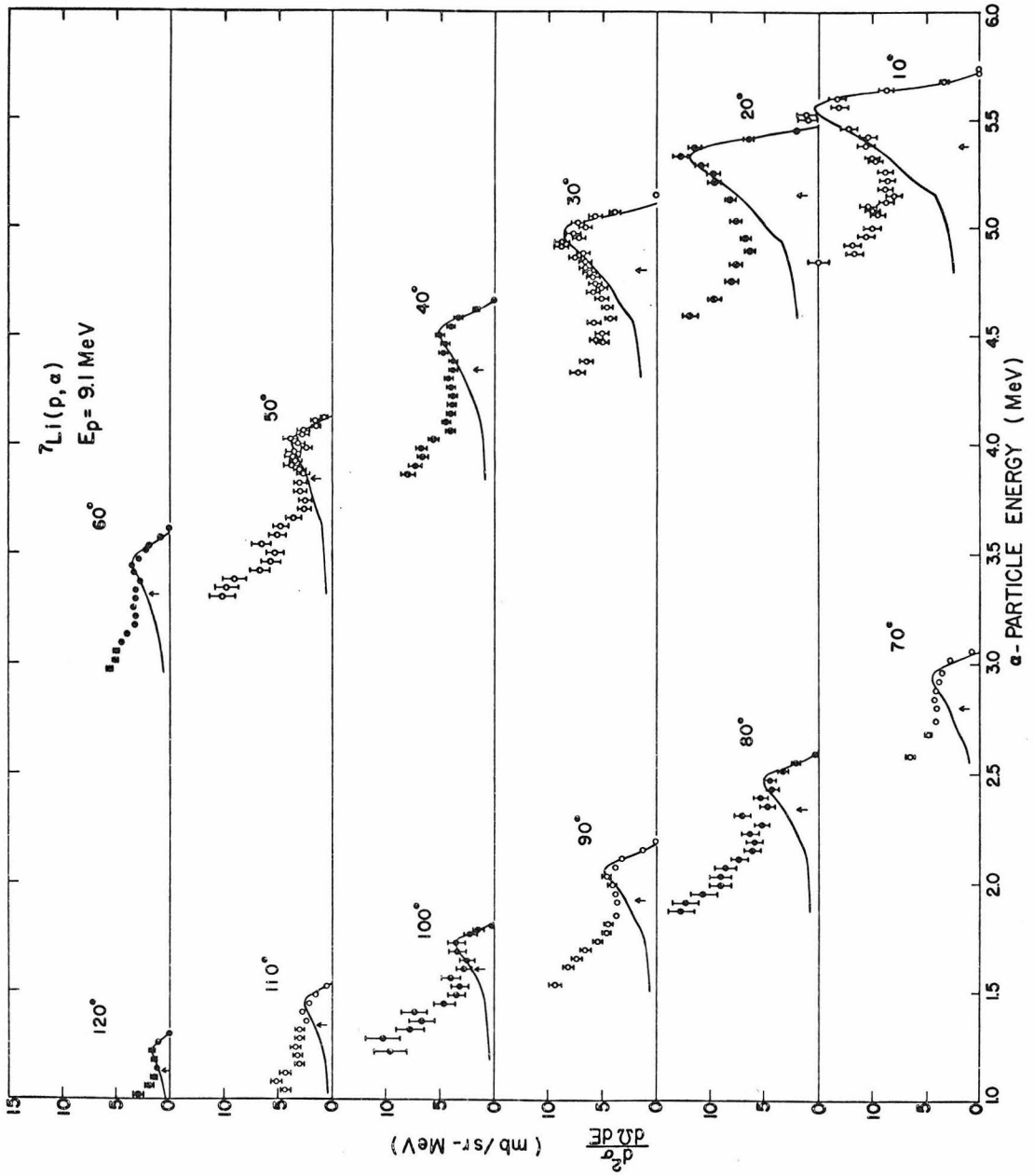
^{7}Li(p, α)
Ep= 9.1 MeV
120°
110°
100°
90°
80°
70°
60°
50°
40°
30°
20°
10°
$\frac{d^2\sigma}{d\Omega\, dE}$ (mb/sr-MeV)
α-PARTICLE ENERGY (MeV)

FIGURE 10. Block Diagram of Slow Coincidence System

The commercial instruments used, for the coincidence measurements from the reaction $^{7}Li(p, \alpha)$, are listed as follows:

TENNELEC Model 100A Low-Noise Preamplifier.

ORTEC 410 Multimode Amplifier. Delay-line mode is used for the pulse shaping.

ORTEC 420 Timing Single-Channel Analyzer (SCA).

ORTEC 409 Linear Gate and Slow Coincidence.

RIDL 400-Channel Analyzer.

For more details, see page 15, Figures 11 and 13.

FIGURE 10

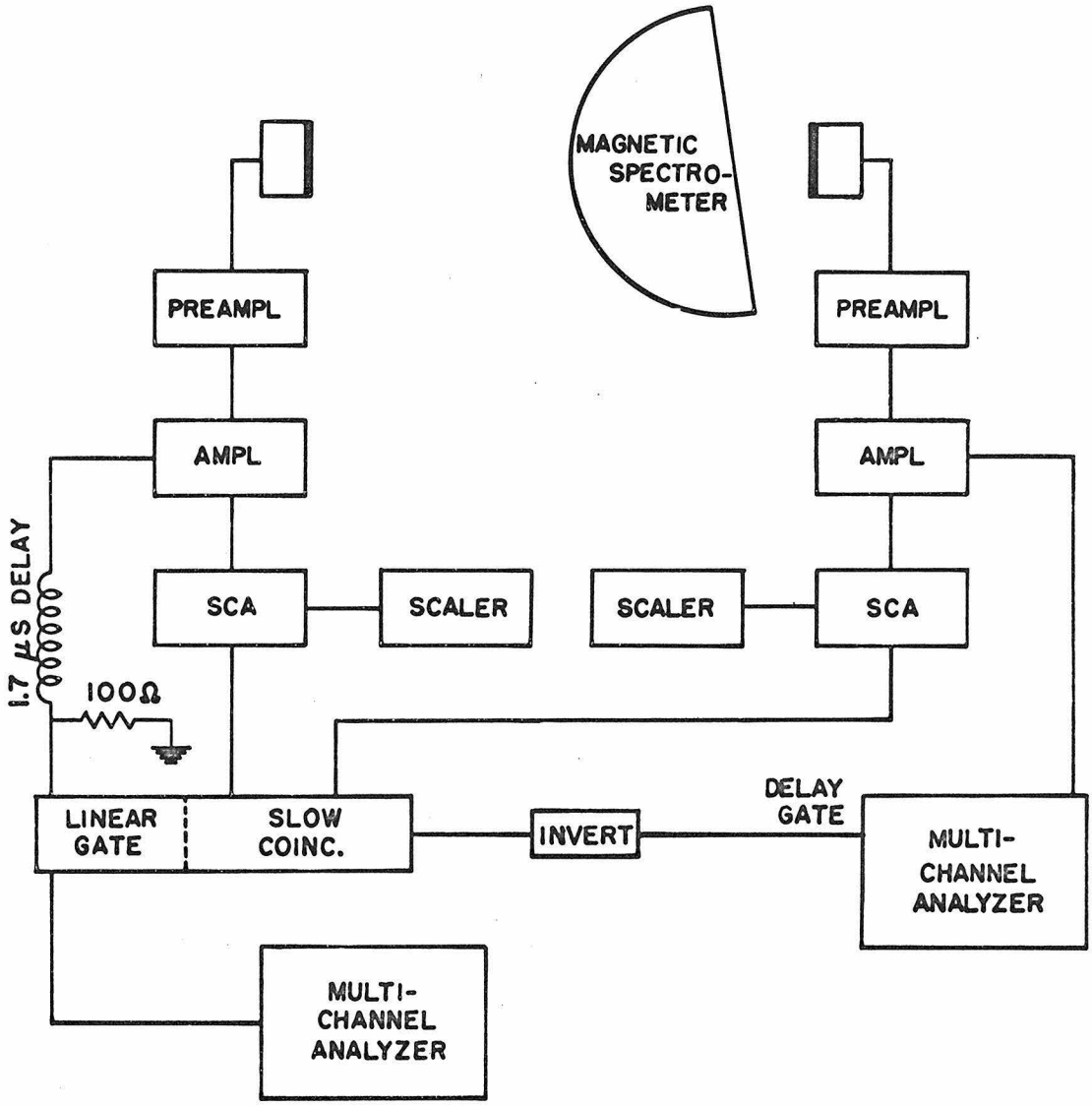

SLOW COINCIDENCE SYSTEM

FIGURE 11. The Coincidence Spectra from $^{7}Li(p, \alpha)$ at $E_{\alpha} = 5.0$ MeV

The protons and tritons from the reaction were detected in coincidence with the 5.0-MeV α-particles. The α-particles were detected at 30° in the magnetic spectrometer whose resolutions were set at $\delta E/E = 1.11\%$, $\delta\Theta = 1°$ and $\delta\Phi = 4°$. The angular apertures of the triton or proton counter in the target chamber were 3.8° and 15.5° respectively along the polar and azimuthal directions. The slow-coincidence resolving time was 1 μs.

The dotted lines are the kinematically predicted loci [cf., Section A, Part III] where the protons and tritons are expected to contribute pulses. For additional details see pages 15 and 16.

FIGURE 11

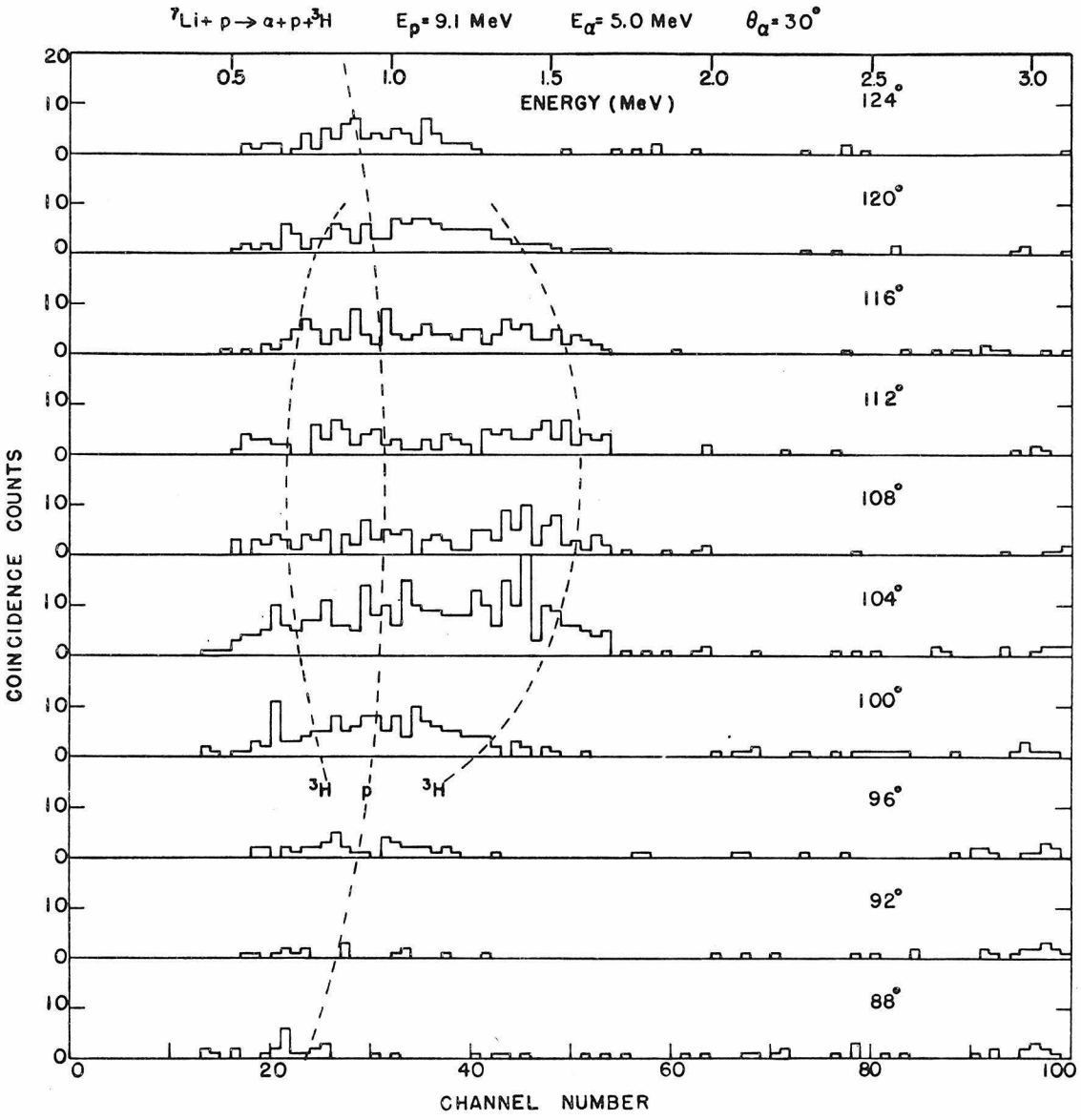
$^{7}Li + p \rightarrow \alpha + p + ^{3}H$ $E_p = 9.1$ MeV $E_\alpha = 5.0$ MeV $\theta_\alpha = 30°$
ENERGY (MeV)
0.5
1.0
1.5
2.0
2.5
3.0
124°
120°
116°
112°
108°
104°
100°
96°
92°
88°
^{3}H
p
^{3}H
COINCIDENCE COUNTS
CHANNEL NUMBER
0
20
40
60
80
100

FIGURE 12. The α - H and α - ^{3}H Angular Correlation from ^{7}Li(p, α) at E_{α} = 5.0 MeV and Θ_{α} = 30°

For each of the coincidence spectra shown in Figure 11, the randoms were estimated and subtracted by comparing with the singles [cf., Section A6, Part II]. Because of the large kinematic $(\partial E/\partial\Theta)\Delta\Theta$ spreading, no attempt was made to separate the protons from tritons. The sum of the α - H and α - ^{3}H coincidence counts was plotted here against the angular positions of the counter in the target chamber. The error bars included the statistical error and the uncertainty in assigning the randoms.

The curve is the geometric efficiency predicted, if an isotropic decay of the excited ^{4}He in its center-of-mass system is assumed. For additional discussion see page 16.

FIGURE 12

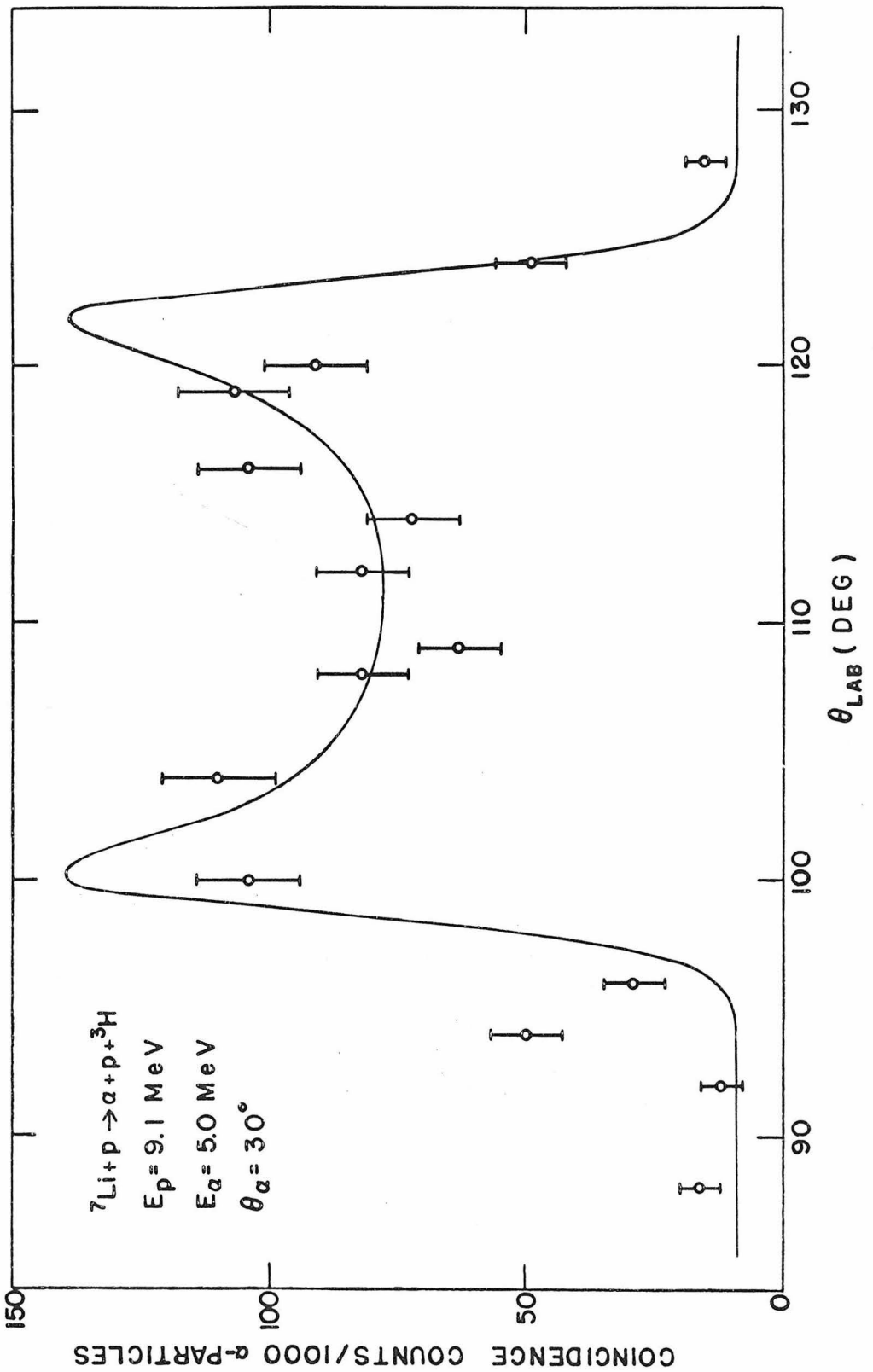
COINCIDENCE COUNTS/1000 α-PARTICLES
150
100
50
0
90
100
110
120
130
θLAB (DEG)
7Li+p →α+p+3H
Ep= 9.1 MeV
Eα= 5.0 MeV
θα= 30°

FIGURE 13. The Coincidence Spectra from $^{7}Li(p, \alpha)$ at $E_{\alpha} = 4.1$ MeV, $\Theta_{\alpha} = 30°$

The protons, tritons and ^{3}He's from the reaction were detected in coincidence with the 4.1-MeV α-particles. The α-particles were detected in the magnetic spectrometer with $\delta E/E = 1.11\%$, $\delta\Theta = 1°$ and $\delta\Phi = 4°$. The angular apertures of the counter in the target chamber were, in this case, set at 7.6° and 15.5° respectively along the polar and azimuthal directions. The slow-coincidence resolving time was 1 μs. The small peaks appearing from channel 110 to 140 follow the two-body kinematics of the elastic scattering of the incoming protons on the ^{12}C target backing. They are randoms.

The dotted lines were drawn from the three-body kinematics. For more details see pages 16 and 17.

FIGURE 13

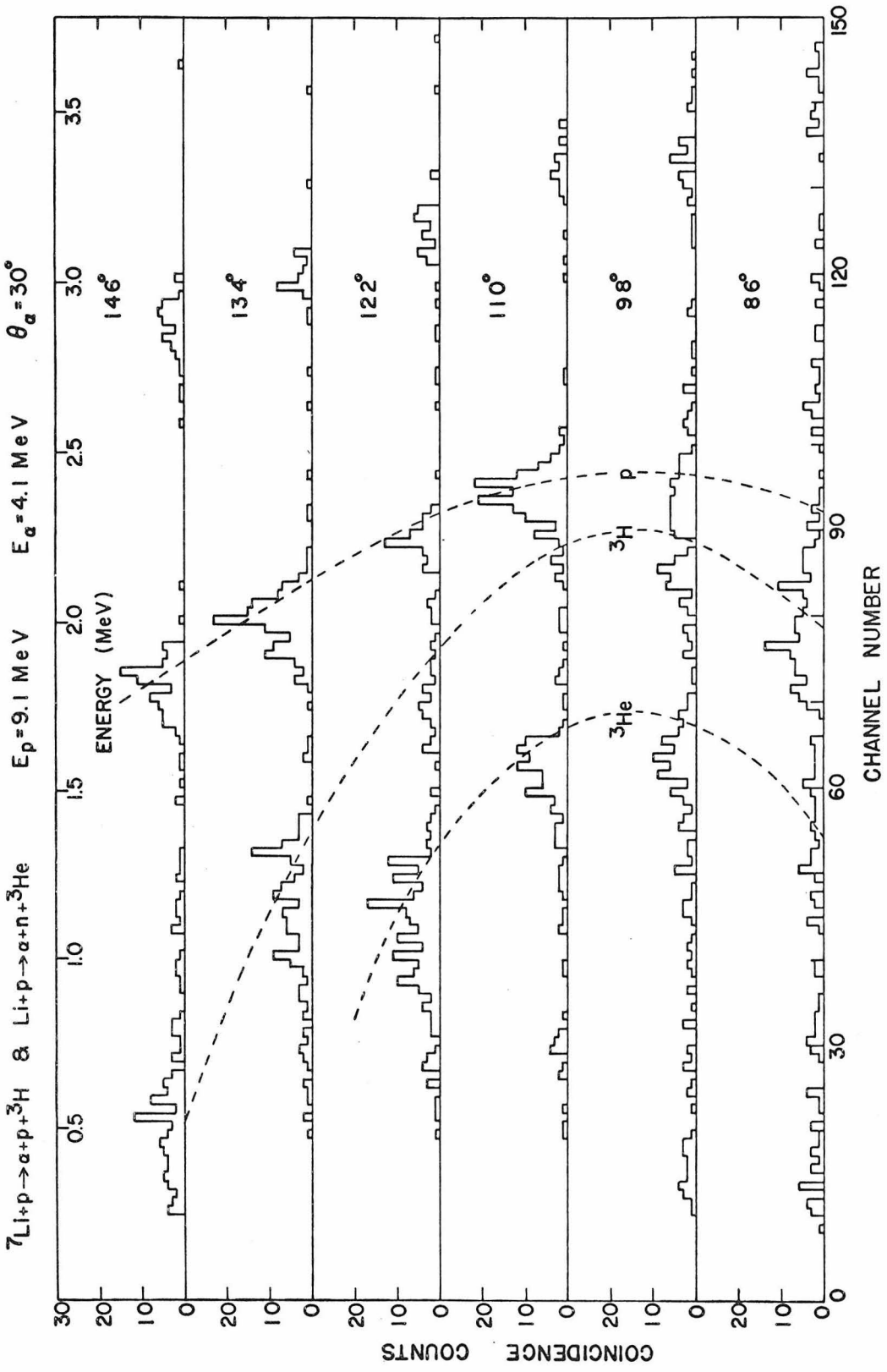
^{7}Li+p→α+p+^{3}H & Li+p→α+n+^{3}He
E_p=9.1 MeV
E_α=4.1 MeV
θ_α=30°
146°
134°
122°
110°
98°
86°
ENERGY (MeV)
0.5
1.0
1.5
2.0
2.5
3.0
3.5
^{3}He
^{3}H
p
COINCIDENCE COUNTS
CHANNEL NUMBER
0
30
60
90
120
150

FIGURE 14. The α - H, α - ^{3}H and α - ^{3}He Angular Correlations from ^{7}Li(p, α) at E_{α} = 4.1 MeV and Θ_{α} = 30°

After subtracting the randoms, the coincidence spectra were reduced to the angular correlation functions. Since there are more energies available in the decay of the ^{4}He system, the kinematic lines, as it was seen in Figure 13, are farther apart. It is possible to separate the different groups of particles from one another. For some angles, however, the error includes the ambiguity in this separation, in addition to those from the statistics and the randoms, [cf., the caption of Figure 12].

The positions indicated by the arrows are the angles where the final-state interactions of α + ^{3}H, α + H and α + N through the relevant compound states are expected to be important. For further explanations see Figure 22 and pages 17 and 30.

FIGURE 14

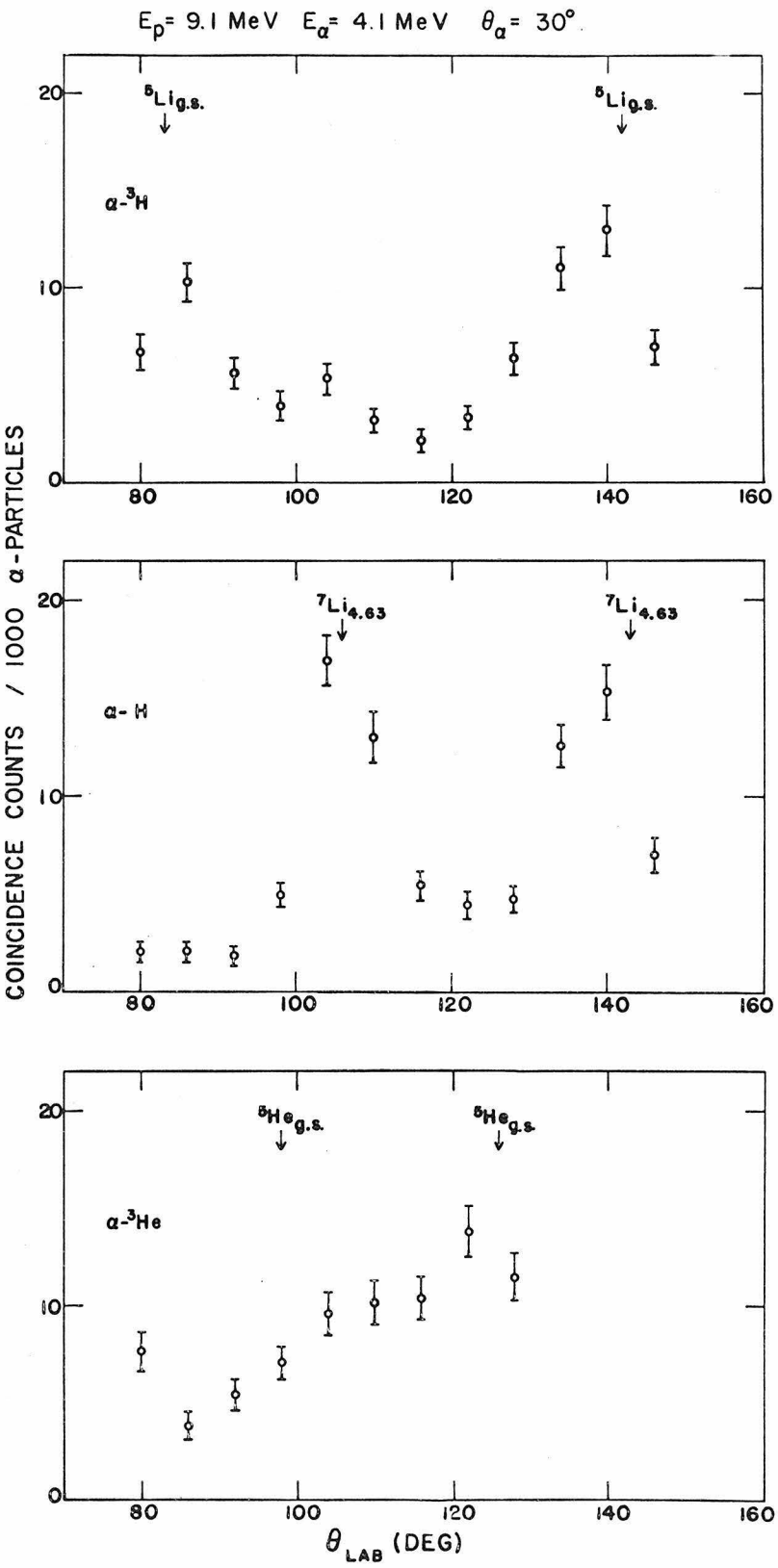
E_p= 9.1 MeV E_α= 4.1 MeV θ_α= 30°
^{5}Li g.s.
^{5}Li g.s.
α-^{3}H
^{7}Li 4.63
^{7}Li 4.63
α-H
^{5}He g.s.
^{5}He g.s.
α-^{3}He
COINCIDENCE COUNTS / 1000 α-PARTICLES
θ_{LAB} (DEG)
0
10
20
80
100
120
140
160

FIGURE 15. Stability of the Deuterated Dotriaiontane Target

In the upper graph (a), the number of the 7.8-MeV protons counted by the magnetic spectrometer, divided by the deuteron counts from D(^{3}He, d) in the counter set at 60° to the beam in the target chamber, is plotted versus the total integrated charge on target. The crosses, opened circles and the dark circles are used to distinguish the points taken with different targets. This shows that the deuterated dotriaiontane targets are stable against the 16.5-MeV ^{3}He beam within 10%.

In the lower graph (b), the same ratio was plotted out as a function of the detected proton energies. These values were used for normalizing from one coincidence spectrum to another.

For additional discussion see pages 19, 20 and 32.

FIGURE 15

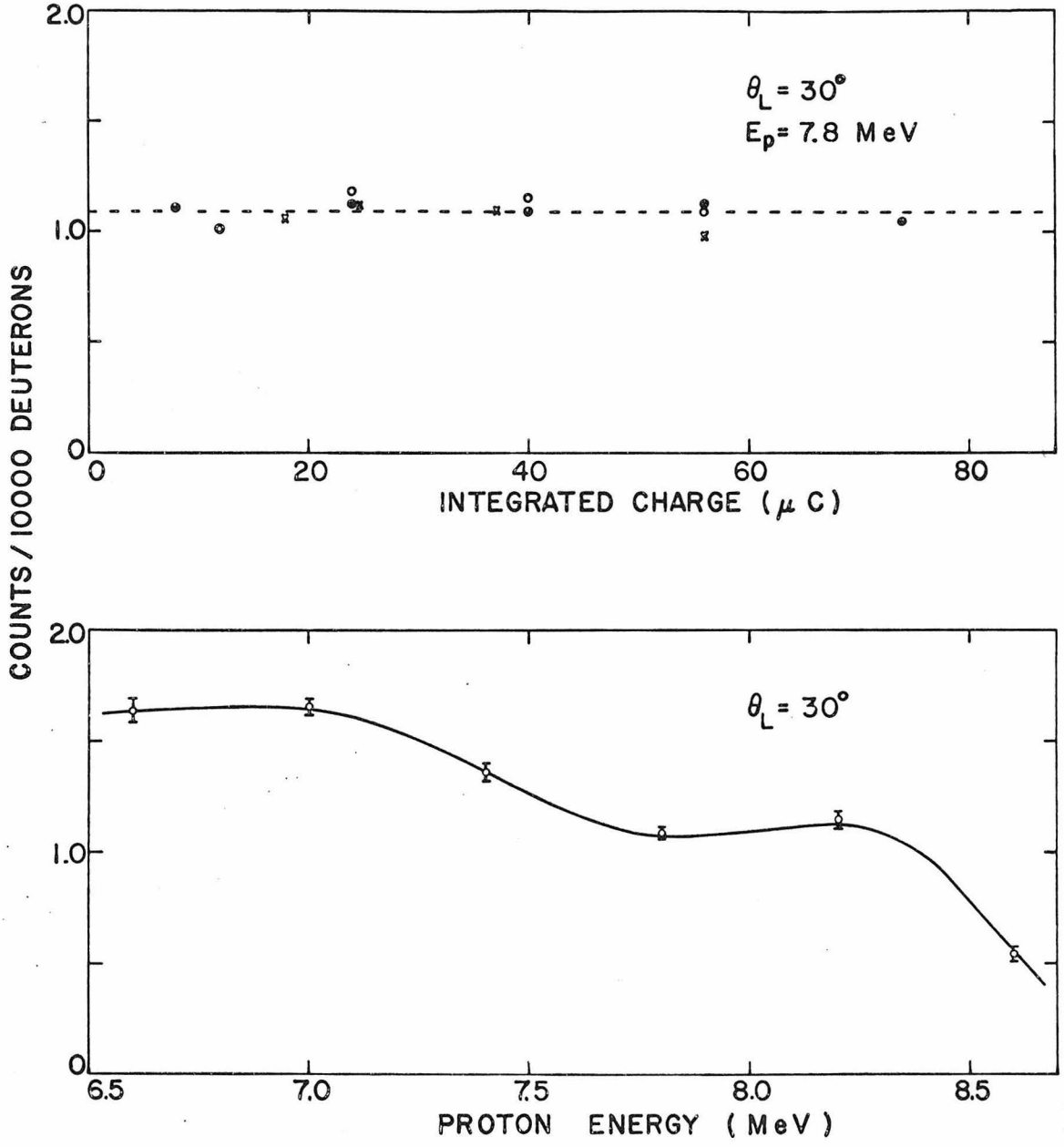
2.0
1.0
0
$\theta_L = 30°$
$E_p = 7.8$ MeV
0
20
40
60
80
INTEGRATED CHARGE (μ C)
COUNTS / 10000 DEUTERONS
2.0
1.0
0
$\theta_L = 30°$
6.5
7.0
7.5
8.0
8.5
PROTON ENERGY (MeV)

FIGURE 16. Particle Spectra at 26°, 36° and 46°

The particles emitted during bombardment of a deuterated dotriaiontane target on copper foil by 16.5-MeV ^{3}He's were detected in the 300-μ surface-barrier counter (see the caption for Figure 3) in the target chamber. Beam defining slits in front of the target chamber were 1.53 mm in both vertical and horizontal directions. The angular apertures were 2° and 8° along the Θ- and Φ-direction. The spectra were complicated by the competing reactions from ^{12}C, such as $^{12}C(^{3}He, ^{3}He')$, $^{12}C(^{3}He, p')$ and $^{12}C(^{3}He, d)$. For more details see page 21.

FIGURE 16

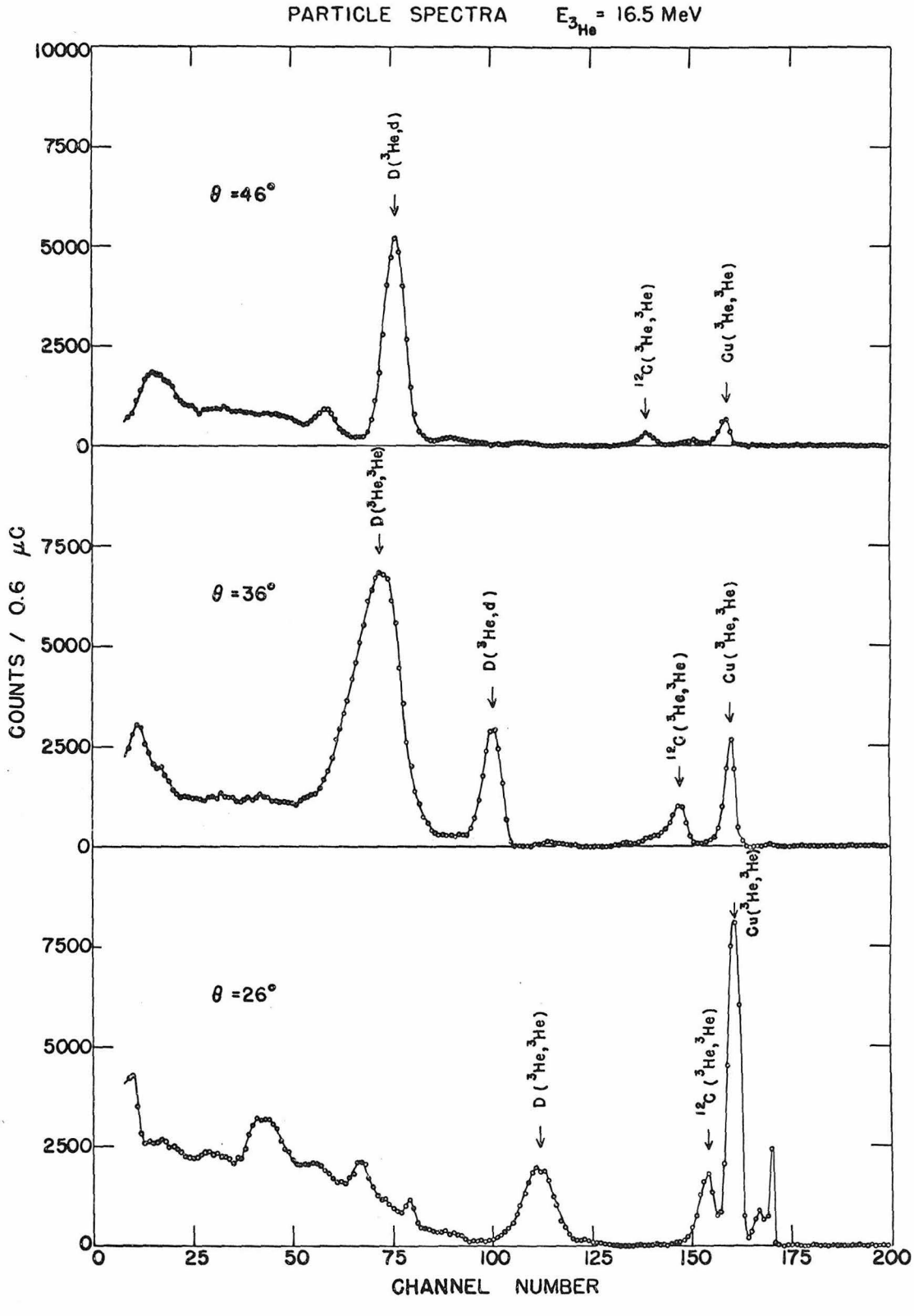
PARTICLE SPECTRA $E_{^3He}$ = 16.5 MeV
θ =46°
θ =36°
θ =26°
D(³He,d)
D(³He,³He)
¹²C(³He,³He)
Cu(³He,³He)
COUNTS / 0.6 μC
CHANNEL NUMBER
0
2500
5000
7500
10000
25
50
75
100
125
150
175
200

FIGURE 17. Angle Calibrations

The loci of the angular positions of the two counters in the coincidence measurement of the elastic scattering, such as $D + {}^3He \rightarrow {}^3He + d$, are independent of the energies involved. The lower graph shows the difference in angles of the counter in the target chamber in order to detect a deuteron or ^3He in coincidence with a ^3He or deuteron from the magnetic spectrometer set at some angles along the abscissa. In the upper graph, the magnetic spectrometer with $\delta\Theta = 0.2°$, $\delta\Phi = 4°$ and $\delta E/E = 1.11\%$ was set at 37.75° according to the reading. The dark (open) circles are the coincidences of the deuterons (^3He's) from the counter in the target chamber, when at the same time the magnetic spectrometer was used to detect the ^3He's (deuterons). The shift in centroids of the two groups was found to be $0.24 \pm 0.05°$. As was indicated by the arrow, the actual position of the magnetic spectrometer was therefore $37.62 \pm 0.04°$. With this the absolute angle of the counter in the target chamber was known to $\pm 0.1°$. For more details see page 23.

FIGURE 17

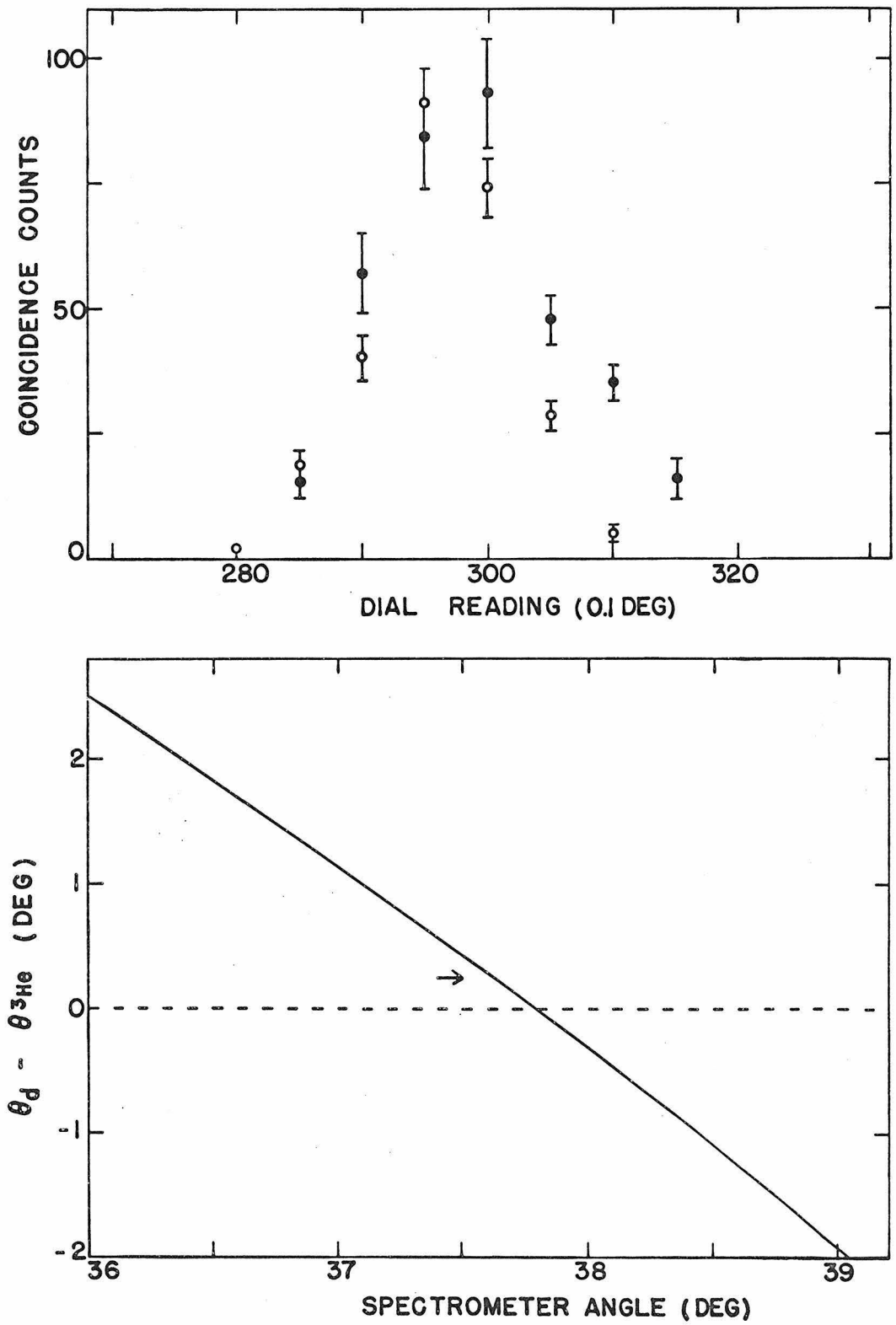
COINCIDENCE COUNTS
100
50
0
280
300
320
DIAL READING (0.1 DEG)
$\theta_d - \theta^3_{He}$ (DEG)
2
1
0
-1
-2
36
37
38
39
SPECTROMETER ANGLE (DEG)

FIGURE 18. A Block Diagram of Fast Coincidence System

In addition to the electronic circuitries used for the coincidence measurements of $^{7}Li(p,\alpha)$, an ORTEC Model 414 Fast Coincidence was inserted to the block diagram shown in Figure 10 for the $D(^{3}He,p)$ coincidence measurements. The fast coincidence resolving time was 110ns. See the caption for Figure 10 and page 24 for additional details.

FIGURE 18

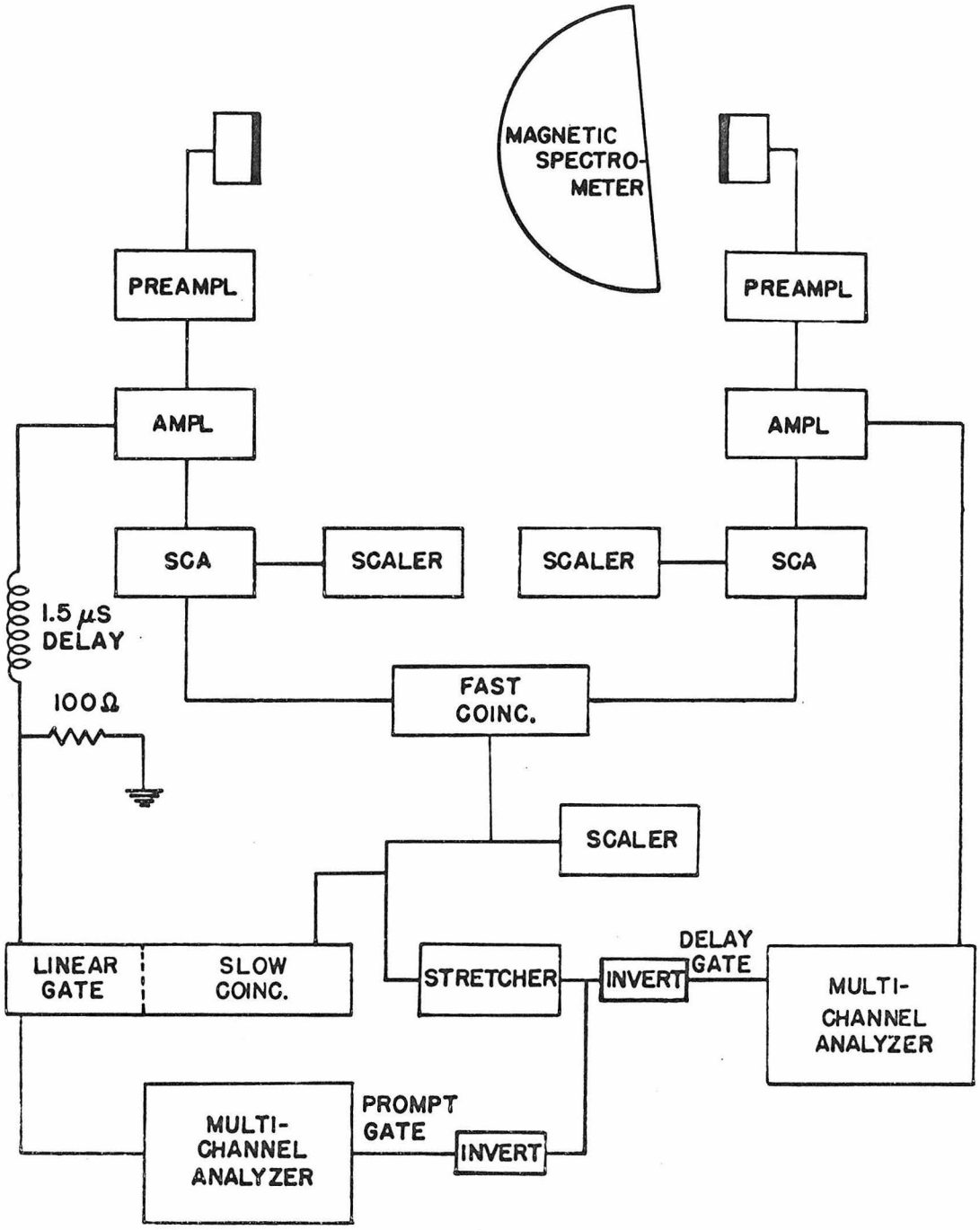

FAST COINCIDENCE SYSTEM

FIGURE 19. The Coincidence Spectra from D(^{3}He, p) at $\Theta_p = 30°$

When the counter in the target chamber was fixed at -20° with respect to the beam, the coincidence spectra obtained for the energy-correlation are shown in this figure. The protons of indicated energies were detected in the magnetic spectrometer, with $\delta\Theta = 1°$, $\delta\Phi = 4°$ and $\delta E/E = 1.11\%$. The angular apertures of the counter in the target chamber were set at 2° and 8° respectively along the polar and azimuthal directions. The fast-coincidence resolving time was 110 ns. The dotted lines are drawn from the three-body kinematics. For more details see page 24.

FIGURE 19

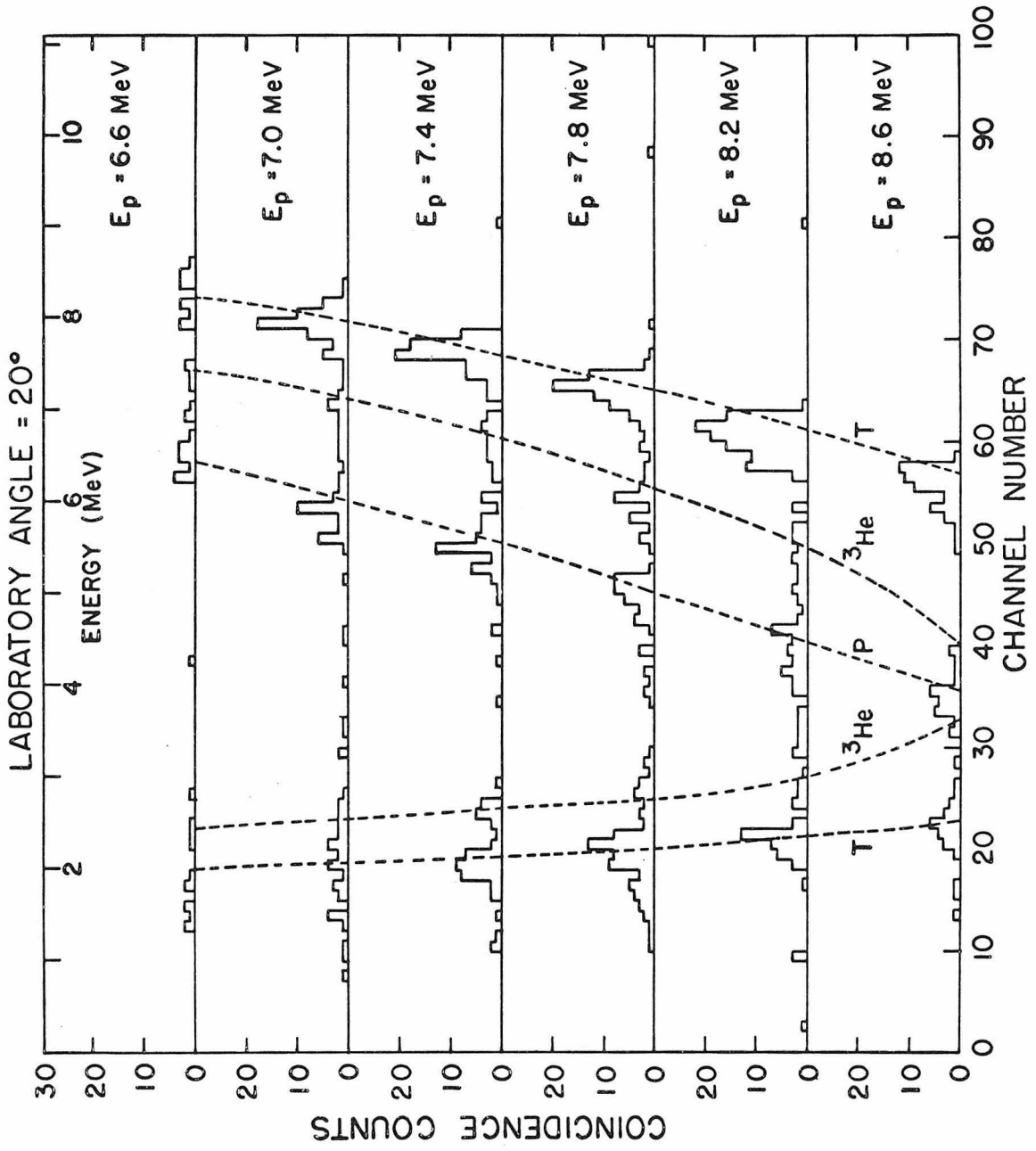
LABORATORY ANGLE = 20°
ENERGY (MeV)
CHANNEL NUMBER
COINCIDENCE COUNTS
E_p = 6.6 MeV
E_p = 7.0 MeV
E_p = 7.4 MeV
E_p = 7.8 MeV
E_p = 8.2 MeV
E_p = 8.6 MeV
T
^{3}He
P
^{3}He
T

FIGURE 20. The Coincidence Spectra from $D(^3He, p)$ at $E_p = 7.8$ MeV

Instead of fixing the position of the counter in the target chamber [cf., Figure 19], it was varied from 16° to 40° for these spectra at fixed proton momentum. See the caption for Figure 19 and page 24 for the resolutions of the detector, the kinematics and other details.

FIGURE 20

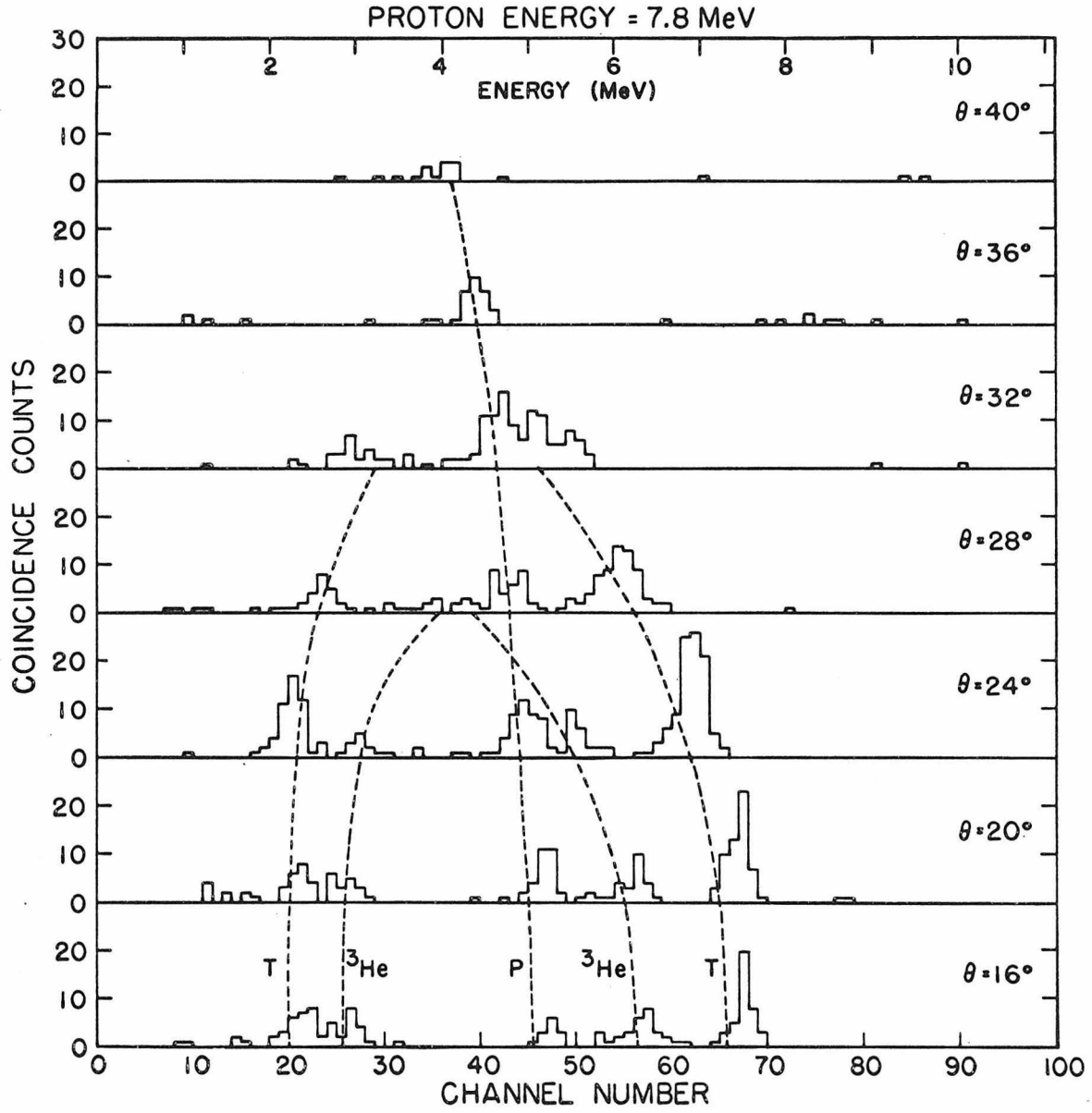
PROTON ENERGY = 7.8 MeV
ENERGY (MeV)
θ=40°
θ=36°
θ=32°
θ=28°
θ=24°
θ=20°
θ=16°
COINCIDENCE COUNTS
CHANNEL NUMBER
T
3He
P
3He
T

FIGURE 21. The Energy and Angle Correlation

After subtraction of the randoms and conversion to the center-of-mass of the recoil ^{4}He system [cf., Section A, Part III], coincidence of spectra shown in Figures 19 and 20 are shown here as an energy and angle correlation. The curves are the results of the modified Born approximation calculation. The bound-state wave functions for the deuteron, triton and ^{3}He were taken from Yu and Meyerhof's work. Rosenfeld's force was used for the nucleon-nucleon interaction. Because there is an axis of symmetry along the recoil ^{4}He direction, the dominant reaction mechanism was assumed to be that the incoming ^{3}He strips its deuteron to the target deuteron and forms a final-state interacting pair of either p + ^{3}H or n + ^{3}He. Following Yu and Meyerhof, a cut-off radius of 5 F was introduced in the calculation. This gives approximately the same amplitudes of the final-state interaction in p-wave and s-wave states. In the fitting , Meyerhof and McElearney's p + ^{3}H phase shifts and Bransden's n + ^{3}He phase shifts [cf., Table III] were used to describe the respective final-state interactions. For further discussions see Figure 27 and pages 25, 60 and 66.

FIGURE 21

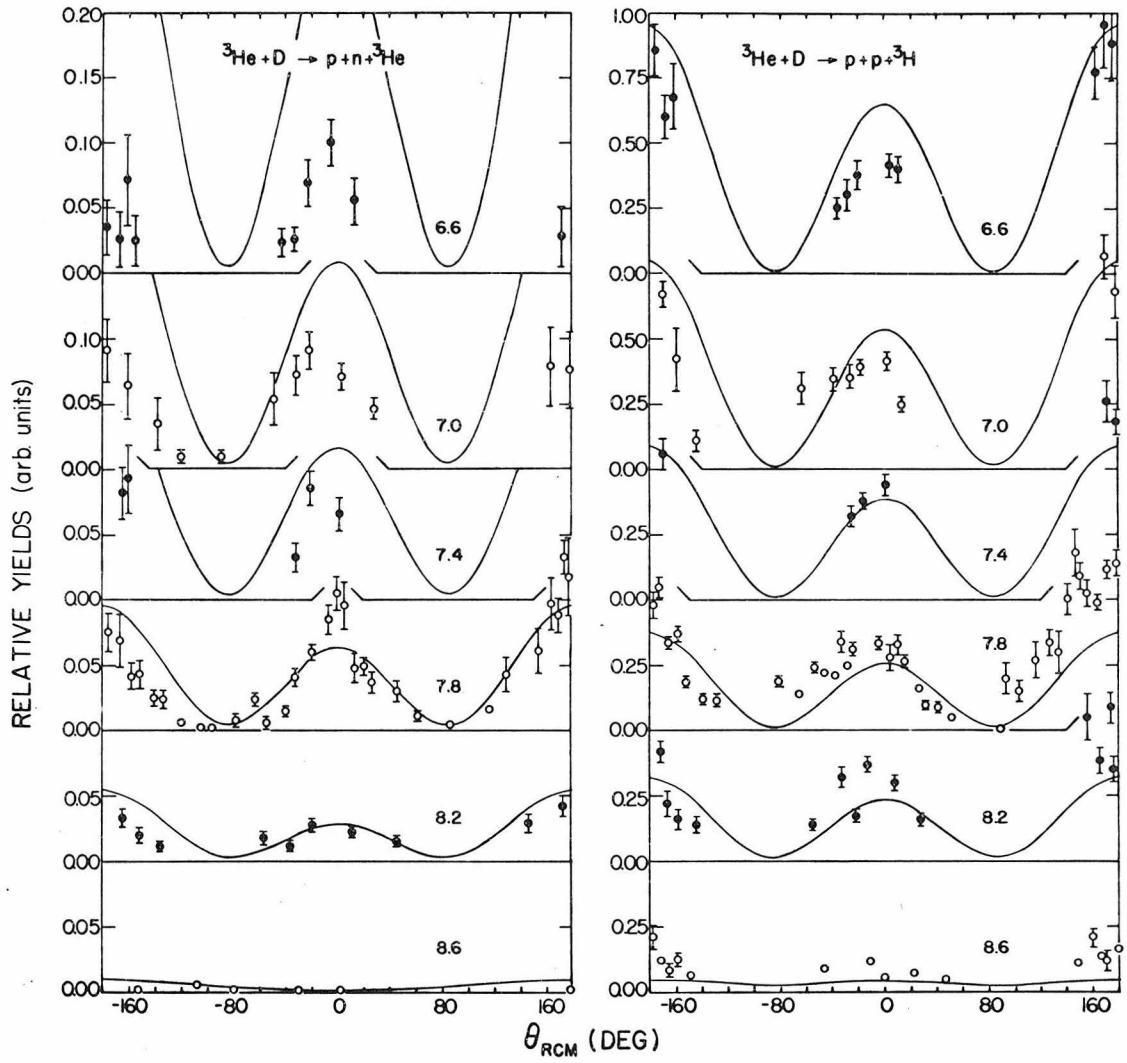
$^3He + D \rightarrow p + n + {}^3He$
$^3He + D \rightarrow p + p + {}^3H$
6.6
7.0
7.4
7.8
8.2
8.6
RELATIVE YIELDS (arb. units)
θ_{RCM} (DEG)
-160
-80
0
80
160

FIGURE 22. The Velocity-Vector Diagram

As it was discussed in Section A, Part III, the relative energy of the particle pair (3 + 5) or (4 + 5), from a three-body reaction $1 + 2 \rightarrow 3 + 4 + 5$, is identical on a cone determined by $\hat{q}_3$ and $\hat{q}_{35}$ or $\hat{q}_{45}$. The unit vector $\hat{q}_i$ is the direction of the relative motion of particle i and the rest of the system, while the unit vector $\hat{q}_{ij}$ is the direction of the relative motion of particles i and j. As an example, the reaction $^7Li + p \rightarrow \alpha + p + {}^3H$ was considered. The final state interaction of α-particle and triton through the 4.63 MeV level in the ^7Li nucleus [cf., Figure 13] will appear at the angles where the energy of the relative motion of α-particle and triton, $\frac{1}{2} M_{35} V_{35}^2$, is 2.16 MeV.

For more details see page 30.

FIGURE 22

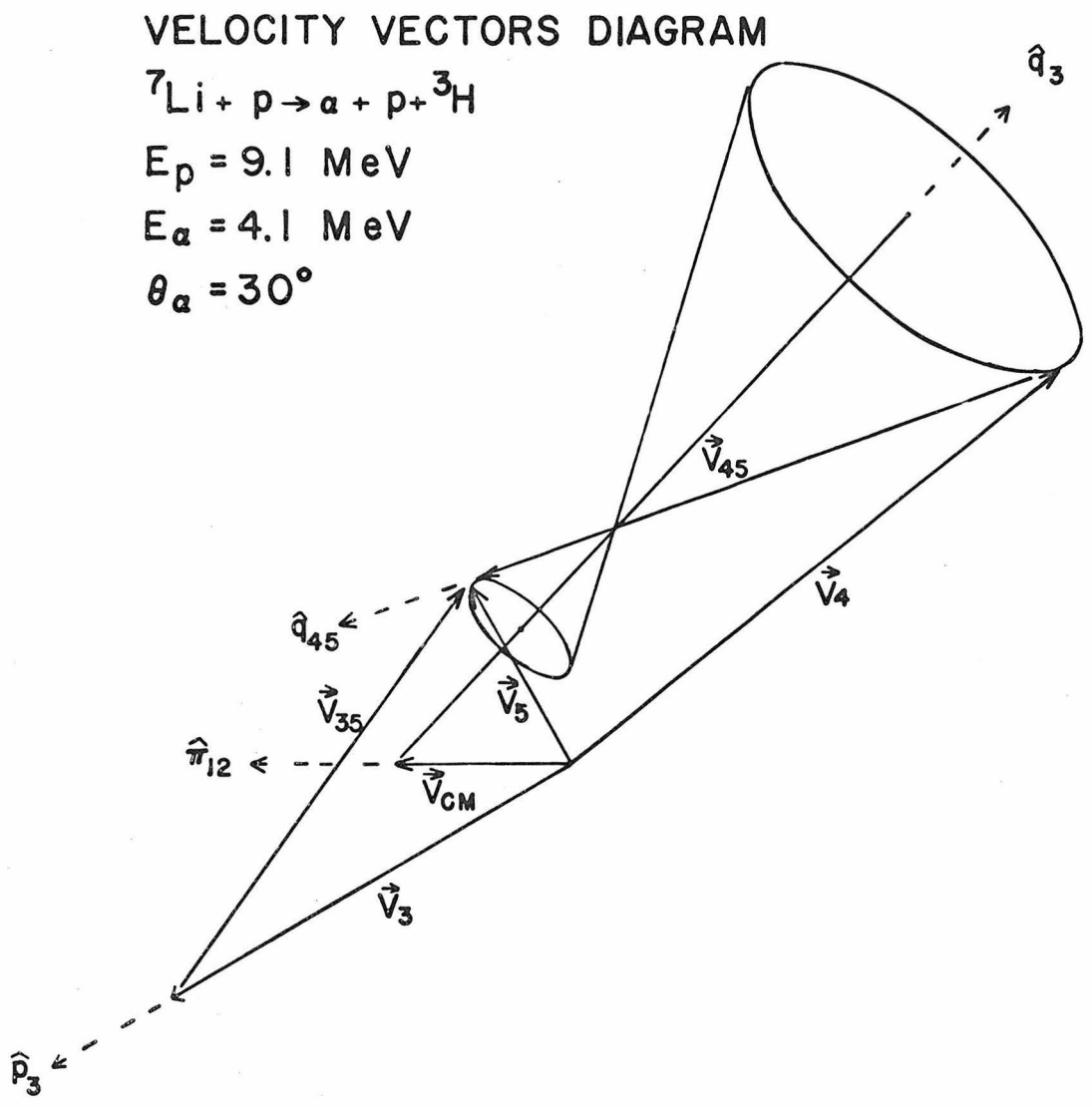
VELOCITY VECTORS DIAGRAM
$^7Li + p \rightarrow \alpha + p + ^3H$
$E_p = 9.1$ MeV
$E_\alpha = 4.1$ MeV
$\theta_\alpha = 30°$
$\hat{q}_3$
$\vec{V}_{45}$
$\vec{V}_4$
$\hat{q}_{45}$
$\vec{V}_{35}$
$\vec{V}_5$
$\hat{\pi}_{12}$
$\vec{V}_{CM}$
$\vec{V}_3$
$\hat{p}_3$

FIGURE 23. The Chi-Squares

With the number of the degrees of freedom equal to 203, the χ^2 of the least-square fit in the searching for the best resonance parameters of the first excited state of the ^{4}He system is plotted around the two sets of solutions (a, E_R, γ_p^2, γ_n^2). The dotted lines indicated the levels of the χ^2 at which the error for each of the parameters was assigned, [cf., Appendix B]. For further discussion see page 44.

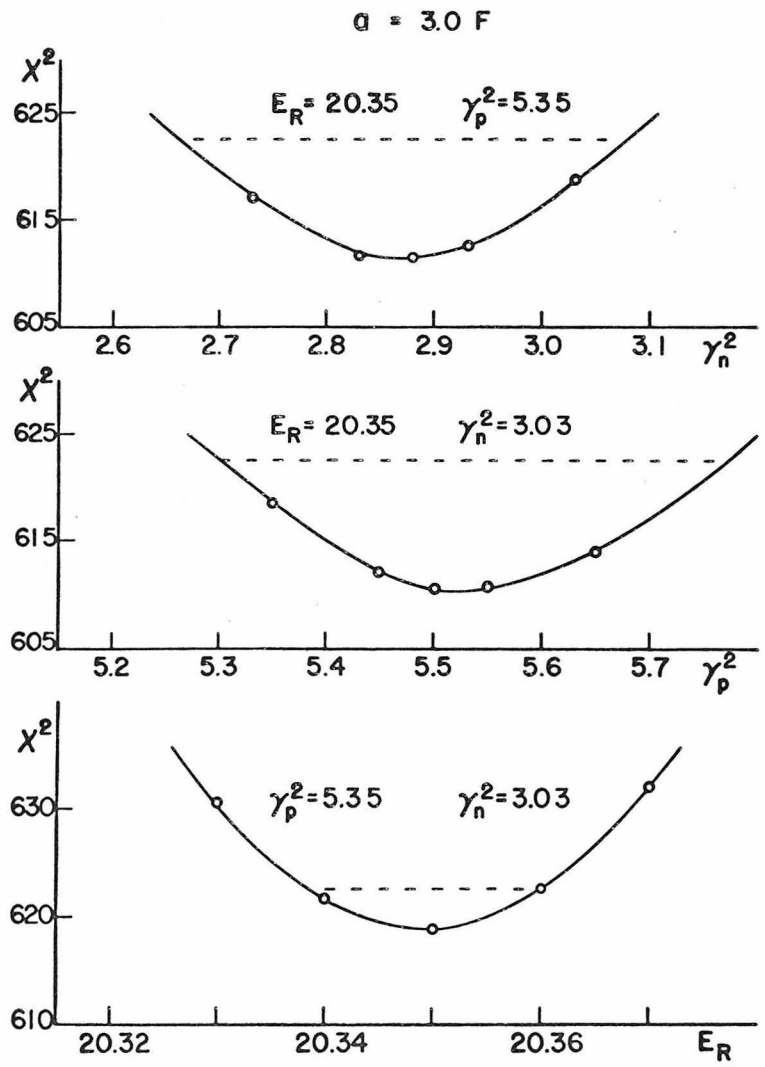
a = 3.0 F
χ^2
625
615
605
E_R= 20.35 γ_p^2=5.35
2.6 2.7 2.8 2.9 3.0 3.1 γ_n^2
χ^2
625
615
605
E_R= 20.35 γ_n^2=3.03
5.2 5.3 5.4 5.5 5.6 5.7 γ_p^2
χ^2
630
620
610
γ_p^2=5.35 γ_n^2=3.03
20.32 20.34 20.36 E_R

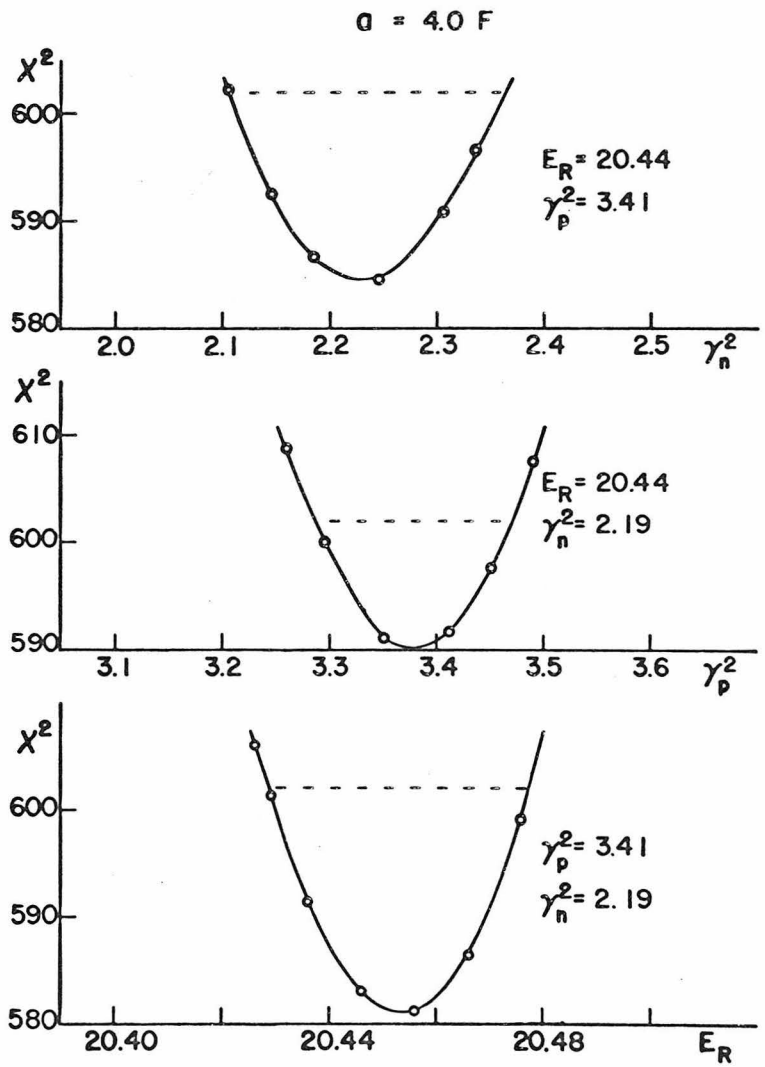
a = 4.0 F
χ^2
600
590
580
E_R= 20.44
γ_p^2= 3.41
2.0 2.1 2.2 2.3 2.4 2.5 γ_n^2
χ^2
610
600
590
E_R= 20.44
γ_n^2= 2.19
3.1 3.2 3.3 3.4 3.5 3.6 γ_p^2
χ^2
600
590
580
γ_p^2= 3.41
γ_n^2= 2.19
20.40 20.44 20.48 E_R

FIGURE 23

FIGURE 24. The ^1S p + ^3H Phase Shifts

The phase shifts calculated from the two sets of resonance parameters (a, E_R, γ_p^2, γ_n^2) obtained from the least-square fit described in Section B, Part IV are shown in this figure together with those given by other authors. The solid line and the dotted line are derived respectively from (3.0, 20.35, 5.53, 2.88) and (4.0, 20.45, 3.38, 2.23). The triangles, squares and circles respectively give the phase shifts by Werntz, Meyerhof et al. and Kurepin et al. The arrow indicates the cut-off energy of 20.30 MeV in ^4He excitation energy, and the least-square fit actually provides the phase shifts up to this energy. See Appendix A, Figures 23 and 25 and pages 44 and 64 for further discussions.

FIGURE 24

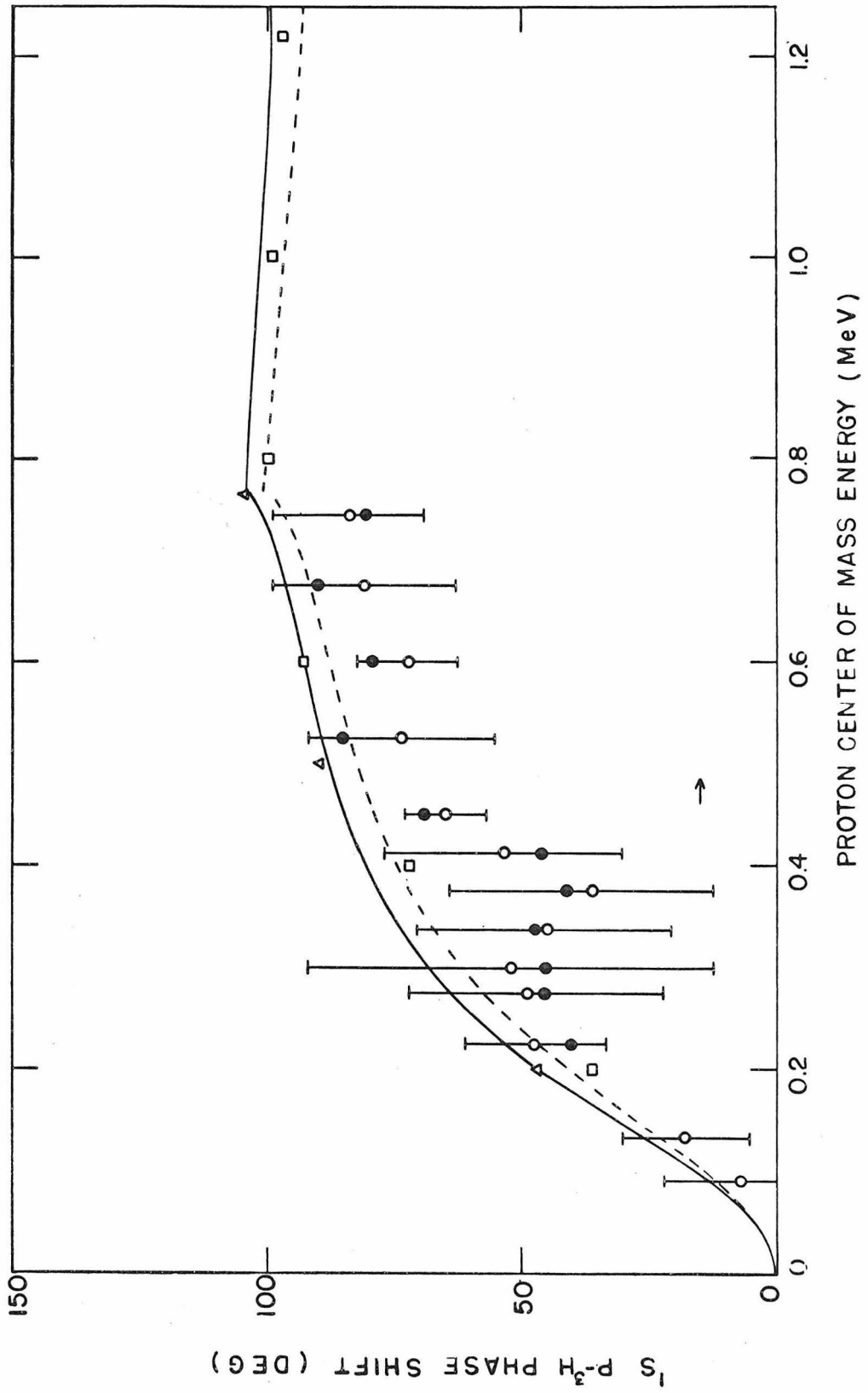
^1S p-^3H PHASE SHIFT (DEG)
150
100
50
0
0
0.2
0.4
0.6
0.8
1.0
1.2
PROTON CENTER OF MASS ENERGY (MeV)

FIGURE 25. The α-Particle Energy Spectra at 15°

To see how different the two sets of resonance parameters are in predicting the spectral shape of the α-particle energy spectrum, here the corresponding calculated shapes are compared with the α-particle energy spectrum at $\Theta_{\alpha} = 15°$. The solid line and dotted line, as they were in Figure 24, are respectively representing the calculations from the sets with a = 3.0 F and a = 4.0 F. The arrow indicates the cut-off energy. For more details see captions for Figures 9 and 24, and page 44.

FIGURE 25

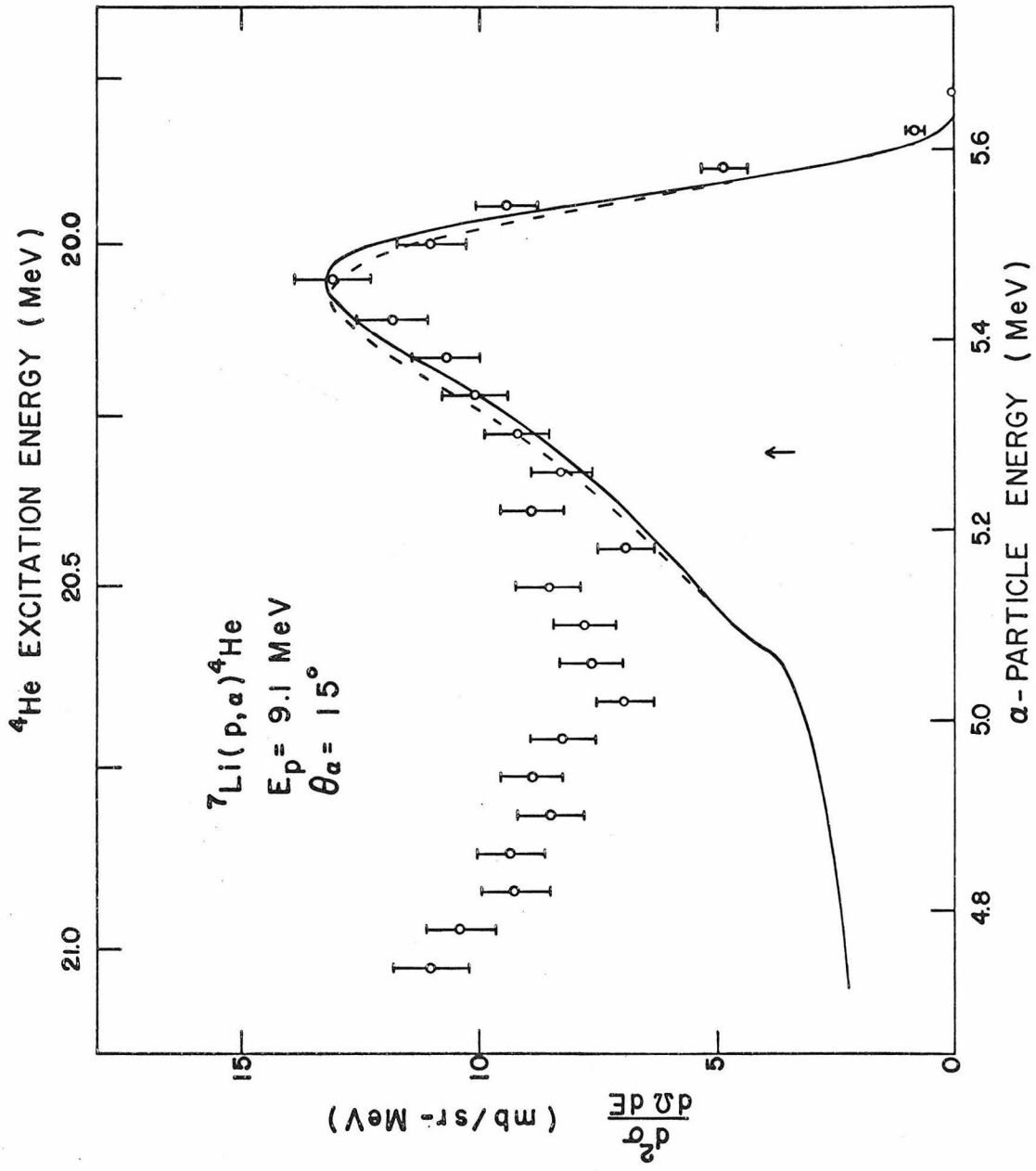
^{4}He EXCITATION ENERGY (MeV)
21.0
20.5
20.0
^{7}Li(p,α)^{4}He
E_p= 9.1 MeV
θ_α= 15°
$\frac{d^2\sigma}{d\Omega\, dE}$ (mb/sr-MeV)
15
10
5
0
4.8
5.0
5.2
5.4
5.6
α-PARTICLE ENERGY (MeV)

FIGURE 26. The Triton Transfer Mechanism in $^{7}Li(p, \alpha)$

In Figure 6, it was shown that the calculation, based on PWBA and a zero-range $p + {}^{3}H$ interaction in the α-particle, was not able to predict the forward peaking in the angular distribution at $E_p = 9.1$ MeV. To improve this, an interaction radius of 3.0 F was used. The dotted curves give the results. As was discussed in Section C, Part IV, this was still not sufficient to explain the behaviors of the angular distribution of the α-particle group leading to the first excited state of ^{4}He. The next attempt was to include the possibility that the incident proton may pick up a triton from the ^{7}Li target forming an α-particle and leaving behind the rest of the system in its excited state. The results are shown in the solid curves. For more details and the explanations for the parameters involved see pages 50-53.

FIGURE 26

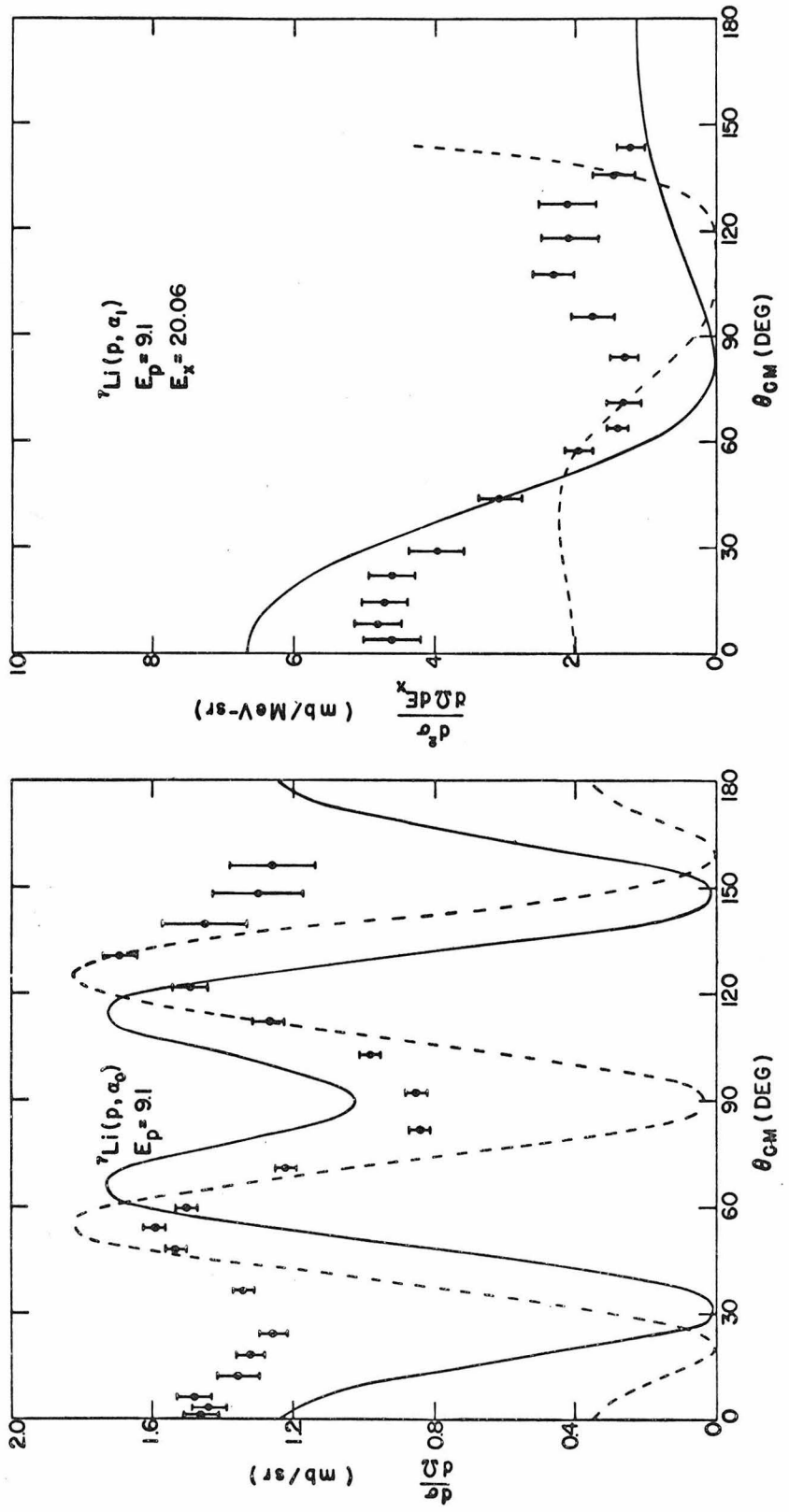
^{7}Li(p, α_0)
E_p=9.1
$\frac{d\sigma}{d\Omega}$ (mb/sr)
θ_{CM} (DEG)
^{7}Li(p, α_1)
E_p=9.1
E_x=20.06
$\frac{d^2\sigma}{d\Omega dE_x}$ (mb/MeV-sr)
θ_{CM} (DEG)

FIGURE 27. The Fit to the Angular Correction from D(^{3}He,p) at $E_p = 7.8$ MeV

To compare the n + ^{3}He phase shifts due to Meyerhof et al. and those due to Bransden et al., the p - ^{3}H and p - ^{3}He angular correlations at $E_p = 7.8$ MeV [cf., Figure 21] were fitted with all the phase shifts given by Meyerhof et al. This is shown by the dotted curves. The fits, especially to the shape of the p - ^{3}He angular correlation and to the branching ratio of the two modes of the reaction, were poor. The solid curves represent the same calculation except that the ^{3}S n + ^{3}He phase shift was replaced by the value of Bransden et al. For further discussion see pages 59, 66 and 67 and Table III.

FIGURE 27

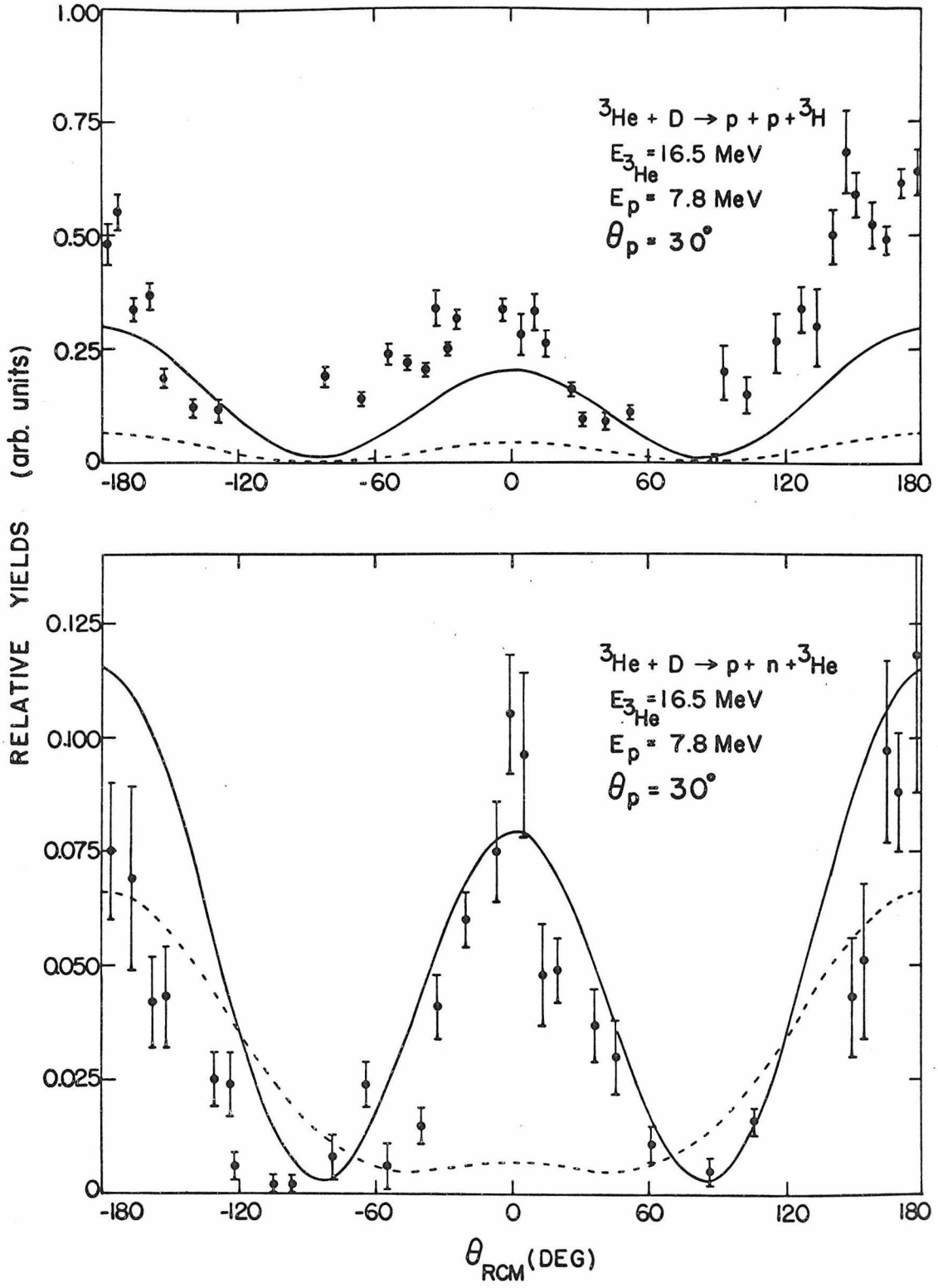
1.00
0.75
0.50
0.25
0
$^3He + D \rightarrow p + p + {}^3H$
$E_{^3He} = 16.5$ MeV
$E_p = 7.8$ MeV
$\theta_p = 30°$
-180
-120
-60
0
60
120
180
RELATIVE YIELDS (arb. units)
0.125
0.100
0.075
0.050
0.025
0
$^3He + D \rightarrow p + n + {}^3He$
$E_{^3He} = 16.5$ MeV
$E_p = 7.8$ MeV
$\theta_p = 30°$
θ_{RCM} (DEG)